AN INVESTIGATION ON THE STABILITY OF BIOCHAR-C IN SOILS AND ITS POTENTIAL USE TO MITIGATE NON-CO_2 GREENHOUSE GASES USING NEAR-INFRARED (NIR) SPECTROSCOPY

A thesis presented in partial fulfillment of the requirements for the degree of

Doctor of Philosophy

in

Soil Science

At Massey University, Manawatu
New Zealand

AINUL FAIZAH MAHMUD

2020

ABSTRACT

The global interest in using biochar for C sequestration-climate mitigation and soil improvement has driven rapid expansion in biochar research to understand its properties and application impacts. The potential for biochar application to increase soil organic carbon (SOC) stocks and its potential agronomic and additional environmental benefits, such as reducing soil nitrous oxide (N_2O) emission, are determined by its stability in the soil, which is dependent on its intrinsic properties and the soil conditions.

The inherent properties of biochar are highly influenced by feedstock type and pyrolysis temperature hence, the use of various types of feedstock and pyrolysis technologies leads to uncertainties in predicting the effect of biochar addition to soils. Previous research has established a general assumption that biochar stability is strongly influenced by the type of feedstock used and maximum pyrolysis temperature. Research is required, however, to produce practical and reliable techniques that can be used to verify the reported maximum pyrolysis temperature, regardless of the type of feedstock used and predict the likely stability of the biochar.

In addition to the pyrolysis process, the final particle size of the biochar and the method of incorporation into the soil may also influence the ability of the biochar to moderate soil properties and function. With previous research, there is general lack of attention given to these potentially influential parameters when assessing the impact of biochar application to soil.

Therefore this thesis evaluates (i) the use of near-infrared (NIR) spectroscopy technique for predicting the maximum pyrolysis temperature of biochar as it is a well-known, non-

destructive, and rapid technique for analyzing organic material; (ii) the effect of biochar application, with special attention to biochar particle size and depth of placement, on N_2O soil emission and SOC stocks; and (iii) the integrated use of NIR spectroscopy for SOC measurement.

In the first study, we hypothesized that NIR spectroscopy can be used to predict the maximum pyrolysis temperature achieved during biochar production. Eighty-two carbonized materials produced from various feedstock types and pyrolysis conditions with the reported pyrolysis temperature ranged between 220 to 800 °C, were scanned using NIR spectrometer and were used as the calibration set. The NIR calibration model was built by correlating the NIR spectral data with the reported pyrolysis temperature using partial least squares regression (PLSR). A separate sample set (n=20) was compiled using laboratory-produced biochar made from pine wood at pyrolysis temperature ranged from 325 to 723 °C. The calibration model validated using (i) leave-one-out cross-validation (LOO-CV) and (ii) the prediction set, yielded good accuracy (LOO-CV: r^2=0.80 and RMSECV:48.8 °C; prediction: r^2=0.82 and RMSEP: 57.7 °C). Results obtained in this study have shown that NIR spectroscopy can be used to predict the maximum pyrolysis temperature of biochar and has the potential to be used as a monitoring tool for biochar production.

In addition to the first study, the predictive ability of the NIR model was evaluated further. We hypothesized that the variation in feedstock types and pyrolysis processes may affect the predictive performance of the NIR model in predicting the maximum pyrolysis temperature of biochar. Therefore, three sample sets were generated from a total of 82 carbonized materials and its subsets (Set A: n=82; Set B: n=68; Set C: n= 48) and were

used for developing three calibration models. The selection of samples for Set B and C was made by reducing the variability associated with production conditions and feedstock type i.e. Set B consist of samples produced by slow pyrolysis and using the same pyrolyzer unit, while for Set C (a subset of Set B), samples produced from "processed feedstocks" were excluded. A separate sample set (n=18) consists of samples produced from animal manure, crop residue, and woody materials were used as the prediction set. This biochar was produced using the slow pyrolysis technique in a laboratory or under relatively high production controlled conditions at temperature ranged from 250 to 550 °C. These calibration models were validated using (i) leave-one-out cross-validation (LOO-CV) and (ii) a prediction set, with the model based on set C gave the best prediction (R2: 0.941; RMSEP: 27.3 °C), followed by the model based on set A (R2: 0.896; RMSEP: 35.6 °C), and set B (R2: 0.928; RMSEP: 37.3 °C). These results indicate that feedstock types have a considerable effect on the performance of the NIR model while the effect of pyrolysis conditions was less pronounced. Thus, data variability from samples needs to be taken into account in developing the NIR calibration model for predicting the maximum pyrolysis temperature of biochar.

Before studying the effect of biochar on N_2O soil emission and SOC stocks, the maximum pyrolysis temperature of biochar to be used in the experiment was predicted using the NIR spectroscopy technique. The estimated pyrolysis temperature – after scanning the 3-year old pine wood biochar and using the NIR model developed – was 500 °C, while the reported temperature was 550 °C.

A controlled glasshouse study was conducted to investigate the effect of biochar particle size and the impact of soil inversion (through simulated mouldboard ploughing) on N_2O

emissions from soils to which cattle urine was applied. We hypothesized that the application of biochar may (i) affect N_2O emissions through changes in soil physical properties, specifically soil aeration and water retention; and (ii) the effects of biochar addition on these properties may differ depending on their particle size (e.g., a larger particle size may increase soil aeration whereas a smaller particle size may clog pores), and their placement in soil (e.g., the incorporation of a large particle size-biochar at depth may promote water movement from the top layer and increase the overall drainage of the soil). Pine biochar (550 °C) with two different particle sizes (<2 mm and >4 mm) was mixed either into the top soil layer at the original 0–10 cm depth in the soil column or at 10–20 cm depth by inverting the top soil to simulate ploughing. Nitrous oxide emissions were monitored every two to three days, up to seven weeks during the summer trial, and measurements were repeated during the autumn trial. The use of large particle size biochar in the inverted soil had a significant impact on increasing the cumulative N_2O emissions in the autumn trial, possibly through changes in the water hydraulic conductivity of the soil column and increased water retention at the boundary between soil layers. Thus, the importance of the role of biochar particle size and the method of biochar placement on soil physical properties and the implications of these on N_2O emissions was highlighted. In the same glasshouse study, the effect of biochar particle size and depth of placement was further evaluated in relation to soil organic C. We hypothesized that (i) the large-particle size biochar may affect soil aeration and accelerate soil C decomposition rate with increased oxygen availability, and this effect is greater when biochar is incorporated at depth due to the more compacted soil at deeper layer with poorer aeration compared to

the surface layer; and (ii) the NIR spectroscopy technique can be used to predict the SOC concentration and SOC stocks in biochar-amended soil.

Carbon stocks were estimated using NIR spectroscopy coupled with partial least-squares regression analysis (NIR/PLSR) and direct organic C measurements using an elemental analyzer. The NIR spectra of the soil were acquired by scanning intact soil cores using the NIR spectrometer. By the end of the glasshouse trial (327 days), the large-particle size biochar applied at depth had induced significant soil C loss (9.20 Mg C ha^{-1} ($P < 0.05$), possibly through the combination of enhanced soil aeration, and the interrupted C supply from new plant inputs at that depth due to soil inversion. This C loss did not occur in the treatment with the small-particle size biochar. Near-infrared (NIR) spectroscopy was able to predict the SOC concentration, however, the prediction accuracy may be negatively affected by an increasing biochar particle size and soil inversion, thus may affect the subsequent SOC estimates.

The information obtained in this thesis will inform the future use of biochar and contribute to the knowledge of possible factors affecting soil N_2O emission from biochar-amended soil, the mineralization of native SOC, and the changes in SOC stocks over time, particularly in the pastoral soils of New Zealand. Also, based on this study, the use of NIR spectroscopy technique may potentially be integrated as part of the methodology for SOC estimation.

ACKNOWLEDGMENTS

I sincerely thank my supervisor Prof. Marta Camps Arbestain for the never-ending patience, guidance, and support throughout these years. I can't thank her enough for not giving up on me. I am also deeply grateful to my co-supervisor, Prof. Mike Hedley for the support and advice during my study.

I sincerely thank the Institute of Agriculture and Environment at Massey University and University Putra Malaysia for the scholarship that made this study possible.

Sincere thanks to Dr. Bambang Kusumo, Dr. Peter Bishop, Dr. Tao Wang, Dr. Roberto Calvelo–Pereira, Mr. Ian Furkert, Ms. Glenys Wallace, Mr. Mike Bretherton, Mr. Ross Wallace, and Mr.Bob Toes for the support they provided me with the field and laboratory work.

Thank you to all my friends in Massey who made everything enjoyable back then. To Qinhua Shen, May Sasikunya, Khadija Malik, Aldrin Rivas, Ahmed Elwan, Neha Jha, Stephen Collins, and many others, thank you so much.

I thank my partner, Ismalinda, for her love, patience, understanding, and support she provided me throughout this journey. I also thank my mom and all my siblings for their support and encouragement. This thesis is dedicated to Mr. Mahmud Ismail. Thank you abah.

TABLE OF CONTENTS

LIST OF TABLES

LIST OF FIGURES

LIST OF ABBREVIATIONS

BD	bulk density
C	Carbon
CEC	cation exchange capacity
CO_2-e	carbon dioxide equivalent
DM	dry matter
EBC	European Biochar Certificate
GHG	greenhouse gas
H/C_{org}	atomic H to organic C ratio
HHT	highest heating temperature
IC	inverted control
IL	inverted large particle size biochar
IS	inverted small particle size biochar
LOO-CV	leave-one-out cross-validation
MSC	multiplicative scatter correction
N	Nitrogen
N_2O	nitrous oxide
NIR	near-infrared
NIRS	near-infrared spectroscopy
PC	principal component
PCA	principal component analysis
PLSR	partial least square regression
RMSE	root mean square error
RMSECV	root mean square error of cross-validation
RMSEP	root mean square error of prediction
RPD	ratio prediction to deviation
SD	standard deviation
SEM	standard error of the mean
SNV	standard normal variate
SOC	soil organic carbon
SOM	soil organic matter
UC	un-inverted control
UL	un-inverted large particle size biochar
US	un-inverted small particle size biochar
Vis-NIR	visible-near infrared
VM	volatile matter
WFPS	water-filled pore space

CHAPTER 1. GENERAL INTRODUCTION

1.1 General background

The use of biochar as soil amendments for improved soil conditions and as a climate-change mitigation approach has gained recognition in the past few years and the interest in biochar research is consistently expanding (Chen et al., 2019). Biochar is a carbon-rich solid obtained from the thermochemical conversion of biomass in an oxygen-limited environment (Lehmann and Joseph, 2015). Due to its resistance towards microbial degradation, it has a mean residence time of 100 years or more, hence, biochar application can impact soil C storage and net CO_2 removals. Biochar addition would also indirectly increase soil C sequestration potential through stabilization of native SOC (Wang et al., 2016). It has been estimated that biochar systems can mitigate up to 2 Gt CO_2 eq/year (Fuss et al., 2018). Biochar as soil amendments may also reduce the N_2O emission from soil (Verhoeven et al., 2017) which further contributed to climate-change mitigation. However, understanding in the exact mechanisms and factors involved in the native SOC stabilization and the reduction of soil N_2O emission following biochar application is still lacking (Lehmann and Joseph, 2015).

The impact of biochar addition on a particular soil is dependent on biochar characteristics that were influenced by the nature of feedstocks and pyrolysis temperature (Li et al., 2019; Majumder et al., 2019). Extensive research has been devoted to the characterization of biochar to understand the variations in biochar physicochemical properties -as a function of production conditions and feedstocks- and its suitability for selected purposes (Igalavithana et al., 2017). Near-infrared (NIR) spectroscopy is one of the recent methods employed for biochar characterization (Kusumo et al., 2014; Yang and Sheng, 2012). This technique is rapid, non-destructible, allows the use of large sample mass, and cost-

efficient. Multivariate analysis (e.g. partial least square regression, PLSR) is used to build the calibration model by correlating the acquired NIR spectral data of the sample with the reference data. This model then can be used to determine the properties of unknown samples. As biochar application is gaining more interest, more biochar is produced by small-scale producers with less control over the production process. Thus, a fast and reliable tool is needed to determine the properties of the biochar, particularly the actual maximum pyrolysis temperature achieved during biochar production which may suggest the likely stability of biochar over time.

In addition, any properties that are measurable by standard methods can be used as the reference data, thus, NIR spectroscopy can also be used with other conventional techniques to minimize analysis cost and time. For example, NIR has been used to measure the soil C content and to estimate the soil C stock of a large area (Segnini et al., 2019). Therefore, NIR has the potential to be used for evaluating the effect of biochar on soil C by measuring the changes in soil C content over time following the application of biochar.

In New Zealand, limited studies have been done to assess the impact of biochar application on soil N_2O emission (Clough et al., 2010; Taghizadeh-Toosi et al., 2011), and on soil C stock (Calvelo Pereira et al., 2016), but have not studied the effect of biochar particle size and placement method. Whereas, although NIR spectroscopy has been used to predict SOC concentration (Kusumo et al., 2011) and SOC stocks (Roudier et al., 2015), no NIR-study has been done to predict SOC content in biochar-amended soil. To date, NIR spectroscopy has only been used for assessing biochar stability indices (Kusumo et al., 2014), with no application on biochar-amended soil.

In this context, the general hypotheses guiding this research were as follows:

- NIR spectroscopy can be used to predict the highest heating temperature achieved during biochar production.
- The varying feedstock types and pyrolysis conditions used for biochar production may decrease the performance of the NIR prediction model due to the presence of data variability.
- The application of biochar may (i) affect N_2O emissions through changes in soil physical properties, specifically soil aeration and water retention; and (ii) the effects of biochar addition on these properties may differ depending on their particle size (e.g., a larger particle size may increase soil aeration whereas a smaller particle size may clog large pores important for aeration and drainage), and their placement in soil (e.g., the incorporation of a large particle size-biochar at depth may promote drainage, aeration, and increase rooting depth).
- The large-particle size biochar may affect soil aeration and accelerate soil C decomposition rate with increased oxygen availability, and this effect is greater when biochar is incorporated at depth due to the more compacted soil at deeper layer with poorer aeration compared to the surface layer.
- NIR spectroscopy can be used to predict the SOC concentration and SOC stocks in biochar-amended soil.

1.2 Research Objectives

1.2.1 Main objectives

Following these identified research gaps and hypotheses, the main objectives of this study are to evaluate the effect of biochar particle size and the method of biochar placement on N_2O soil emission and SOC stocks, as well as to develop a reliable technique using NIR spectroscopy to predict the pyrolysis temperature of biochar, and by extension, the SOC stocks of biochar-amended soil.

1.2.2 Specific objectives

1. To develop a technique using near-infrared spectroscopy (NIRS) combined with partial least squares regression (PLSR) to reliably predict the highest heating temperature achieved during biochar production as a method of selecting more stable biochar.
2. To evaluate the effects of feedstock types and pyrolysis conditions, as sources of data variability, on the performance of near-infrared (NIR) models for predicting the highest heating temperature of biochar.
3. To investigate the effect of biochar particle size and the impact of soil inversion—through simulated mouldboard ploughing—on N_2O emissions from soils to which cattle urine was applied.
4. To examine the effect of biochar particle size and the method of biochar placement on soil organic C (SOC) stocks.
5. To evaluate the potential of using NIR spectroscopy technique to predict the SOC concentration and SOC stocks.

1.3 Thesis outline

In this thesis, the focus is divided into evaluating the use of NIR spectroscopy as a method of selecting more stable biochar by predicting the highest heating temperature achieved during biochar production as presented in Chapters 3 and 4, followed by the investigation on the effect of biochar addition on soil N_2O and soil C as presented in Chapters 5 and 6, respectively. The biochar used in Chapters 5 and 6 was also scanned using NIR technique written in Chapters 3 and 4. Moreover, the use of NIR spectroscopy in the earlier chapters act as prelude to a more comprehensive use of NIR spectroscopy on biochar-amended soil presented in Chapter 6. The whole thesis includes 7 chapters as follows:

Chapter 1 gives an introduction to the entire thesis, general background, and specifies the objectives of the current research and the outline of this thesis.

Chapter 2 provides a literature review based on the previous related findings including research gaps.

Chapter 3 presents a near-infrared (NIR) calibration model that can be used to predict the highest heating temperature (HHT) at which biochar was produced.

Chapter 4 evaluates the effect of different feedstock types and pyrolysis conditions on the predictive performance of NIR models used for predicting the maximum pyrolysis temperature of biochar.

Chapter 5 investigates the effect of biochar particle size and the impact of soil inversion (through simulated mouldboard ploughing) on N_2O emissions from soils to which cattle urine was applied.

Chapter 6 investigates the influence of biochar particle size and depth of placement on soil organic C (SOC) stocks and the use of NIR spectroscopy coupled with partial least-squares regression analysis (NIR/PLSR) for SOC measurement.

Chapter 7 is the overall conclusions and future research recommendations.

CHAPTER 2. LITERATURE REVIEW

2.1 Biochar overview

Biochar is a C-rich product obtained when biomass is thermally degraded in the absence of, or with a limited amount of oxygen (pyrolysis) that could be used as a soil amendment for improved agronomic and environmental outcomes (Lehmann and Joseph, 2015). The European Biochar Certificate (EBC) (2016) and the International Biochar Initiative (2015) have established a series of thresholds for a charred material to be considered as biochar which includes a carbon content higher than 10% (dry mass basis), an atomic H/C_{org} ratio of 0.7 or lower, and with specific maximum values of heavy metals and organic contaminants.

Biochar can be produced from wide ranges of feedstocks such as woody materials, e.g., pine chips (Gonzaga et al., 2018); agricultural wastes, e.g., rice husk, rice straw, and corn cob (Jindo et al., 2014; Kanouo et al., 2019); animal waste (Cantrell et al., 2012); paper mill waste (Enders et al., 2012); and sewage sludge (de Figueiredo et al., 2019). The type of feedstocks used and the pyrolysis conditions applied, such as temperature, time, heating rate, and level of oxygen, determine the characteristics of biochar (Panwar et al., 2019; Wei et al., 2019).

Pyrolysis is defined as "the thermal degradation of biomass by heat in the absence of oxygen, which results in the production of charcoal (solid), bio-oil (liquid), and fuel gas products" (Demirbas and Arin, 2002). Major organic compounds such as cellulose, hemicellulose, and lignin are expected to break down during pyrolysis. Hemicellulose breaks down first (220-315 °C), followed by cellulose (315-400 °C), and lignin (>400 °C) (Yang et al., 2006). The main types of pyrolysis methods used are slow (conventional) pyrolysis, fast pyrolysis, flash pyrolysis, and intermediate pyrolysis (Tripathi et al., 2016).

The operating parameters for each pyrolysis method are shown in Table 2.1. These parameters determine the rate and extent of biomass degradation.

Table 2-1. Range of the main operating parameters for the pyrolysis process, as adapted from Demirbas and Arin (2002) and Zhang et al. (2010).

Condition	Slow	Fast	Flash	Intermediate
Pyrolysis temperature	250-700	500-950	>1000	500-650
Heating rate (°C /s)	0.1-1	10-200	>1000	1.0-10
Particle size (mm)	5-50	<1	<0.5	0.5-20
Residence time (s)	450-550	0.5-10	<0.5	10-20
Pressure (MPa)	0.1	0.1	0.1	0.1

There is a strong relationship between the pyrolysis conditions, i.e. temperature and the chemical structure of biochars. Carbon concentration increases as pyrolysis temperature increases, whereas 'H' and 'O' concentrations gradually decrease (Novak et al., 2009). When the pyrolysis happens at relatively lower temperatures, i.e. <400 °C, biochar rich in C=O and C-H functional groups are formed. The yield recovery is high at low pyrolysis temperature range, and the dominant organic compounds are aliphatic or less stable cellulose-like structures, which can be easily degraded by microbes. At high pyrolysis temperatures (400–700 °C), the feedstock is converted into relatively stable poly-condensed-aromatic structures that contain high C (Kaal et al., 2012). The changes in biochar elemental contents (C, H, and O) such as the decrease in both atomic ratios of H/C and O/C with the increase of heating temperature has been used as an indicator of biochar's structure and stability (European Biochar Certificate (EBC), 2016; International Biochar Initiative, 2015).

Physical properties of biochar such as surface morphology, porosity, pore-volume, surface area, and other physical structures are also influenced by feedstock types and

production conditions (Kan et al., 2016a). At high temperature (600°C), Brodowski et al. (2005) observed complete destruction of the original structure of the feedstock. The structure of biochar produced at a lower temperature (~400°C) was similar to that found in amorphous carbons, while biochar produced at a higher temperature (>500°C) have structures which were more similar to the thermally-reduced graphene oxides (Guizani et al., 2017; McDonald-Wharry et al., 2013). Brewer et al. (2014) found that biochar porosity is influenced by feedstock type with biochar produced from grass has a higher porosity than woody biochar, while generally, both pore volume and surface area of biochar increase with the increase of heating temperature (Fu et al., 2012; Weber and Quicker, 2018).

To date, research on biochar characteristics as a function of feedstock types and pyrolysis temperature has been extensive (Igalavithana et al., 2017; Leng and Huang, 2018) as the physicochemical properties (elemental compositions, moisture, fixed C, volatile matter, ash contents, pH, CEC, surface area, and pore size) including its molecular and structural compositions of biochar determine its stability and suitability for specific applications (Leng and Huang, 2018; Li and Chen, 2018). Based on a recent review and meta-analysis of 154 studies by Li et al. (2019), the possibility to link biochar production (pyrolysis temperature and feedstock type) with its properties and performance was highlighted. This suggested the possibility of predicting the outcomes of specific biochar application based on the pyrolysis temperature and type of feedstock used for its production. Recent guide-lines by IPCC also emphasize the practical need to identify biochar's production temper-ature and feedstock type to estimate the change in SOC stocks from biochar amendments to soils (IPCC, 2019). However, although this information is commonly available, it is

well known that due to the exothermic nature of pyrolysis reaction (Ripberger et al., 2015) and the varying thermal behavior of feedstock (Di Blasi et al., 2014), the control of pyrolysis temperature can be difficult and thus, the reported temperature may be inaccurate and need to be verified.

2.2 Agronomic and environmental benefits of biochar

The use of biochar is not only limited to C sequestration (Lehmann and Joseph, 2015), but its application to soil has been reported to give positive effects on soil qualities such as the increases of ion exchange capacity, liming ability, nutrient retention, soil organic C, and plant growth (Laird et al., 2010; Shi et al., 2017; Zhang et al., 2012). The addition of biochar may also improve soil aeration, soil aggregation, and other soil hydrologic functions (Blanco-Canqui, 2017; Omondi et al., 2016; Ouyang et al., 2013). Under specific conditions, biochar application has also been shown to reduce the greenhouse gas (GHG) emissions such as the nitrous oxide (N_2O) and methane (CH_4) from soil (Cayuela et al., 2015; Jeffery et al., 2016; Van Zwieten et al., 2015). The next sections will explore more on the effect of biochar application on soil N_2O emission and soil organic C.

2.2.1 Biochar effect on nitrous oxide (N_2O) emission from soil

New Zealand has committed to reducing greenhouse gas (GHG) emissions to 5 and 11% below the 1990 level by the year 2020 and 2030, followed by a net-zero target for CO_2 and N_2O by 2050 according to the Climate Change Response (Zero Carbon) Amendment Act introduced in 2019 (Ministry for the Environment, 2019a). The primary sources of nitrous oxide (N_2O) in New Zealand are excreta (urine and dung) from grazing animals; contributed to 14% (5435.3 kt CO_2-e) of total N_2O emissions from the agricultural sector

in 2017 which represent a 5.8% increase since 1990, followed by urea and farm dairy effluent applied to soils (Ministry for the Environment, 2019b).

Nitrous oxide is produced in soil by microbial processes that occur during (i) the oxidation of NH_4^+ to NO_3^- (nitrification), (ii) during the dissimilatory reduction of NO_3^- and NO_2^- to N_2 when oxygen is depleted (denitrification) (Robertson and Tiedje, 1984) or (iii) from the nitrifier-denitrification reaction, in which ammonia oxidizers reduce NO_2^- to N_2O or N_2. Nitrifier-denitrification can happen in both aerobic and anaerobic conditions (Wrage et al., 2001). These microbial processes are affected by several factors such as the availability of N sources, organic matter content, and the physical condition of the soil i.e, low soil aeration, high soil water content and soil compaction (de Klein and Ledgard, 2005; Saggar et al., 2004). Denitrification is the main reaction responsible for N_2O production when the water-filled pore spaces (WFPS) of soils is over 70% while, nitrification is the main source under drier soil conditions (Khalil and Baggs, 2005). However, the emissions of N_2O in New Zealand pastoral soils mostly originate from denitrification processes (Saggar et al., 2004).

The use of biochar as soil amendments has been suggested as a potential tool to reduce the N_2O emission from soil (Van Zwieten et al., 2015), however, its application has been reported to have contrasting effects. Several authors (Nelissen et al., 2014; Taghizadeh-Toosi et al., 2011; Thomazini et al., 2015) claimed the emissions of N_2O from soil were reduced after the application of biochar, while other studies showed biochar increased (Chen et al., 2015; Shane M. Troy et al., 2013; Yoo and Kang, 2012) or did not affect soil N_2O emissions (Angst et al., 2014; van Zwieten et al., 2019). Nonetheless, multiples meta-analyses confirmed that N_2O emissions are reduced with biochar application rates. Based

on the meta-analysis done by Cayuela et al. (2014), biochar applications reduced soil N_2O emission by 54% in both laboratory and field studies. However, later they updated their finding with a lower N_2O mean reduction of 49% (Cayuela et al., 2015) with field studies shown lower N_2O reductions (28%) compared to laboratory studies (54%). Further meta-analyses done by Liu et al. (2018) and Borchard et al. (2019) also found reduced soil N_2O emission by 32 and 38%, respectively, along with decreased NO_3^- leaching after biochar applications.

2.2.1.1 Soil factors and the role of biochar in controlling N_2O emissions

There are several possible factors involving biochar application in soil that may affect N_2O emissions, such as the changes in soil pH, soil aeration, and interactions between biochar with available N in soil (Cayuela et al., 2014, 2013). Changes in soil pH may affect N_2O emissions due to the need for an optimum pH for nitrifiers and denitrifiers to perform well in soil. Decreasing soil pH may increase the N_2O product ratios of both nitrification ($N_2O/(NO_2^-+NO_3^-)$); due to enhanced denitrification of NO_2^- (Mørkved et al., 2007), and denitrification ($N_2O/(N_2+N_2O)$); possibly due to hindered synthesis of the functional N_2O reductase enzyme (Bakken et al., 2012). The liming properties of biochar have been reported in several articles where the application of biochar was found to alleviate soil pH in acidic soil (Chintala et al., 2014; Verheijen et al., 2010). In studies done by Isadora et al. (2019), Obia et al. (2015), and Van Zwieten et al. (2010), the reduction in N_2O emissions from acidic soils after having increased its pH with the application of biochar were observed. However, the change in pH of a specific soil with the addition of specific biochar will also largely dependent on the pH-buffering capacity

of the specific soil. Thus, the response of soil pH to biochar application might be varied (Camps-Arbestain et al., 2015).

Biochar application may also alter soil physical properties such as improving soil aeration, porosity, moisture, and aggregation while reducing compaction and bulk density (Blanco-Canqui, 2017; Herath et al., 2013; Masiello et al., 2015). These changes may affect soil N_2O emissions by influencing the generation of N_2O and its diffusion (Chapuis-lardy et al., 2007; Heincke and Kaupenjohann, 1999). The addition of biochar may increase oxygen availability and lower the WFPS, thus decreasing soil N_2O emissions by hampering the activity of denitrifiers. Yanai et al. (2007) and Rogovska et al. (2011) suggested that biochar addition enhanced soil aeration and contributed to the reduction in N_2O emissions in their incubation studies. However, in an incubation study done by Case et al. (2012), it was suggested that the effect of biochar on soil pH and aeration only provided a minimal contribution to the reduction of N_2O emission from basic soil. These researchers incubated soil cores with different doses of biochar and wetted them to a uniform 78% WFPS. They found that despite all soil cores has the same soil aeration, soil amended with higher biochar rate had lower cumulative N_2O production compared to control. Although biochar-amended soils having higher soil pH values than non-amended soils, they were only slightly differed (8.02-8.22), and thus the reduction of N_2O production due to the pH changes in basic soils was considered as unlikely. In such conditions, another factor such as the interaction between biochar and the available N (NO_3^- or NH_4^+) in soil was hypothesized as a potential contributor to the suppression of N_2O soil emission. Nevertheless, this study only focused on the effect of biochar addition

in basic soil. Thus, the result found cannot simply be used to represent the effect of biochar addition on N_2O emission in all soil types and conditions.

The availability of reactive N in the soil, such as NO_3^- or NH_4^+, is important for microbial activities related to N_2O production. Biochar application to soil may limit the availability of N in soil possibly by immobilization of the available NH_4^+ (Hina et al., 2010; Saleh et al., 2012) and/or NO_3^- (Haider et al., 2017; Kammann et al., 2015; Yao et al., 2012), thus lowering the N_2O emissions by reducing the availability of the substrate used for the production of N_2O. Considerable reductions in soil extractable NO_3^- and a decrease in N_2O emission over time has been observed after the application of biochar (Bruun et al., 2011; Case et al., 2012; L. Van Zwieten et al., 2010; Van Zwieten et al., 2014). However, the mechanisms involved and the interaction between biochar properties; such as the function of pyrolysis temperature, feedstock type, and its application rate, with soil available N on N_2O production remains elusive and require further evaluation (Cayuela et al., 2014; Q. Liu et al., 2018; Verhoeven et al., 2017). Contrary to the studies above-mentioned, Singh et al. (2010) and Jones et al. (2012) found that biochar had little or no effect on the leaching of NO_3^- in biochar-amended soils. Both of these studies involved relatively long-term experiments. The authors suggested the aging of biochar in soils had also affected the available N and subsequently the N_2O emissions.

Most of the studies on the effect of biochar application on soil N_2O emission still lack insights and understanding of the mechanisms involved (Kammann et al., 2017; Woolf et al., 2018a). Mukherjee and Lal (2013), Clough et al. (2013), and Omondi et al. (2016) emphasized the lack of research focusing on the effect of biochar application on soil physical properties, such as the formation and stability of soil aggregates, which are

closely related to soil aeration, porosity, and drainage facility of soil, and thus may also indirectly impact N_2O soil emission.

Clough et al. (2013) also highlighted the need to assess the influence of biochar particle size, which often gets overlooked in N_2O emissions studies. In a comparison study done by Felber and Leifeld (2013) in which N_2O emissions from controlled laboratory conditions experiment and a field experiment were measured, it was suggested that the efficiency of biochar for reducing N_2O emissions was also related to the effectiveness of mixing of biochar in soil and its possible effect on NO_3^- immobilization. The ineffective mixing of biochar in the field left larger soil aggregates without having biochar incorporated inside and this reduced the contact of biochar particles with soil and affected the ability of biochar to retain NO_3^- (Felber et al., 2013). Soil-biochar contact is also affected by the biochar incorporation technique (e.g., whether the biochar is spread on the soil surface, uniformly mixed into the topsoil or incorporated at certain soil depth) and yet this also has received little attention (Verheijen et al., 2010). In a review done by Blanco-Canqui (2017), biochar particle size and placement method were identified as factors that can potentially influence soil physical properties, and yet there is very limited research on this.

2.2.2 Biochar effect on soil C

Soil carbon (C) plays an important role in varying soil functions such as in the conservation and filtration of water, storage and recycling of nutrients, biomass production, habitat for biological activity, and carbon storage. Soil C is also considered as one of the key indicators of soil function in regards to agricultural productivity, water security, and climate regulation (FAO, 2015; Wiesmeier et al., 2019). The estimated size

of the soil organic C (SOC) pool to 1-m depth is 1462–1548 Pg (petagram = 10^{15} g or 10^{9} t), almost twice as much as the atmospheric stocks (Batjes, 2014). Therefore, even small changes in the SOC stocks would affect the atmospheric stock (Smith, 2008) with small gains in soil organic C can result in a considerable reduction in atmospheric CO_2 concentrations (4 per 1000 Initiative, 2015). SOC decomposition rate can be affected by several factors such as the inherent soil characteristics, climate, and land use e.g. agricultural activities (Lal, 2018). Unsustainable agricultural practices have resulted in a major depletion of SOC stocks by ~133 Pg C in the top 2-m of agricultural soils (Sanderman et al., 2018).

The SOC stocks can be maintained or increased by (i) reducing soil tillage and thus less SOC mineralization from soil disruptions, (ii) increasing below-grounds C inputs through the selection of deep-rooting crop varieties with higher fine-root density at depths, and/or (iii) the addition of organic C amendments (e.g. animal manure, compost, or biochar) (Chenu et al., 2019; Dignac et al., 2017; Whitehead et al., 2018). The incorporation of biochar into the soil has not only been promoted as a strategy for direct C sequestration due to its high C content and high recalcitrance (Lehmann, 2007; Woolf et al., 2018a) but also as an agricultural management practice with beneficial effects on soil physical and chemical properties (Chen et al., 2019; Ye et al., 2019). However, biochar addition has been found to affect the mineralization rate of native SOC (S. Liu et al., 2016; Wang et al., 2016), referred to as “priming”, where “positive priming” is the increased mineralization of native SOC while, “negative priming” is the reduced mineralization of native SOC, following biochar additions (Zimmerman et al., 2011).

Several mechanisms have been proposed to explain the biochar-induced negative priming effect such as (i) enhanced physical protection of SOC from increased soil aggregation (Hernandez-Soriano et al., 2016; Kerré et al., 2016), (ii) sorption of SOC on biochar surfaces and thus limiting its availability to microbes (Keith et al., 2015; Maestrini et al., 2014; Whitman et al., 2014), (iii) increased formation of organo-mineral complexes through adsorption and ligand exchange (Joseph et al., 2010; Weng et al., 2017) and/or (iv) the inhibition of microbial activity due to toxic substances in biochar (Palansooriya et al., 2019; Whitman et al., 2015), while the addition of biochar may accelerate the mineralization rate of SOC (positive priming) by (i) stimulated microbial activity from the addition of labile C in biochar, also known as co-metabolic effect (Luo et al., 2011; Singh and Cowie, 2014) and/or (ii) improved soil condition favorably for microbes e.g. changes in soil pH, nutrient availability, and soil moisture regime (Paetsch et al., 2018; Whitman et al., 2015).

Mixed responses of SOC mineralization following biochar additions are common, for example, in a meta-analysis study by Maestrini et al. (2015), a mean increase of 15% in native SOC mineralization (positive priming) after biochar additions to the soil was observed, in contrast with a mean decrease of 3.8% in SOC mineralization with biochar additions (negative priming effect) reported in a meta-analysis study done by Wang et al. (2016). These contrast may be due to the differences in the number of studies included in each meta-analysis and/or the transient nature of priming effect, changing from positive to negative or vice versa which sometimes can only be observed if the study was carried out for a certain duration. Several studies reported that the positive priming effect occurred for more than 1.5 years after biochar addition and shifting towards negative

priming afterward (Ding et al., 2018; Maestrini et al., 2015), whereas other studies found that following biochar addition the priming effect was negative for up to 0.5 years, with no significant priming effect was observed later on (Kerré et al., 2016; Wang et al., 2016).

The changes in the direction and magnitude of SOC priming in soil amended with biochar were not only influenced by study duration but also other experimental conditions such as the setting (whether it was done in the laboratory, glasshouse or the field), the presence/absence of plants, biochar application rate, as well as the varying soil and biochar properties incorporated in each study (Ding et al., 2018; Han et al., 2020; Maestrini et al., 2015; Wang et al., 2016). Compare to field studies, controlled experiments i.e. laboratory incubations and glasshouse pot studies were less representative of realistic field conditions due to the lack of variations in factors affecting biochar-SOC dynamics such as the moisture, temperature, and interactions between biochar, SOC, and plant inputs (Cui et al., 2017; Fang et al., 2017; Paetsch et al., 2018), thus the overall effect of biochar addition on native SOC can be difficult to assess. Weng et al. (2015) highlighted the importance of incorporating plants into the study when assessing the extent of biochar-induced priming of SOC as labile plant inputs and root exudates may cause negative priming of SOC due to the preferential substrate utilization by microorganisms that favor easily degradable plant inputs compare to the more stable SOC (Weng et al., 2015) and also stabilized the SOC through biochar-enhanced organo-mineral interactions (Weng et al., 2017). Plant inputs may also induce co-metabolic decomposition and thus promote the positive priming effect (Dong et al., 2018).

Additionally, the amount of biochar applied was an influencing factor for SOC priming. Based on the meta-analysis by Wang et al. (2016), a low application amount of biochar ≤

1% (w/w) induced significant negative priming on SOC, whereas no significant priming effect was observed with higher biochar application rate (up to 20% w/w). In a 90-day incubation study by Abbruzzini et al. (2017), with a biochar application rate of 0.4 to 1.9% (w/w) they found significant negative priming effect on SOC in biochar-amended soils compared to the soil alone, possibly due to preferential utilization of easily available C source by soil microorganisms. Yet, in another short-term incubation study by Liu et al. (2018) the negative priming effect of biochar was only significant when the application rate was 5% (w/w) with no significant differences when biochar was applied at a lower rate. The low amount of biochar may be insufficient to physically protect the native SOC from mineralization. Conversely, based on a review by (Han et al., 2020), positive priming effect was observed in studies with a biochar addition rate lower than 15% (w/w).

Furthermore, soil properties such as soil textures may affect the SOC mineralization rate as positive priming effect has been observed when biochar was mixed with sandy or coarser soil -possibly due to the greatly improved soil aeration (S. Liu et al., 2016) and increased accessibility of the weakly protected SOC for microbial degradation (Han et al., 2020)-, whereas, negative or no priming effect was found in fine-textured soil. Likewise, biochar properties such as the labile C fraction and ash content that vary with feedstock type and pyrolysis conditions also affect the native SOC decomposition rate following its application (Han et al., 2020). For example, biochar produced at a lower temperature or made from manure, and crop residues would have higher labile C fraction than high temperature, woody-based biochar (Enders et al., 2012; Pariyar et al., 2020), and thus contributed to the increased mineralization of native SOC through the stimulation of microbial activity by the labile C contained within the biochar or temporary negative

priming effect due to preferential substrate utilization of biochar-C instead of the native SOC by soil microorganism (Singh and Cowie, 2014; Yu et al., 2018).

Although most possible factors (and its related mechanisms) affecting biochar-derived priming effect has been identified and investigated, other aspects such as the biochar incorporation technique (Maestrini et al., 2015) and its application depth -which may also affect soil processes and SOC dynamics (Blanco-Canqui, 2017; Verheijen et al., 2010)- is lacking and need to be taken into consideration in evaluating the effect and predictive understanding of biochar addition on native SOC decomposition.

2.3 Near-infrared (NIR) spectroscopy for biochar characterization and soil organic C (SOC) measurement

2.3.1 Near-infrared (NIR) spectroscopy overview

Near–infrared (NIR) spectroscopy technique has been developed for its use in agriculture sector in the last 40 years for determining the composition of agricultural products such as cereals, fruit, vegetables, meat, etc. (Bellon-Maurel and McBratney, 2011; Burns and Ciurczak, 2007; Workman Jr, 2016).`It has also been successfully used to measure soil moisture content (Kuang and Mouazen, 2011; Mouazen et al., 2005a), soil texture (Deiss et al., 2017; Mouazen et al., 2005b), total soil C, organic C, total N (Brunet et al., 2008; Chang and Laird, 2002; Viscarra Rossel et al., 2016; Yang et al., 2012), cation exchange capacity (CEC) (Sudduth and Hummel, 1993; Ulusoy et al., 2016), mineralisable N (Moron and Cozzolino, 2004), potentially mineralisable C (Ludwig et al., 2002; Sarkhot et al., 2011), microbial biomass C and N (Linsler et al., 2017; Ludwig et al., 2002; Zornoza

et al., 2008), root density (Kusumo et al., 2010; Xu et al., 2016), and the composition of organic matter in soil and litter (Kang et al., 2017; Terhoeven-Urselmans et al., 2006).

Near-infrared (NIR) spectroscopy is known as a rapid, cost-effective, non-destructive technique and can be used in both laboratory and on-site (Nocita et al., 2015a). It works based on the interaction of near-infrared radiation with sample constituents, particularly the covalent bonds of small atoms such as O, C, H, and N, abundant in organic matter. The signal reflected from the object (e.g. soil) is based on the vibration of the small atoms, such as C-H, O-H, N-H bonds which produces spectral signatures that are defined by their absorbance or reflectance as a function of wavelength in the electromagnetic spectrum. The near-infrared (NIR) spectral region encompasses wavelengths between 700 nm to 2500 nm, which generally consists of weak overtones and combinations of vibrational bands of atoms (Viscarra Rossel et al., 2006; Williams and Norris, 2001).

The overlapping of overtones and combination bands makes the separation and identification of individual NIR bands difficult. However, the quantitative analysis of samples based on the NIR spectra can be improved using chemometric techniques, such as the performance of a multivariate calibration for the determination of sample constituents. Chemometric can be defined as a discipline within chemistry that deals with statistical and mathematical methods to extract useful information from chemical measurement and relate it to the compound of interest followed by the development of a predictive model (classification or regression) (Williams and Norris, 2001).

2.3.2 NIR spectral pre-processing techniques and the use of multivariate analysis

2.3.2.1 NIR data preprocessing

Generally, analysis of NIR spectra involves pre-processing techniques to remove or minimize unwanted spectral variance (e.g. baseline shift, trend, scattering, noise) and enhance the data. This includes data transformation to reduce nonlinearity such as from reflectance (R) spectra to log (1/R), spectral normalization using the multiplicative scatter correction (MSC) or standard normal variate (SNV) to reduce signal fluctuation caused by light scattering in reflectance measurements from variation in the particle size distribution of the sample, detrending for baseline correction, data smoothing and differentiation using Savitzky–Golay method to reduce random noise and increase the signal-to-noise ratio, also data autoscaling using mean centering and variance scaling (Sun et al., 2009; Varmuza and Filzmoser, 2009; Workman Jr, 2016). NIR spectral pre-processing is followed by the implementation of multivariate analysis to produce qualitative or quantitative models. Two well-known multivariate techniques commonly used for NIR data are the principal component analysis (PCA) and the partial least square regression (PLSR).

2.3.2.2 Principal component analysis (PCA) and partial least square regression (PLSR).

The principal component analysis (PCA) is an exploratory method that reduced the dimension of original data by projecting the original highly correlated x-variables into a smaller set of uncorrelated latent variables called principal components (PCs). Each PC contains explained variance (information) of the data structure. The data plotted in the scatter plot (score plot) is well presented if the total variance retained in a few PCs is high.

Most of the data variability can be explained in the first two principal components; PC1 and PC2 (Miller and Miller, 2010). PCA is usually run before any other multivariate technique to check for outliers or any discernable pattern from sample distributions shown in the scores plot (Esbensen et al., 2002).

Whereas, the PLSR analysis is carried out to build the calibration model by correlating the pre-processed NIR spectral data with the reference data. Briefly, PLSR involves the use of latent variables (also known as components or factors) obtained from X-variables that relate well with the Y-variables (through internal regression), and also best describe the variation of X-variables itself. This transformation of original X variables into latent variables involves maximizing covariance between latent variables (components/factor) and Y variables, i.e. by having maximum explained variance of X-variables and maximum correlation with Y-variables (Varmuza and Filzmoser, 2009; Wold and Eriksson, 2001). The optimum number of components/factors that produce low root mean square error (RMSE) and low Akaike Information Criterion(Viscarra Rossel, 2008) are used to establish the calibration model. Then, the model is validated using leave-one-out-cross-validation (LOO-CV) to check for over-fitting and later validated using the prediction set.

The predictive ability of the model is evaluated based on statistical parameters such as the root mean square error of LOO-CV (RMSECV), root mean square root of prediction (RMSEP), the coefficient determination (R^2) and RPD (ratio of prediction to deviation); RPD is the standard deviation of the reference data divided by the root mean square error (SD/RMSE) (Kusumo et al., 2011). The steps for chemometric analysis of NIR spectra is illustrated as follows:

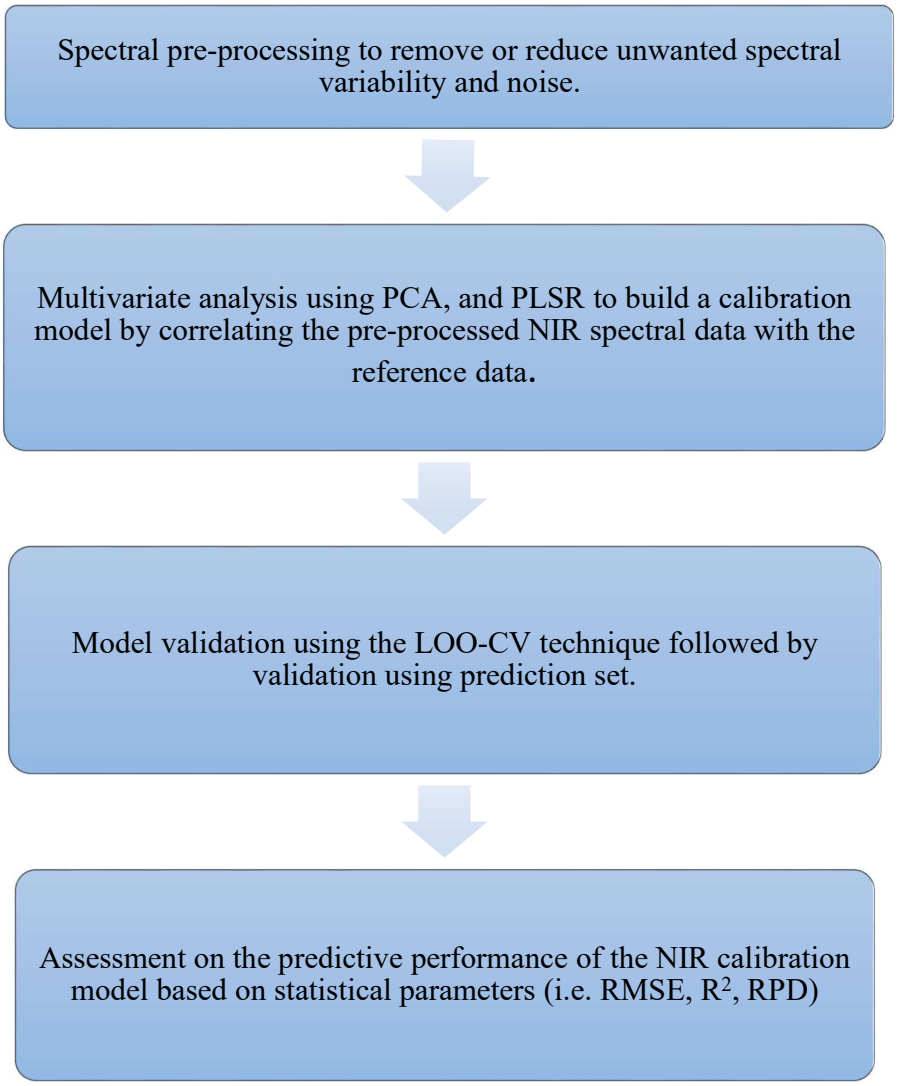

Figure 2-1. Steps for chemometric analysis of NIR spectra

2.3.3 The use of NIR spectroscopy for biochar characterization

To date, only a few studies on the characterization of charred materials, including biochar, using NIR have been done. Reeves et al. (2007) successfully determined some chemical properties (total acids, carboxylic acids, lactones, and phenols) of charred pine wood, bark, cellulose, and lignin. Monteiro et al. (2010) carried out a quality assessment of charcoal and were able to distinguish between charcoal obtained from an industrial process and that obtained in a laboratory furnace. Davrieux et al. (2010) and De Muñiz et

al. (2013) used NIR to distinguish charcoal produced from wood of different tree species. Andrade et al. (2012) estimated the fixed C content, volatile matter content, and gravimetric yield of *Eucalyptus* charcoal produced at different production temperatures; 350°C, 450°C, 550°C, and 900°C.

Whereas, Yang and Sheng (2012) used NIR spectroscopy to estimate ash, volatile matter, fixed C contents, and pyrolysis temperature of biochar made from pine wood, cedarwood, and cotton stalk produced at different pyrolysis temperatures. Kusumo et al. (2014) also used NIR to predict the production temperature of biochar, ash, volatile matter, and other biochar properties such as condensed aromatic C, fixed C, H/C_{org}. In a more recent study, Ramalho et al. (2017), differentiated charcoal produced from wood as coming from either native forest or commercial plantation. They also showed that NIR can be used to discriminate these charcoal according to their production temperatures. Costa et al. (2018) also used NIR spectroscopy to predict final production temperature of charcoal produced from *Eucalyptus* wood at a final temperature of 400 °C, 500 °C, 600 °C, and 700 °C.

NIR spectroscopy has been proven to be a useful technique for estimating the properties of charred material including biochar, however, most reported NIR studies were used on charcoal produced from wood and for the specific industrial purpose (e.g. as an energy source, for barbeques) (Costa et al., 2019), whereas biochar is produced from various types of feedstock at varying temperature range and production conditions which may affect NIR prediction.

2.3.4 Near-infrared (NIR) spectroscopy as an alternative method for SOC estimation.

Biochar application is one of the management practices that has been shown to affect soil organic carbon (SOC) storage (Bai et al., 2019; Ngo et al., 2014). In a recent study by Blanco-Canqui et al. (2020), the negative priming effect of biochar and its potential use as a C sequestration agent has been highlighted, where SOC stocks were increased by twice the amount of C added with the biochar after six years in the field in the Midwestern USA. Currently, the common methods used to measure the organic C concentration and the overall C stocks of the untreated soil (not containing biochar) are also applicable for biochar-amended soils. In general, SOC can be estimated based on the standard and conventional direct measurements or by using the relatively recent spectroscopic methods (Bellon-Maurel and McBratney, 2011; Nayak et al., 2019; Paustian et al., 2019).

2.3.4.1 Direct measurement for SOC determination

Direct measurement of SOC stocks relies on appropriate physical sampling and sample processing, followed by laboratory analysis for SOC concentration determination (Paustian et al., 2019; Smith et al., 2020). However due to the slow rate of SOC changes and the large spatial variability in SOC content, the detection of any measurable changes can be difficult (Nayak et al., 2019). The SOC stocks for a given depth is calculated from bulk density, SOC concentration, and soil depth (FAO, 2019; IPCC, 2006). Therefore, an effective sampling design involving adequate sample size and sampling interval, the correct sampling depth, accurate bulk density, and SOC content measurements is crucial. If the expected change in SOC stocks can be estimated for a given period, the minimum number of samples required can be determined based on the concept of the minimum

detectable difference (MDD) (FAO, 2019; Zar, 2010) with the MDD value should be smaller than the expected change in SOC stocks.

Based on a review comprising of 41 studies by Davis et al. (2017), sampling depth for SOC assessment was found to vary between 10 cm to 100 cm. However, IPCC (2006) recommended SOC measurement to be done in the top 30 cm depth, whereas FAO (2019) suggested deeper soil sampling, although lower depth may be considered depending on the objectives of the study. Soil bulk density is the mass per unit volume of the soil and generally measured using the undisturbed (intact) core method (FAO, 2019). However, soil bulk density is influenced by soil texture and land use causing differences in the amount of soil sampled within a given sampling depth (Ellert and Bettany, 1995), thus, the "equivalent soil mass" approach is recommended when calculating for SOC stocks (Ellert et al., 2007; FAO, 2019; Wendt and Hauser, 2013).

2.3.4.2 Standard laboratory methods for SOC measurement

Common laboratory analyses for SOC measurements include dry combustion in an elemental analyzer, wet oxidation/digestion, and the loss-on-ignition method. Dry combustion technique works based on the combustion of SOC at a high temperature and is the most accurate for measuring the soil C content (Nayak et al., 2019). However, the cost for the initial purchase and maintenance is relatively high, moreover, this technique requires a very small sample mass (a few milligrams), thus it is important to ensure the samples analyzed are representative (FAO, 2019).

Wet oxidation based on the Walkley and Black (1934) procedure is a well-known technique used to determine the organic matter content in the soil. This method assumes that 77% of the organic carbon is oxidized by chromic acid and that soil organic matter

contains 58% C (Schulte and Hoskins, 1995), thus, a correction factor of 1.3 is needed to adjust the result. This technique is relatively rapid and easy, however, unlike the dry combustion method, the recovery rate of this technique may vary and is affected by the differences in soil constituents and the presence of recalcitrant material like charcoal (FAO, 2019; Schulte and Hoskins, 1995). Thus, this technique is also used to determine the chemical oxidative stability of biochar and for the quantification of biochar in the soil (Leng et al., 2019).

Another routinely used method to determine SOC content is the loss-on-ignition (LOI) which is based on the oxidation of soil at a temperature ranging from 360 to 550 °C for two hours or more (FAO, 2019; Schulte and Hoskins, 1995). The SOM content i.e. the difference between the soil mass before and after ignition, will need to be multiplied with 0.58 or individual conversion factor to get the SOC value. This technique is not only simple and cheap but it also allows the use of larger sample mass ≥20 grams. However, similar to the wet oxidation technique, LOI value is affected by soil compositions such as the clay content and the presence of charcoal (Abella and Zimmer, 2007; De Vos et al., 2005).

2.3.4.3 SOC measurement using spectroscopic methods

Spectroscopic techniques such as the visible-near-infrared (Vis-NIR), near-infrared (NIR), or mid-infrared (MIR) spectroscopy, laser-induced breakdown spectroscopy (LIBS), and inelastic neutron scattering (INS), are increasingly applied for SOC measurement as they are relatively rapid, efficient for large sample numbers, cost-effective, and non-destructive than the conventional methods (England and Rossel, 2018; Nayak et al., 2019).

The infrared (Vis-NIR, NIR, or MIR) spectroscopy has been used for over 30 years to investigate soil properties including SOC content (Bellon-Maurel and McBratney, 2011; Nocita et al., 2015a) and thus this technique is more established compared to other spectroscopic techniques (Knadel et al., 2017). Infrared spectroscopy is suitable for soil organic C analysis since absorption bands of organic molecules are detected within these spectral regions (Vis: 350-700 nm; NIR: 780-2500 nm; MIR: 2500-25000 nm) (Williams and Norris, 2001). Generally, the spectrometer used for Vis-NIR and NIR spectroscopy technique is similar, whereas MIR spectroscopy uses a separate spectrometer. In the laboratory setting, MIR spectroscopy can predict the SOC concentration of the oven- or air-dried and finely ground soil sample with higher accuracy than using both Vis-NIR and NIR spectroscopy, however, the latter are superior for in-situ SOC measurement as MIR spectra is more affected by soil moisture variations (Hutengs et al., 2019; Soriano-Disla et al., 2014). Thus, the use of Vis-NIR and NIR spectroscopy were more prevalent due to the minimum sample preparation (Nocita et al., 2015a).

Figure 2-2. Quantitative estimation and validation of soil properties based on spectral libraries. Source: Nocita et al. (2015b).

In a review by England and Rossel (2018), Vis-NIR was promoted as the most suitable cost-effective spectroscopy technique for soil C stock accounting as it can measure soil C concentration in-situ or with minimal preparation. Figure 2-2 shows the prediction step for measuring soil properties using Vis-NIR spectrscopy technique.

However, to date, there were only a few studies attempted to estimate the soil C stock using Vis-NIR spectroscopy, even though soil C stocks represent more important information than soil C concentration. In a study by Roudier et al. (2015), the feasibility of using Vis-NIR for the in-situ measurement of SOC concentration and the subsequent prediction of SOC stocks were reported. Guo et al. (2017), Guo et al. (2019), and (Segnini et al., 2019) also successfully used Vis-NIR and NIR to estimate SOC stock using the

measured SOC concentration. However, they used dried, finely-ground, and sieved soil samples. Based on this study, it shows the potential of integrating the Vis-NIR or NIR spectroscopy in SOC stock estimation study for reducing research time and cost.

The use of Vis-NIR or NIR spectroscopy for measuring SOC in soil-amended biochar is very much lacking. To date, there were only three published studies on the use of NIR spectroscopy on soil-amended with biochar; Reeves et al. (2010) showed that the addition of biochar to soil may affect the NIR spectral signature of the original soil C, while, Allen & Laird (2013) and Uchimiya et al. (2019) showed that NIR spectroscopy can be used to predict the total C of soils amended with biochar. In both studies, soil samples were air-dried and sieved prior to NIR scanning and the range of NIR wavelength used was between 1100 to 2500 nm.

2.4 Research gaps

According to the literature review, current research gaps related to (i) biochar characterization, (ii) the use of biochar to reduce nitrous oxide (N_2O) soil emission, (iii) the use of biochar to increase soil organic C (SOC) stocks while reducing the mineralization of native SOC, and (iv) how the use of near-infrared spectroscopy can be well-suited into a biochar-related study, can be summarised as follows:

i) Based on the vast literature on biochar characterization, biochar characteristics are highly influenced by pyrolysis temperature and feedstock type. Thus, it can be concluded that biochar produced from a certain type of feedstock at a certain pyrolysis temperature is expected to have particular characteristics, and by knowing this information (pyrolysis temperature and feedstock type) it would be sufficient to predict its suitability for potential purposes. For example, it is preferable to apply wood-based biochar produced at a high pyrolysis temperature for soil C sequestration due to its high C content (Woolf et al., 2018a). However, due to lack of standardization in biochar production, the reported temperature can only be verified indirectly i.e. by measuring the C content (and the H/C_{org} ratio) using laboratory techniques and comparing the values with the literature. Therefore, there is a need for a relatively cheaper and rapid alternative method to verify the reported pyrolysis temperature, for instance, by using the NIR spectroscopy technique.

ii) Although the use of biochar as soil amendments has been suggested as a potential tool to reduce the N_2O emission from the soil, there have been mixed results. Based on the literature, there are two parameters in biochar studies; the particle size of

biochar and placement depth, which may potentially affect soil N_2O emission, but have been generally overlooked and are still not well studied.

iii) Mixed responses of SOC mineralization following biochar additions are common and extensive literature has been devoted to understanding the effect of biochar application to SOC stocks and the involving mechanisms. Yet, studies focusing on the effect of biochar incorporation technique which determines the placement of biochar in soil, and the use of biochar with different particle sizes are lacking.

iv) The determination of SOC using direct measurement requires extensive and laborious sampling and laboratory analyses. The NIR spectroscopy technique has been promoted as a suitable tool for SOC concentration measurement and SOC stock estimation. Yet, it's usages on soil-amended with biochar is extremely limited.

CHAPTER 3. NEAR-INFRARED SPECTROSCOPY (NIRS) FOR PREDICTING THE MAXIMUM PYROLYSIS TEMPERATURE OF BIOCHAR

Abstract

Biochar produced by pyrolyzing feedstock at temperatures 350 °C or above has atomic H/C_{org} ratio of 0.7 or less and has low degradability in soils and suitable for carbon sequestration. This study investigates whether the near-infrared reflectance spectra (NIRS) of biochar can be used to reliably predict the maximum pyrolysis temperature achieved during biochar production as a method of selecting more stable biochar. A calibration model was developed using partial least squares regression (PLSR) of NIR spectral data (780-2450 nm), acquired from 82 carbonized materials produced from different types of feedstock and ranges of maximum pyrolysis temperatures (220 °C to 800 °C). The calibration model was validated using (i) leave-one-out cross-validation (LOO-CV) and (ii) a prediction set, yielded good accuracy (R^2 = 0.82) with root mean square error (RMSE) of 48.8 °C and 57.7 °C, respectively. These results indicate that NIRS has the potential to be used as a monitoring and quality control tool for biochar production.

Keywords

Near-infrared spectroscopy; NIR; Biochar; Pyrolysis temperature; Partial least squares regression (PLSR)

3.1 Introduction

According to International Biochar Initiative (2015) and European Biochar Certificate (2016), a charred material is considered as biochar if its atomic H/C_{org} ratio is 0.7 or less, which is commonly achieved by pyrolyzing feedstock at the highest heating temperature (HHT) of 350 °C or above. Generally, the HHT of the pyrolysis process through which biochar is produced ranges from 350 to 1000 °C, and has a strong influence on biochar C content, surface area, and degree of aromatic C condensation (Keiluweit et al., 2010; Weber and Quicker, 2018). These properties, in turn, have a strong influence on biochar degradability, with those produced at a higher temperature having higher persistence (Singh et al., 2012; Wang et al., 2016).

Temperature gradients are common inside the kiln (between and within feedstock particles) due to the non-uniform heat transfer, especially as the feedstock particle size and/or that of the reactor increases (Van de Velden et al., 2010). Temperature gradients may cause the condensation of volatile pyrolysis products onto/within the biochar particles. If not re-pyrolyzed, these volatiles can sometimes have toxic effects on soil biota and plants (Buss and Mašek, 2014), although beneficial effects have also been reported (Graber et al., 2010; Joseph et al., 2013). Some may include PAH (polycyclic aromatic hydrocarbons) compounds, although these have only been found to be in considerable amounts in biochar when produced in poorly controlled pyrolysis conditions (Hale et al., 2012) and their eco-toxicological risk to the soil environment is unlikely (Cornelissen and Hale, 2017). If re-pyrolyzed, the resultant products (e.g., coke) may have negative effects on the macroscopic structure of the biochar by blocking pores (Liaw and Wu, 2015). Another major challenge faced by biochar producers is the exothermic nature of pyrolysis

reactions, which makes the control of pyrolysis temperature below 400 °C difficult (Ripberger et al., 2015). This raises the need for a "market" quality control tool able to predict the maximum temperature at which the biochar has been produced. Besides, it could be used as a quality tool during biochar manufacturing as the practice of installing multiple thermocouples at different positions inside the kiln for monitoring the pyrolysis temperature (Li et al., 1999; Park et al., 2010) or by placing additional thermocouples within the samples are practically difficult (Aguiar et al., 2008; Di Blasi et al., 2013).

Attempts have been made to determine the HHT at which carbonized materials have been produced using Raman spectroscopy technique, specifically by establishing correlations between the changes observed in characteristic bands with the increasing HHT of known samples (McDonald-Wharry et al., 2013; Yamauchi and Kurimoto, 2003). However, several shortcomings of this method include (i) the requirement of a suitable laser power setting on a sample-to-sample basis to acquire a high quality of signals, (ii) the fact that an excess of energy from the laser radiation may burn the sample, thus requiring additional preliminary testing to choose appropriate settings before routine analysis, and (iii) the high maintenance costs of the instrument (e.g., the annual cost of laser replacement) (Jestel, 2010; Smith and Dent, 2019). Schneider et al. (2010) determined the aromaticity of benzene polycarboxylic acid (BPCA) content of biochars with increasing HHT of carbonized materials. This technique may potentially be used to predict HHT (Schmidt et al., 2017); however, this method requires multiple analytical steps and is very time-consuming.

Near-infrared spectroscopy (NIRS) has not yet been thoroughly tested for such purpose, but it has already been proven to be valuable in industrial quality control and assessment,

especially in the agriculture sector. Among others, NIRS has been used by USDA (United States Department of Agriculture) as a standard method for the determination of protein content in grains, and also by the AOAC (Association of Official Analytical Chemists) to assess the quality of animal feed and forages (Kawano, 2008). To date, NIRS has been proven to be a suitable technique to predict specific biochar properties which are affected by thermal degradation, such as indices of biochar C persistence (condensed aromatic C, fixed C, H/C_{org}) (Kusumo et al., 2014), and other biochar properties (e.g., ash, volatile matter) (Andrade et al., 2012; Yang and Sheng, 2012). Therefore, the suitability of using NIRS to also predict the production temperature of biochar is expected as reported by Yang and Sheng (2012) and Kusumo et al. (2014), that found a 69 and 88% accuracy, respectively, in the prediction of pyrolysis temperature for their biochar samples using NIR data coupled with principal components—linear discriminant analysis (PC-LDA). The relatively moderate predictive accuracy was attributed to the small number of samples used (Yang and Sheng, 2012) and possibly due to the poor control of the production temperature including the existence of variable temperature gradients within the pyrolyzer (Kusumo et al., 2014), however, no detailed explanation was given.

To our knowledge, other than the studies done by Yang and Sheng (2012) and Kusumo et al. (2014), no other study has been done using NIRS to predict the HHT at which biochar has been produced. This paper aims to evaluate whether NIRS combined with PLSR analysis can be reliably used to predict the HHT at which biochar was produced so that this can be used as a tool for quality control in biochar manufacture and C sequestration value.

3.2 Materials and methods

3.2.1 Samples

Eighty-two carbonized materials were used as the original calibration set. These samples were previously studied by Enders et al. (2012) and Whitman et al. (2013) (details are provided in Table S3-1) and received in powder form for this study. They were produced from animal manures (bull manure, dairy manure, composted dairy manure, digested dairy manure, poultry manure), crop residues (corn, mixed plant residues, rice husk, soybean, switchgrass), nutshells (hazelnuts, peanut), mixed waste (food, paper, mixtures), woody materials (pine shavings, oak shavings, mixed hardwood chips, mixed softwood chips, mixed woodchips), and yard waste (brush, grass clippings, leaves). A large number of these carbonized materials (n=68) were produced by the same commercial company (Best Energies, Inc., Cashton, WI, USA) through slow pyrolysis using a Daisy Reactor pyrolyzer unit, while the rest of them (n=14) were produced using other production techniques (ablative updraft pyrolysis, fast pyrolysis, intermediate pyrolysis, fixed bed gasification, torrefaction, and updraft pyrolysis). The pyrolysis temperatures used ranged from 220 °C to 800 °C.

An additional set of 20 carbonized samples (Table S3-2) were gathered from another study and used as the prediction set. This prediction set consists of carbonaceous samples made from a single type of feedstock (pine wood) and was produced using slow pyrolysis technique in a 5 L gas-fired rotating drum kiln at varying HHT ranged from 325 to 723 °C (Ripberger et al., 2015). These samples had three different sizes: small (15 mm x 15 mm x 17.5 mm; n=2); medium (32 mm x 32 mm x 17.5 mm; n=7) and large (67 mm x 67 mm x 17.5 mm; n=11).

Out of the total 102 samples used in calibration and prediction sets, 82 samples complied with an atomic H/C_{org} ratio of 0.7 or lower (Table 3-1), as established by the International Biochar Initiative, (2015) and European Biochar Certificate (2016) as the threshold value for a charred material to be considered biochar, while 20 samples had an H/C_{org} ratio higher than 0.7. There were 17 samples for which only the H/C ratio was available (Tables S3-1 and S3-2). Despite this variability, in this document, all the samples will be referred to as biochar. The samples were ground to a particle size less than 100 μm to achieve homogenous fine powder before spectral acquisition.

Table 3-1. Number of samples grouped according to feedstock and highest heating temperature (HHT)

		Feedstock groups						
		Animal manure	Crop residues	Nutshells	Mixed wastes (food, paper, mixture)	Woody materials	Yard wastes	Total samples in each temperature group
HHT	X<300 °C	0	0	0	2+0	0	0	2 (0)
	300 ≥ X > 400 °C	7(1)+0	2(1)+0	2(2)+0	2(1)+0	4(2)+4(3)	0	21 (11)
	400 ≥ X > 500 °C	8(8)+0	2(2)+0	2(2)+0	2(1)+0	3(3)+4 (4)	0	21 (18)
	500 ≥ X > 600 °C	10(10)+0	7(6)+0	3(3)+0	2(1)+0	8(7)+6 (6)	3(2)+0	38 (28)
	X ≥600 °C	5(4)+0	2(1)+0	1(1)+0	2(2)+0	3(3)+6 (6)	0	19 (16)
	Total samples in each feedstock group	30 (23)	13(10)	8(8)	10(5)	38(34)	3(2)	102 (82)

* n_1(n)+(n_2) with n_1 is the number of biochar from Enders, et al., (2012) and n_2 is the number of biochar from Ripberger et al., 2015, while (n) is the number of true biochar with H/C_{org} ≤0.7 within specific HHT and feedstock groups.

3.2.2 Spectral acquisition and pre-processing

A soil contact probe attached by fiber optic cable to the spectrometer (ASD FieldSpec 3 V-NIR Spectrometer, Analytical Spectral Device, Boulder, CO) was used to collect the UV-Visible NIR spectral reflectance. The spectrometer provides spectra from 350 nm to 2500 nm with 1 nm resolution. One spectrum recorded per sample was the average of 30 spectra acquisitions. Indico Pro (Ver. 6.0) was used to correct the splice in the spectrum and all the data collected were saved in an ASCII text file.

A chemometric analysis software-ParLeS (Viscarra Rossel, 2008) was used to pre-process the spectral data as follows: data were transformed from reflectance (R) to log (1/R) and were pre-processed using wavelet detrending (with 0.2 and 5, trend and decomposition level, respectively). A Savitzky–Golay filter with a third-order polynomial algorithm and

a window size of 15 nm was used to reduce the noise. The smoothed data were thereafter processed into the first derivative, and then finally treated using mean centering (Savitzky and Golay, 1964).

3.2.3 Brief description of data analysis

3.2.3.1 Principal component analysis (PCA)

A principal component analysis (PCA) was run prior to any other multivariate technique using the pre-processed NIRS data to check for outliers or any discernable pattern from sample distributions shown in the scores plot (Esbensen et al., 2002). The most representative wavelengths were identified from the loading plot as proposed by Kamruzzaman et al., (2011).

3.2.3.2 Partial least square regression (PLSR)

Following the PCA analysis, partial least square regression (PLSR) was carried out to build the calibration model using the 82 samples of Enders et al. (2012) by correlating the pre-processed NIR spectral data with the reference data i.e. HHT. The optimum number of factors that produce low root mean square error (RMSE) and low Akaike Information Criterion (Viscarra Rossel et al., 2006) were used in the calibration model. The model was first validated using leave-one-out-cross-validation (LOO-CV) to check for over-fitting and later validated using the prediction set (n=20). The accuracy of the established model was determined based on the root mean square error of LOO-CV (RMSECV), root mean square root of prediction (RMSEP), the coefficient determination (R^2) and RPD (ratio of prediction to deviation); RPD is the standard deviation of the reference data divided by the root mean square error (SD/RMSE) (Kusumo et al., 2011). Minitab 16 (Minitab Inc., State College, Pennsylvania) was used for PCA.

Only pre-processed NIR spectral data at selected wavelength ranges of 780-2450 nm were used rather than the full recorded bands of 350-2500 nm to obtain optimal calibration and greater accuracy in prediction as proposed by Kusumo et al., (2014). The steps in data analysis are presented in Figure 3-1.

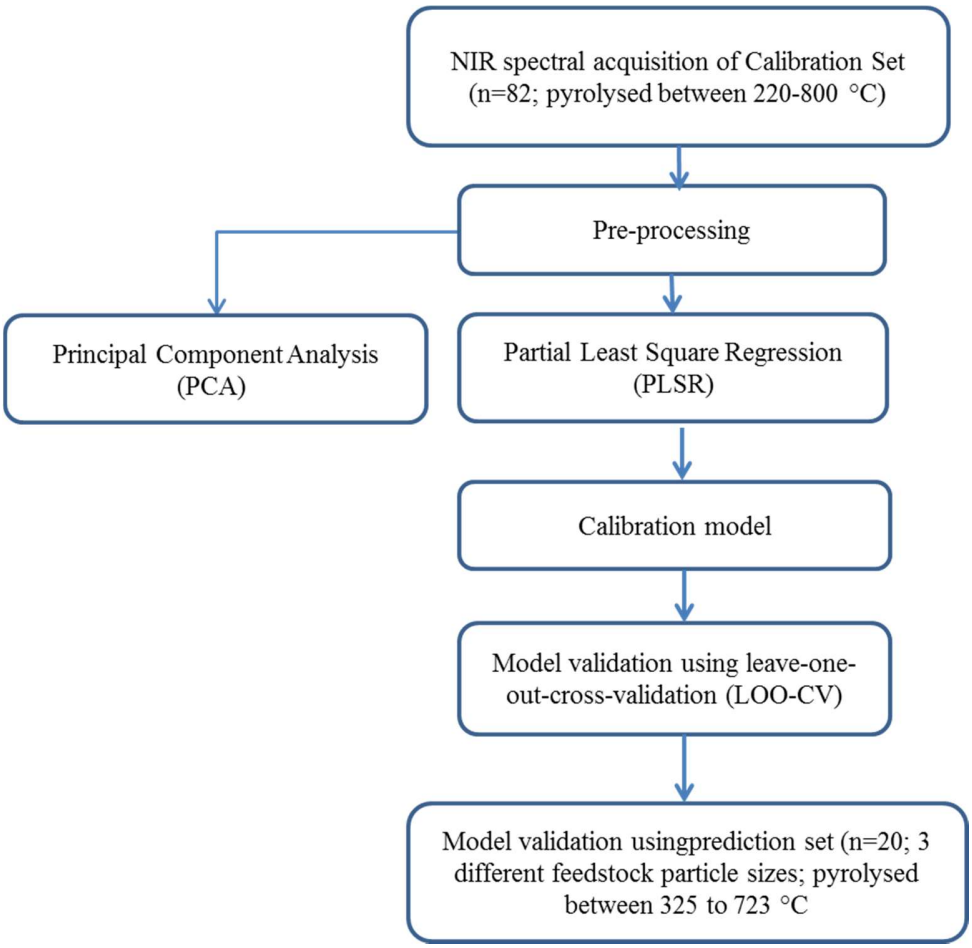

Figure 3-1. Proposed methods and model optimization for predicting maximum pyrolysis temperature of biochar using PLSR.

3.3 Results

3.3.1 Spectral absorbance of biochar

The averaged spectral absorbance of biochar samples based on pyrolysis temperature, as depicted in Figure 3-2, shows that biochars produced at pyrolysis temperature ≤400 °C

had some recognizable peaks and lower absorbances than the biochars produced at temperatures > 400 °C, which showed flat spectra. The 1325-1390 nm bands can be assigned to the C-H stretching vibration in the first overtone and the 1550- 1700 nm can be assigned to the aromatic groups from lignin. The peak at 1940 nm, which was detected in the absorbance spectra of biochars pyrolyzed at temperatures ≤ 400 °C, is attributed to the presence of moisture, while the 2155-2225 nm and 2287-2447 nm bands could be assigned to the O-H, C-O, C-H stretch, aromatic skeletal, and alkyl groups (Schwanninger et al., 2011; Workman Jr and Weyer, 2012).

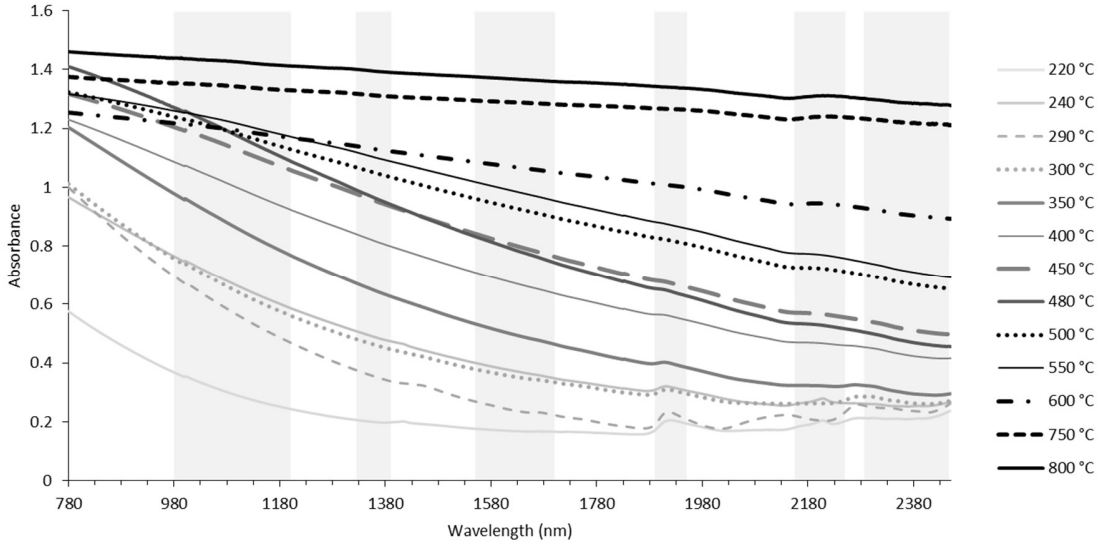

Figure 3-2. Averaged spectral absorbance of biochar samples (n=82) grouped based on pyrolysis temperature; absorbance = log (1/reflectance). Shaded areas represent band regions associated with sample variations.

3.3.2 Principal Component Analysis (PCA)

Seven principal components represent almost 91% of the total variation in NIRS data obtained from all 82 samples, with PC 1 and PC 2 accounting for 64% and 9%, respectively (Figure 3-3). Clear trends or clusters could be seen from the PCA scores plot

based on the HHT of the biochar under study. Poorly carbonized material produced in at HHT ≤ 350 °C plotted all in Quadrants I and IV, except for one sample (biochar produced from oak shavings at 300 °C). At higher HHT, samples tended to plot towards the left, mostly in Quadrants II and III, with biochar produced at HHT ≥ 600 all plotting in Quadrant III.

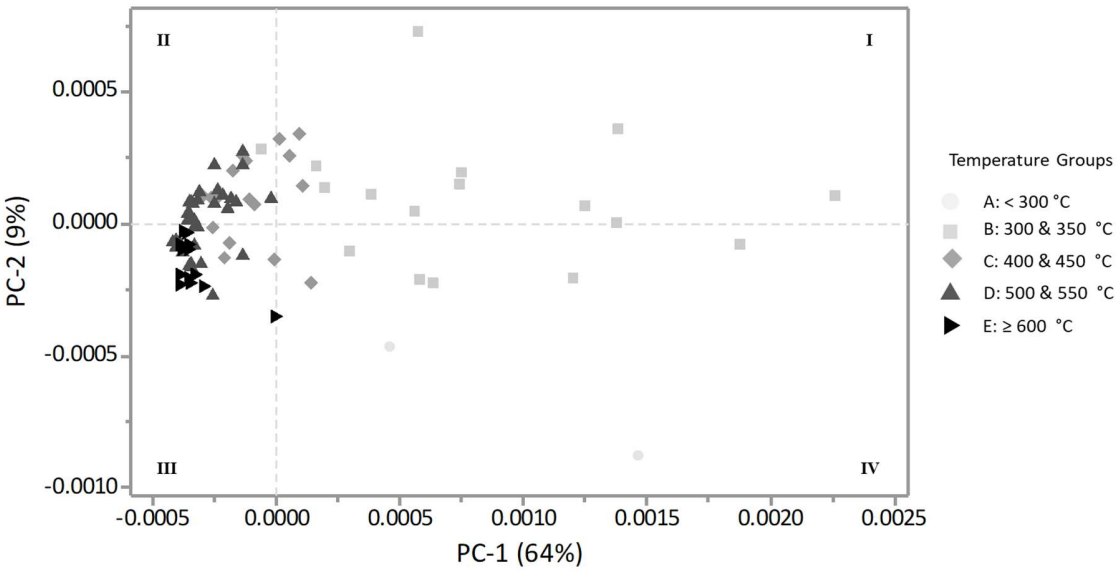

Figure 3-3. PCA scores plot of biochar samples in the calibration set (n=82) according to temperature groups**.**

3.3.3 Partial Least Square Regression (PLSR) for predicting maximum pyrolysis temperature

Based on the LOO-CV technique, the calibration model obtained using the pre-processed NIR spectral data at wavelengths ranging between 780 to 2450 nm had a good ability (r^2 = 0.8) to predict the HHT at which biochars were produced, with the RMSE values of cross-validation being below 50 °C and the RPD values higher than 2 (Table 3-2, Figure 3-4a). Models with RPD values > 2 are considered to be good models and may be

sufficient for quantitative prediction depending on the intended application of the model (Chang et al., 2001; Dunn et al., 2002; Viscarra Rossel et al., 2006). In addition to LOO-CV, the calibration models were also validated using the prediction set (n=20). The validation model explained 82% of the variation in HHT (Figure 3-4b) with an RMSE value of prediction of 58 °C and an RPD value higher than 2.

Table 3-2. Validation of calibration models using LOO-CV technique and prediction set

No. of samples	Band region used (nm)	No. of Factors for PLSR model	Leave-one-out -cross-validation			Validation using prediction set (n=20)		
			R^2	RMSECV	RPD	R^2	RMSEP	RPD
82	780-2450	6	0.803	48.78 °C	2.26	0.824	57.68 °C	2.39

*RMSECV: root mean square error of leave-one-out-cross-validation; RMSEP: root mean square error of prediction; RPD: the ratio of prediction to deviation.

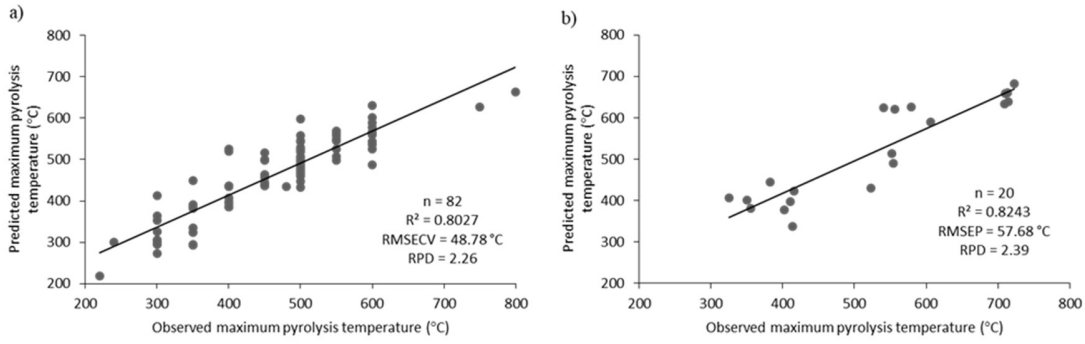

Figure 3-4. PLSR plot of the observed versus predicted maximum pyrolysis temperature using leave-one-out-cross-validated calibration model (a) and validation using prediction set (b).

3.4 Discussion

The averaged reflectance spectra of biochar samples produced at 50 °C increments of HHT (220-800 °C) were distinguishable from each other (Figure 3-2). The mean absorbance increased with HHT providing early evidence that the NIRS technique was capable of distinguishing biochars based on their HHT of production, even at relatively small temperature differences. The higher absorbance at higher HHT resulted from chemical changes within the charcoal structure and the darkness intensification that occurs at increasing HHT (Nassau, 2001). Reflectance in the 780-1400 nm bands is also useful to explain the variability that is caused by the physical properties of samples, i.e., the color and the particle size of scanned samples (Schwanninger et al., 2011). Although here the latter does not apply as all samples were ground into a homogenous fine powder to avoid the spectral baseline shifts that may happen by scanning an unground sample of varying particle size (Williams and Norris, 1987).

The PCA analysis that was carried out using pre-processed NIR spectral data of all 82 samples further provided a general idea of the overall distribution of the samples, showing that biochar samples having similar properties clustered together. The fact that a gradient in the distribution of samples based on HHT was distinguishable (Figure 3-3) further indicated that PLSR would be capable of developing a calibration model to predict the HHT of biochar samples.

Despite the fact that the biochar used in the model were produced from different types of feedstock and particle sizes, and, in some instances, from different pyrolysis kilns, the model was able to predict the HHT of the biochar when performing the LOO-CV with RMSE of 48.8 °C. It should be noted that part of the variability could be due to the

occurrence of uneven heating and temperature gradients during biochar manufacture (Hasan et al., 2017; Park et al., 2010), which supports previous findings reported by Kusumo et al., (2014) and may explain why a sample produced at 300 °C has plotted along with those pyrolyzed at higher temperatures. Although the uneven heating between and within feedstock particles may be minimized by reducing the particle size and improving control on the heat transfer inside the kiln (Atreya et al., 2017; Kan et al., 2016a), it is a common practice for the particle sizes of feedstocks to range between 0.5 and 50 mm or even larger depending on the type of pyrolysis method used (Demirbas and Arin, 2002). Based on studies of heat transfer in the production of charred materials (including biochar), other than the thermal lag that usually exists between the samples and the thermocouple temperature (Stenseng et al., 2001; White et al., 2011), the occurrence of exothermic reactions could also cause the temperature in hot spots in the kiln to rise to 50 °C or higher than the temperature setpoint depending on the production conditions (Di Blasi et al., 2014; Park et al., 2010). Thus, temperature measurement discrepancies in biochar manufacture seem inevitable and the temperature assigned for each biochar can only be considered as a proxy. One hypothesis is that the prediction model may well predict the true HHT that occurred during pyrolysis of the biochar sample provided but the true HHT was unable to be recorded accurately in the larger charge size in the kiln. This hypothesis further supported when the calibration model was tested using the prediction set (n=20), which rendered a slightly larger RMSE (57.7 °C) than the one obtained by LOO-CV. Samples in the prediction set were produced from pine wood chips that had a relatively wide range of feedstock particle sizes (from 15 to 67 mm) and the differences between small, medium and large samples was evident thus the effect of

uneven heating due to different particle sizes were expected to be amplified. Yet, the model still gave a good prediction, highlighting the flexibility of the model. The fact that the validation of the model using LOO-CV and prediction set yielded a relatively low and similar RMSE; 50-60 °C, is remarkable.

The ease of sample scanning and data collection using the NIRS technique provides an opportunity for this calibration data set to be enlarged and the model to be continually improved over time by increasing the sample collections to be incorporated into the calibration set to cater the variability that exists from different operating conditions.

3.5 Conclusion

A calibration model developed using PLSR based on the NIR spectral data (780-2450 nm) successfully predicted the maximum pyrolysis temperature at which the biochar samples were produced. Based on the high prediction accuracy established by the model using leave-one-out-cross-validation (LOO-CV) and a prediction set, this NIR model may be considered as a suitable alternative for non-destructive screening and quality control of biochar production.

CHAPTER 4. NEAR-INFRARED SPECTROSCOPY (NIRS) FOR PREDICTING THE MAXIMUM PYROLYSIS TEMPERATURE OF BIOCHAR: THE EFFECT OF FEEDSTOCK TYPES AND PYROLYSIS CONDITION

The study in this chapter was conducted to expand the findings in Chapter 3, where it was found that the near-infrared (NIR) spectroscopy technique can be used to predict the highest heating temperature (HHT) achieved during biochar production. However, the effect of feedstock types and pyrolysis conditions, as sources of data variability, may affect the performance of NIR model and this was evaluated in this chapter.

Abstract

Different feedstock types and pyrolysis techniques are used for biochar production and it is well-accepted that biochar properties are not only dependent on the maximum pyrolysis temperature but also the type of feedstock and pyrolysis process used. This study investigates whether variation in feedstock type and/or pyrolysis processes affect the predictive performance of near-infrared (NIR) model to predict the maximum pyrolysis temperature of biochar. Three calibration models were developed using partial least squares regression (PLSR) of the NIR spectral data (780-2450 nm) acquired from three sample sets. These sample sets were generated from a total of 82 carbonized materials and its subsets (Set A: n=82; Set B: n=68; Set C: n= 48). The selection of sample for Set B and C was made by reducing the variability associated with production conditions and feedstock type i.e. Set B consist of samples produced by slow pyrolysis and using the same pyrolyzer unit, while Set C (a subset of Set B) excluded samples produced from "processed feedstocks". These calibration models were validated using (i) leave-one-out cross-validation (LOO-CV) and (ii) a prediction set, with the model based on set C gave the best prediction (R^2: 0.941; RMSEP: 27.3 °C), followed by the model based on set A (R^2: 0.896; RMSEP: 35.6 °C), and set B (R^2: 0.928; RMSEP: 37.3 °C). These results indicate that feedstock types have a substantial effect on the performance of the NIR model while the effect of pyrolysis conditions was less pronounced.

Keywords

Near-infrared spectroscopy; NIR; Biochar; Pyrolysis temperature; Feedstock; Partial least squares regression (PLSR)

4.1 Introduction

Currently, a wide range of feedstocks has been used to manufacture biochar, varying from woody materials, agricultural residues, animal and human waste, as well as industrial waste (Tripathi et al., 2016). Pyrolysis plants for biochar production can vary widely as well, with the main types being slow pyrolysis, intermediate pyrolysis, fast pyrolysis, flash pyrolysis, and gasification, which vary depending on the different ranges of temperature, heating rates, vapor residence time, and reactor configurations (e.g., ablative, auger, fixed bed, fluidized bed, heated kiln, rotating cone, and vacuum pyrolyzers) (Kan et al., 2016b). It has been generally accepted that the properties of resulting biochars (e.g., condensed aromatic C, fixed C, H/C_{org}, ash, and volatile matter contents) are dependent on the maximum pyrolysis temperature (referred to as highest heating temperature; HHT), and also the type of feedstock and pyrolysis process used (Antal and Grønli, 2003; Harsh et al., 2016). Although all these variations provide the opportunity to produce tailor-made biochars optimized for particular needs (Ronsse et al., 2013), they also create additional challenges in the biochar production, specifically in regulating the heat generated inside the pyrolyzer and thus achieving the desired product at a specific HHT. The chemical composition of each feedstock determines the type of reactions leading towards thermal degradation (Gani and Naruse, 2007), including the occurrence of exothermic reactions able to cause sudden temperature spikes during pyrolysis (Di Blasi, 2008; White et al., 2011). Di Blasi et al. (2014) compared the thermal behavior of different types of feedstock (agriculture residues vs. woods) and found higher temperature overshoots with respect to the fixed heating temperature for agricultural residues relative to woods (up to a factor of 2 to 4). These were attributed to the specific chemical composition and high ash content

of the former. The feedstock particle size, along with the wide range of operating conditions and their technical limitations also influence the heat transfer inside the pyrolyser thus affecting the thermal decomposition of feedstock (Jahirul et al., 2012) and cause deviations from the intended HHT. Given that the actual maximum temperature experienced by the feedstock is difficult to know, the biochar manufacturer generally provides information on the HHT – usually measured and monitored using thermocouples–.

The potential use of NIR spectroscopy as a tool to estimate the maximum pyrolysis temperature of biochar has been discussed in the previous chapter and the ability of NIR model to give good prediction despite the possible existence of temperature gradients attributed to the use of feedstock with different particle sizes, was highlighted. However, the effect of different feedstock types and pyrolysis conditions on the predictive ability of NIR models are yet to be evaluated. We hypothesized that the NIR model predictive ability is affected by variation in feedstock type and/or pyrolysis processes and the NIR calibration model's performance can be further improved by refining sample selection for calibration set.

Therefore, the objective of our research was to examine how feedstock types and pyrolysis conditions affect the efficiency of NIR model to predict the HHT of biochar and to identify whether the NIR calibration model's performance can be further improved from reducing sample variations i.e., by choosing selectively the samples to be included in the calibration set.

4.2 Materials and methods

4.2.1 Samples

Eighty-two carbonized samples were used as the original calibration set and details of the samples were previously described in Chapter 3. Briefly, these samples were previously studied by Enders et al. (2012) and Whitman et al. (2013). They were produced from animal manures, crop residues, nutshells, mixed waste (food, paper, or mixtures of crushed brick and cement kiln residues), woody materials, and yard waste. Sixty-eight carbonized materials (n=68) was produced through slow pyrolysis (Best Energies, Inc., Cashton, WI, USA), while the rest of them (n=14) were produced using other production techniques (ablative updraft pyrolysis, fast pyrolysis, intermediate pyrolysis, fixed bed gasification, torrefaction, and updraft pyrolysis). The pyrolysis temperatures used ranged from 220 °C to 800 °C.

An additional set of 18 carbonized samples (Table S4-1) were gathered from other studies and used as the prediction set. They were produced from animal manure (including mixtures of eucalyptus wood chips with either biosolids or cattle manure), crop residue (corn stover), and woody materials (pine, poplar, and willow woodchips). The pyrolysis temperatures used ranged from 250 °C to 550 °C (Calvelo Pereira et al., 2011a; Gregory et al., 2014; Herath et al., 2013; Shen et al., 2016; Wang et al., 2012b). All the feedstocks used had particle size ranging between 3 to 50 mm and were dried overnight at 65 °C before pyrolyzed in small batches (~200 g) using slow pyrolysis technique, under relatively high production controlled conditions (Calvelo Pereira et al., 2011).

Out of the total 100 samples used in calibration and prediction sets, 75 samples complied with the molar H/C_{org} ratio of 0.7 or lower (Table 4-1), as established by the International

Biochar Initiative, (2012) and European Biochar Certificate (2012) as the threshold value for a charred material to be considered biochar, while 25 samples had H/C_{org} ratio higher than 0.7. There were 17 samples for which only the H/C ratio was available (Table S4-1). Despite this, all the samples will be referred to as biochars in this document to facilitate its flow. The samples were ground to a particle size less than 100 μm to achieve homogenous fine powder before spectral acquisition.

Table 4-1. Number of samples grouped according to feedstock and HHT

		Feedstock groups						
		Animal manure	Crop residues	Nutshells	Mixed wastes (food, paper, mixture)	Woody materials	Yard wastes	Total samples in each temperature group
HHT	<300 °C	0+2	0	0	2+0	0+1	0	5 (0)
	300&350 °C	7(1)+2	2(1)+1(1)	2(2)+0	2(1)+0	4(2)+0	0	20 (8)
	400&450 °C	8(8)+2(2)	2(2)+0	2(2)+0	2(1)+0	3(3)+3(2)	0	22 (20)
	500&550 °C	10(10)+1(1)	7(6)+1(1)	3(3)+0	2(1)+0	8(7)+5(5)	3(2)+0	40 (36)
	≥600 °C	5(4)+0	2(1)+0	1(1)+0	2(2)+0	3(3)+0	0	13 (11)
	Total samples in each feedstock group	37 (26)	15(12)	8(8)	10(5)	27(22)	3(2)	100(75)

* $n_1(n)+(n_2)$ with n_1 is the number of biochar from Enders, et al., (2012) and n_2 is the number of biochar from other researchers, while (n) is the number of true biochar with $H/C_{org} \leq 0.7$ within specific feedstock and HHT groups.

4.2.2 Spectral acquisition and pre-processing

The UV-Visible NIR spectral reflectance of the sample was collected using a spectrometer (ASD FieldSpec 3 V-NIR Spectrometer, Analytical Spectral Device, Boulder, CO). The spectrometer provides spectra from 350 nm to 2500 nm with 1 nm resolution. One spectrum recorded per sample was the average of 30 spectra acquisitions. The splice in

the spectrum was corrected using Indico Pro (Ver. 6.0) and all the data were saved as an ASCII text file. The pre-processing and data treatment of the spectral were done according to steps in Chapter 3 using ParLeS (Viscarra Rossel, 2008).

4.2.3 Brief description of data analysis and samples selection for calibration and prediction sets

In this study, principal component analysis (PCA), followed by partial least square regression (PLSR), were carried out to correlate the pre-processed NIR spectral data (780-2450 nm) with the reference data (HHT). Details on the PCA and the use of PLSR for the generation of the calibration model have been described in Chapter 3.

Initially, a PLSR calibration model was built using the 82 samples of Enders et al. (2012) (set A) by correlating the pre-processed NIR spectral data (780-2450 nm) with the HHT (as described in Chapter 3). Next, a subset of these 82 samples was selected (set B; n=68) – these were all produced by slow pyrolysis and using the same pyrolyzer unit – in order to determine whether the prediction ability could be improved by reducing the variability of production conditions. Later, a subset from set B (set C; n=48) was compiled to produce a more refined calibration model and to decrease the variability associated with feedstock type by further reducing the sample size by eliminating those biochar produced from "processed feedstocks" i.e. the type of feedstock that has been chemically or biologically treated thus the original composition of feedstock were changed such as food and paper, including the type of feedstock that can be classified as a new type through substantial material changes after certain pretreatment such as the digested manure (International Biochar Initiative, 2012). Set C included thermosequences of biochar (from 300 to 600°C) produced from the following feedstocks only: bull manure, corn, dairy manure, hazelnut,

oak, pine, and poultry manure. Finally, an independent set of 18 biochar was used as the prediction set. The steps on sample selection and data analysis are presented in Figure 4.1.

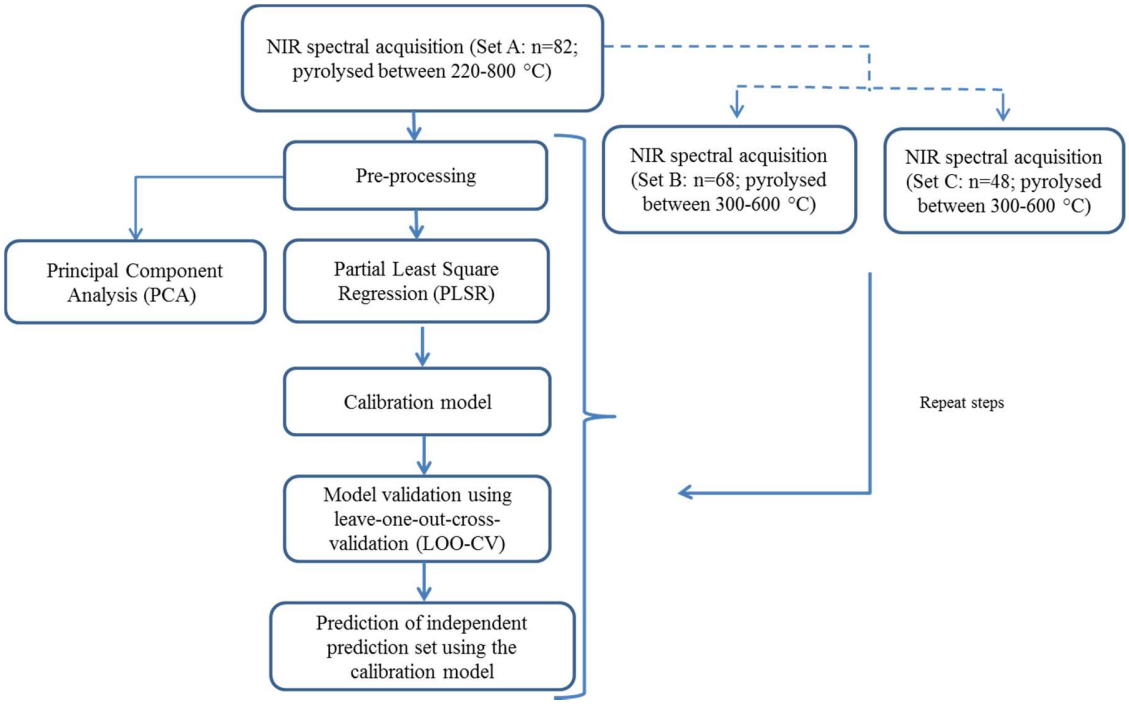

Figure 4-1. Proposed methods and model optimization for predicting maximum pyrolysis temperature of biochar using PLSR. Set A: all 82 samples; Set B: 68 from 82 samples produced using slow pyrolysis using the same pyrolyzer unit; Set C: 48 from 82 samples produced in thermosequence (from 300 to 600 °C) using only 7 types of feedstock.

4.3 Results

4.3.1 Spectral absorbance of biochar

Based on the spectral absorbance of the selected biochar samples shown in Figure 4-2, biochar produced at pyrolysis temperature > 400 °C have generally flat spectra (or smaller peaks). This is associated with the fact that biomass components have been thermally degraded (De Muñiz et al., 2013) and the higher absorbance of high-temperature biochars due to their blackness as the degree of carbonization increases (Lestander et al., 2014). The sensitivity of NIR towards the color of the samples is made evident in the spectra of

biochar samples produced from paper sludge as these have lower absorbance due to its lighter color, emphasizing the effect of feedstock type in this study. Interestingly, both spectra of digested dairy manure produced at 400 and 450 °C were grouped together with other biochar produced at 500 °C (Figure 4-2) (no 500 °C digested dairy manure was produced, therefore sample produced at 450 °C was chosen to be included here). In Figure 4-2, the most noticeable band seen at 1940 nm is associated with the presence of moisture, common for biochar produced at ≤400 °C. Details on other bands assignments were provided in Chapter 3.

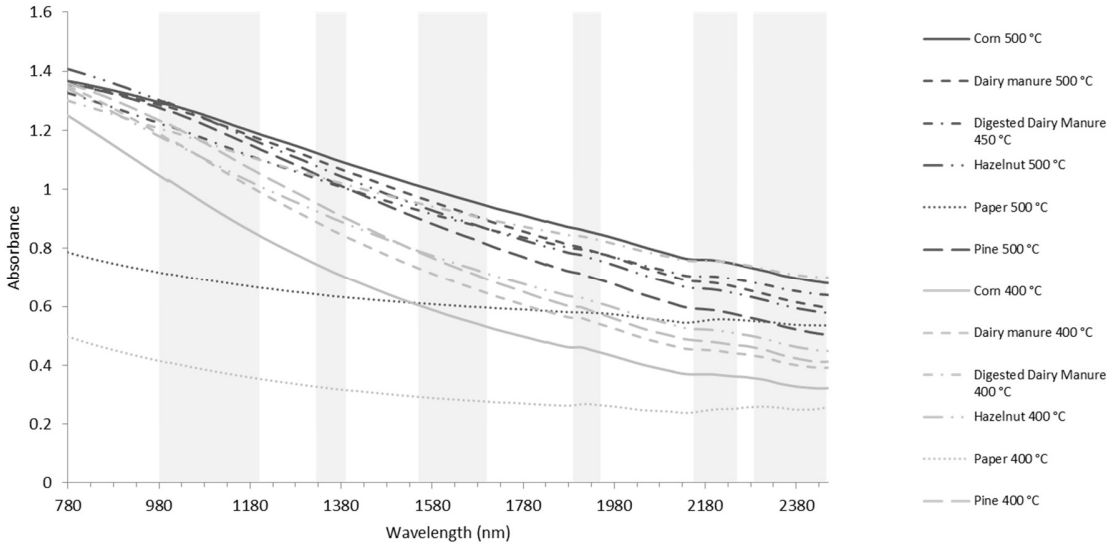

Figure 4-2. Spectral absorbance of selected biochar samples; absorbance = log (1/reflectance). Shaded areas represent bands regions associated with samples variations (all samples shown here were produced using slow pyrolysis technique using the same pyrolyzer)

4.3.2 Principal Component Analysis (PCA)

Seven principal components represent almost 91% of the total variation in NIRS data obtained from all 82 samples (Calibration set A), with PC 1 and PC 2 accounting for 64% and 9%, respectively. The scores of samples obtained from the first two PCs were used to

construct the ordination of biochar samples based on their feedstock and pyrolysis temperature (Figure 4-3a). As HHT increased, biochar samples shifted from the right (Quadrant I and IV) to the left (Quadrant I and III). For biochars produced at low HHT i.e., ≤400 °C, the type of feedstock seemed to have a major influence, with woody materials plotting into the far positive space of PC1 and into Quadrant I, whereas all biochars produced from mixed waste (food, paper, or mixtures of crushed brick and cement kiln residues) except 1 plotted in Quadrant IV, whereas neither animal manure nor crop residues seemed to have a consistent pattern. On the other hand, the contribution of the type of feedstock to the total variation was smaller at high HHT (≥500 °C) as samples tended to be clustered in the negative space of the PC1 axis.

The loading graph of the two PCs (Figure 4-3b) identifies those wavelengths mostly responsible for the discrimination among samples (bands with high positive or negative loadings) (Figure 4-3a). These wavelengths can be identified and assigned to specific chemical structures. Absorbance band around 1000 nm can be associated with the stretching of O-H bonds, while the region around 1080 nm is related to the stretching and deformation of C-H bonds. The band at 1837 nm is associated with O–H stretching and C–O stretching of cellulose, while, 1906 nm is associated with C=O stretching of hemicellulose. The region around 1923-1940 nm is attributed to a combination of O-H stretching and O-H deformation of water molecules. The region around 2200 nm is associated with C-H and C=O stretching of lignin while, 2265 nm is associated with O-H and C-O stretching of lignin. Bands around 2324-2327 nm are associated with C-H stretching and deformation of cellulose and hemicellulose (Schwanninger et al., 2011; Xu et al., 2013).

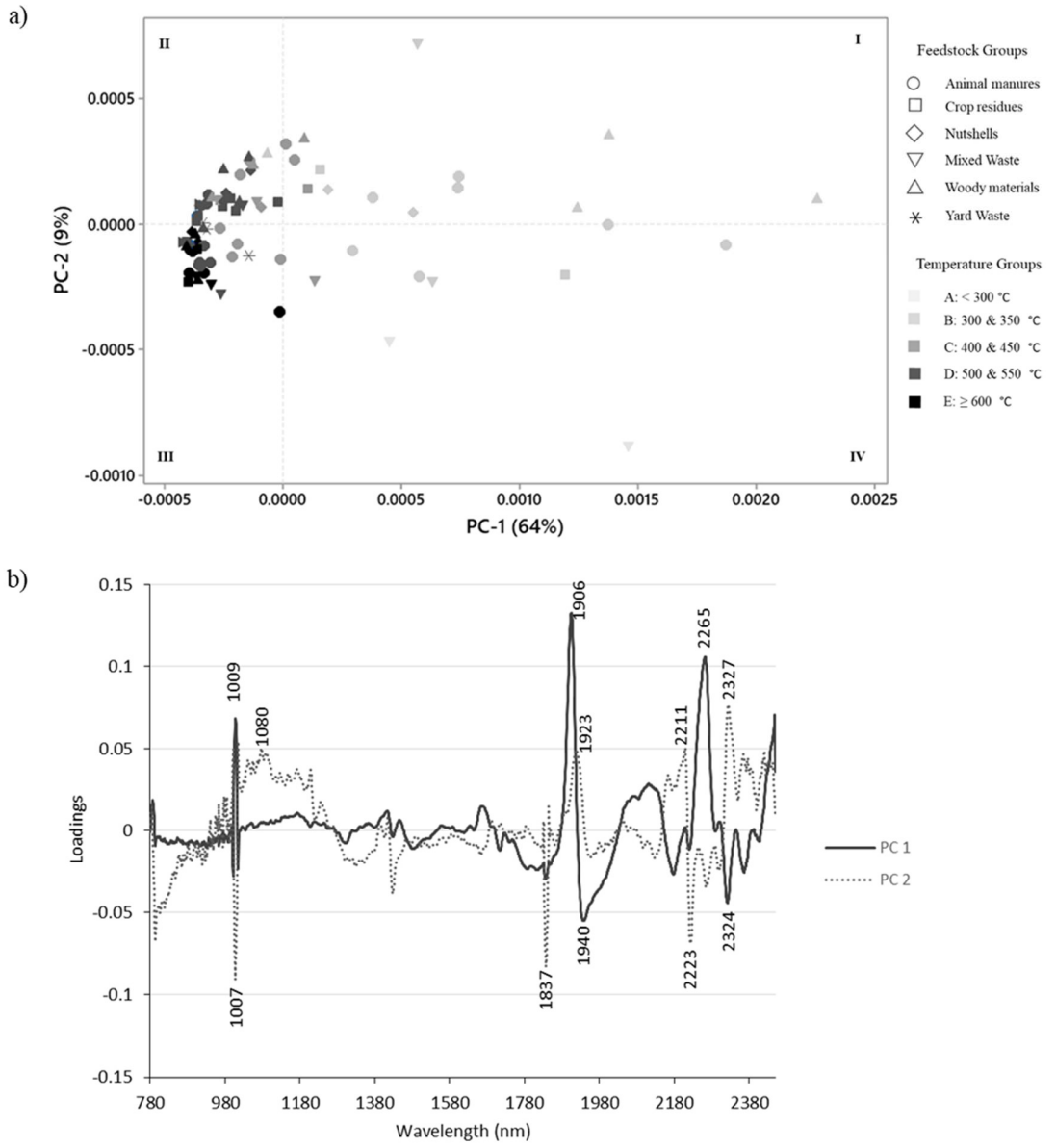

Figure 4-3. a) PCA scores plot of biochar samples in the calibration set (n=82) according to feedstock and temperature groups. b) Loadings plot of the first two principal components (shown are the wavelengths mostly responsible for the discrimination among samples.)

4.3.3 Partial Least Square Regression (PLSR) for predicting maximum pyrolysis temperature

Based on the LOO-CV technique, all three calibration models – obtained using set A (n = 82), B (n = 68) and C (n = 48) – rendered a relatively good prediction ability, with the overall RMSE values of cross-validation (RMSECV) being below 50 °C and the RPD values higher than 2 (Table 4-2). PLSR models with RPD values > 2 are considered to be good models and may be sufficient for quantitative prediction depending on the intended application of the model (Chang et al., 2001; Dunn et al., 2002; Viscarra Rossel et al., 2006). The calibration model based on set C gave the best prediction (R^2: 0.857; RMSECV: 38.1°C; RPD: 2.67) (Table 4-2).

Table 4-2. Validation of calibration models using the LOO-CV technique.

Set	No. of samples	Band region used (nm)	No. of Factors for PLSR model	Leave-one-out –cross-validation		
				R^2	RMSECV	RPD
A	82	780-2450	6	0.803	48.8 °C	2.26
B	68		6	0.793	44.8 °C	2.19
C	48		5	0.857	38.1 °C	2.67

*Set A: all 82 samples produced at 220 to 800 °C; Set B: 68 from 82 samples, produced using slow pyrolysis using the same pyrolyzer unit at 300 to 600 °C; Set C: 48 from 82 samples, produced in thermosequence at 300 to 600 °C and using only 7 types of feedstock.
*RMSECV: root mean square error of leave-one-out-cross-validation; RPD: the ratio of prediction to deviation

Each calibration model was further tested using the independent prediction set. All model gave good predictions, but again, calibration model based on set C gave the best prediction (R^2: 0.941; RMSEP: 27.3 °C; RPD: 4.05), followed by the model based on set A (R^2: 0.896; RMSEP: 35.6 °C; RPD: 3.11) and set B (R^2: 0.928; RMSEP: 37.3 °C; RPD: 2.96) (Table 4-3). Figure 4-4 showed the relationships between observed versus predicted HHT

for models obtained using sets A, B, and C, when validating via cross-validation (Figure 4-4a,c,e) and using the independent set (Figure 4-4b,d,f).

Table 4-3. Validation of calibration models using independent prediction set

Set	No. of samples in calibration set	No. of samples in prediction set	Band region used (nm)	No. of Factors for PLSR model	Validation using the separate prediction set		
					R^2	RMSEP	RPD
A	82	18	780-2450	6	0.896	35.6 °C	3.11
B	68	18		6	0.928	37.3 °C	2.96
C	48	18		5	0.941	27.3 °C	4.05

*Set A: all 82 samples produced at 220 to 800 °C; Set B: 68 from 82 samples, produced using slow pyrolysis using the same pyrolyzer unit at 300 to 600 °C; Set C: 48 from 82 samples, produced in thermosequence at 300 to 600 °C using only 7 types of feedstock. Prediction set: 18 samples produced at 250 to 550 °C.
*RMSEP: root mean square error of prediction; RPD: the ratio of prediction to deviation.

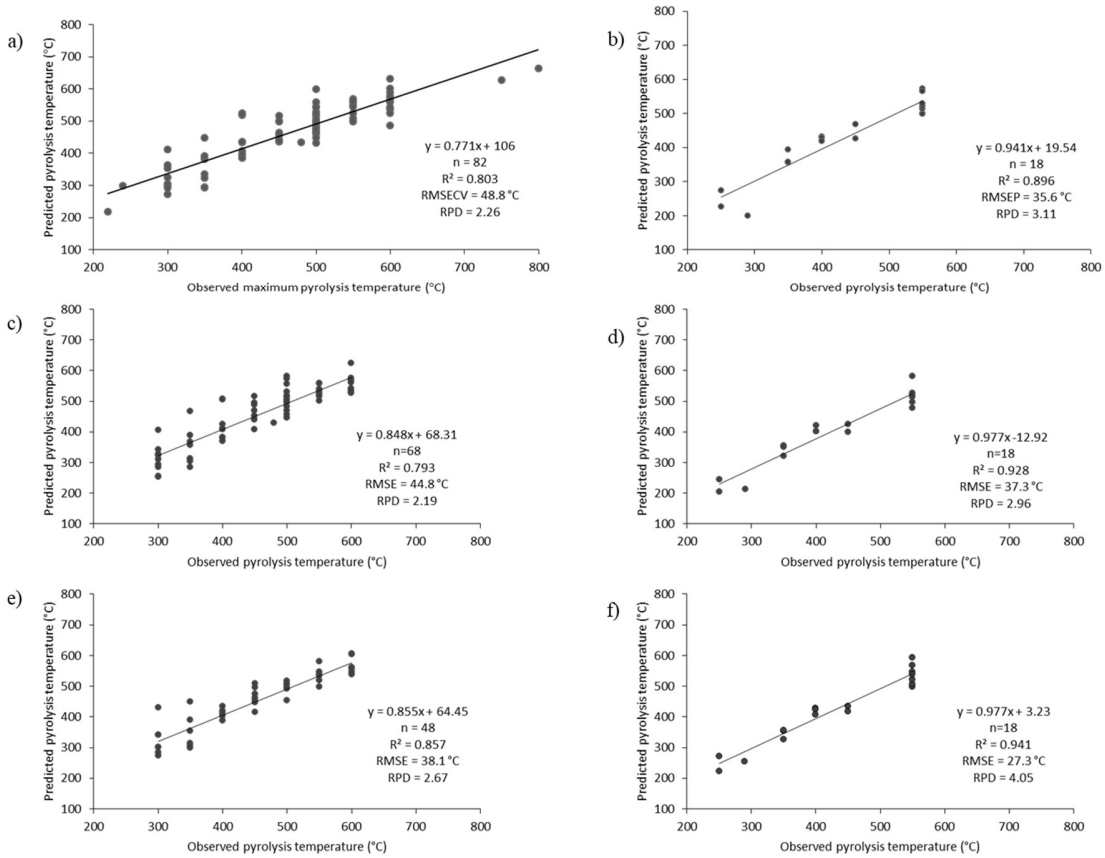

Figure 4-4. Observed versus predicted pyrolysis temperature PLSR plots of each leave-one-out-cross-validated calibration model; a) set A; c) set B; e) set C and their prediction using independent prediction set (b, d, f), respectively.

4.4 Discussion

Based on the spectral absorbance of the selected biochar samples shown in Figure 4-2, the spectra of biochar produced at the same pyrolysis temperature but from different feedstock can be differentiated. Spectra of biochar produced from paper are obviously separated from other samples suggest that differences in the chemical composition of feedstock can still be seen even after being pyrolyzed. Papermill waste contains varieties of contaminants and chemicals (Van Zwieten et al., 2010) that may react differently towards thermal degradation and subsequently produced biochar with unique characteristics. Changes in chemical properties of dairy manure after the digestion process

(Jensen et al., 2016; Spelter et al., 2008), may also affect the thermal degradation rate of the feedstock as compared with undigested dairy manure. Thus, it may explain why the spectra of digested manure produced at 400 and 450 °C were grouped together with other biochar produced at a higher temperature (500 °C). The noticeable moisture bands at 1940 nm in the spectra of biochar produced from corn stoves, paper, and dairy manure (high cellulose feedstock) at 400 °C may suggest the presence of hygroscopic cellulose which is not fully degraded by pyrolysis (Santos et al., 2015).

The influence of feedstock can also be seen from the PCA score plot (Figure 4-3a) although overall its influence lessens with the increase of HHT, whereas the effect of using different pyrolysis conditions for sample production was not apparent. It has been reported that biochar structures become increasingly homogenous at a higher temperature (>500 °C) regardless of feedstock types (Ascough et al., 2008; Leng and Huang, 2018). This can be associated with thermal decomposition of cellulose, hemicellulose, and lignin -common constituents of biochar feedstock- which happened at different temperature ranges. Hemicellulose and cellulose decomposition occur at 220-315 °C and 315–400 °C, respectively, while the lignin thermal decomposition occurs at temperature > 400 °C (Yang et al., 2006). Therefore, biochar produced at a lower temperature (<400 °C) that have more similar chemical properties with the original feedstock (Ramalho et al., 2017) was more scattered but clustered together at a higher temperature (≥ 500 °C) (Figure 4-3a). The presence of these constituents; cellulose, hemicellulose, and lignin which have not undergone complete decomposition, can be seen from the identified wavelengths shown in the loadings plot (Figure 4-3b).

The predictive ability of the first calibration model (Set A) was considered to be good based on the validations using LOO-CV (RPD: 2.26) and the external set (RPD: 3.11). However, since the biochar samples used in this model were produced using a different type of feedstock and pyrolysis condition it was expected that these differences were responsible for the predictive errors (RMSECV: 48.8 °C; RMSEP: 35.6 °C). Therefore, we expected that the inclusion of only the selected relevant variability would result in a more accurate model as in the use of calibration model built using samples from Set B in which variation from pyrolysis conditions was limited to the slow pyrolysis technique only and yet, although the RMSECV error obtained was slightly lower (44.8 °C), the RMSEP was higher (37.3 °C). One possible reason is that the effect of pyrolysis technique in this study was trivial relative to other variations (HHT and feedstock types), as visualized in the PCA score plot (Figure 4-3a) and thus although we used calibration model built using samples produced from one type of pyrolysis technique only (Set B), the accuracy of the prediction did not improve. It was also possible that due to the long residence time of slow pyrolysis technique favoring the completion of secondary reactions (Anca-Couce, 2016; Tripathi et al., 2016), the HHT deviation was prone to happen especially in the presence of certain chemical composition such as the high ash content (Di Blasi et al., 2014), thus masking the effect of different pyrolysis technique itself, if any.

In set C, all of these samples were also pyrolyzed using the slow pyrolysis technique (subset form set B) however, processed samples (biochar from digested manure, paper, and foods) were excluded, and thus the variability of the calibration set was reduced further. The higher prediction performance of the calibration model using Set C confirmed

the substantial effect of feedstock types on data variability and the subsequent predictive ability of the model. The changed in the original chemical compositions of the feedstock after being chemically or biologically treated may affect its pyrolytic behavior resulting in greater or lesser reaction toward thermal degradation at the assigned temperature setpoint (Di Blasi et al., 2015; Shane M Troy et al., 2013). The inclusion of this atypical data, as seen from the NIR spectra of biochar produced from paper and digested manure in Figure 4-2 which were noticeably different from other biochar samples produced at the same HHT, resulted in models with larger errors (calibration model using Set A and B).

4.5 Conclusion

In this study, the effect of different feedstock types and pyrolysis conditions on the predictive ability of NIR models were evaluated. Feedstock types have a substantial effect on the performance of the NIR model while the effect of pyrolysis conditions was less pronounced. Yet, the overall findings in this study suggest that a good prediction can be still be achieved using a calibration model built with relatively high sample size and data variability, especially when prior knowledge of the unknown samples was not available and thus the appropriate range of variability needed was not known. However, if the calibration model is built specifically for biochar produced from a certain type of feedstock, the prediction error can be reduced by incorporating only the relevant data variability.

CHAPTER 5. INVESTIGATING THE INFLUENCE OF BIOCHAR PARTICLE SIZE AND DEPTH OF PLACEMENT ON NITROUS OXIDE (N_2O) EMISSIONS FROM SIMULATED URINE PATCHES

A paper from this study has been published as:

Mahmud, A. F., Camps-Arbestain, M., & Hedley, M. (2018). Investigating the Influence of Biochar Particle Size and Depth of Placement on Nitrous Oxide (N_2O) Emissions from Simulated Urine Patches. *Agriculture*, *8*(11), 175.

In previous chapters (Chapter 3 and 4), the use of NIR spectroscopy to predict the highest heating temperature (HHT) achieved during biochar production as a method of selecting more stable biochar was addressed. Biochar produced at high temperature (≥ 500 °C) is predicted to last longer in soil than that produced at a lower temperatures. This is important as the biochar in soil should be stable enough to provide long-term benefits to the environment. However, other than biochar stability gauged from the production temperature, the final particle size of the biochar and the method of incorporation into the soil may also influence the ability of the biochar to moderate soil properties and function. This chapter (Chapter 5) describes a glasshouse study, which investigates the effect of biochar particle size and depth of placement on soil nitrous oxide (N_2O) emissions.

Following the objectives and hypotheses mentioned in Chapter 1, we hypothesized that the application of biochar may (i) affect N_2O emissions through changes in soil physical properties, specifically soil aeration and water retention; and (ii) the effects of biochar addition on these properties may differ depending on their particle size (e.g., a larger particle size may increase soil aeration whereas a smaller particle size may clog pores), and their placement in soil (e.g., the incorporation of a large particle size-biochar at depth may promote water movement from the top layer and increase the overall drainage of the soil).

In this study, a pine biochar produced at 550 °C was used. The HHT of this biochar was also predicted using the NIR spectroscopy model developed in Chapter 3 and the predicted temperature of this biochar was 500 °C. This provides further confirmation that this biochar would be relatively stable over time and any influence that may increase the variability in this study such as additional labile C would be minimal.

Abstract

The use of biochar reduces nitrous oxide (N_2O) emissions from soils under specific conditions yet the mechanisms through which interactions occur are not fully understood. The objectives of this glasshouse study were to investigate the effect of (i) biochar particle size, and (ii) the impact of soil inversion—through simulated mouldboard ploughing—on N_2O emissions from soils to which cattle urine was applied. Pine biochar (550 °C) with two different particle sizes (<2 mm and >4 mm) was mixed either into the top soil layer at the original 0–10 cm depth in the soil column or at 10–20 cm depth by inverting the top soil to simulate ploughing. Nitrous oxide emissions were monitored for every two to three days, up to seven weeks during the summer trial and measurements were repeated during the autumn trial. We found that the use of large particle size biochar in the inverted soil had significant impact on increasing the cumulative N_2O emissions in autumn trial, possibly through changes in the water hydraulic conductivity of the soil column and increased water retention at the boundary between soil layers. This study thus highlights the importance of the role of biochar particle size and the method of biochar placement on soil physical properties and the implications of these on N_2O emissions.

Keywords

Nitrous oxide emission; biochar; biochar particle size; soil inversion; soil water retention

5.1 Introduction

The primary sources of nitrous oxide (N_2O) emissions from New Zealand pastoral soils are excreta (urine and dung) from grazing animals, followed by urea and farm dairy effluent applied to soils (Van der Weerden et al., 2016). Excreta deposited by grazing animal alone contributed to 14.2% (5503.3 kt CO_2-e) of total N_2O emissions from the agricultural sector, which represent a 7.2% increase since 1990 (Ministry for the Environment, 2018a). In 2013, the New Zealand Government adopted the unconditional targets of reducing greenhouse gas (GHG) emissions to 5% below the 1990 level by year 2020, followed by post-2020 commitments to reduce greenhouse gas emissions to 11 and 50% below the 1990 level by year 2030 and 2050 (Ministry for the Environment, 2018b), respectively, which forces the need to develop economically and technically feasible options in order to achieve such goal.

Nitrous oxide can be produced in soil via nitrification, denitrification and nitrifier-denitrification. The nitrification process involves the oxidation of ammonium (NH_4^+) into nitrite (NO_2^-) and this into nitrate (NO_3^-) producing N_2O as by-product, while the denitrification process involves the reduction of NO_3^- into gaseous nitrogen (N) compounds, mainly N_2O and dinitrogen gas (N_2). Nitrifier-denitrification by NH_4^+-oxidizing bacteria may also contribute to the formation of N_2O in soils (de Klein et al., 2001; Wrage et al., 2001). Environmental conditions influencing N_2O emissions include soil mineral N concentration, soil moisture, dissolved organic carbon (C) concentration, temperature, and pH (de Klein et al., 2001; Tiedje, 1988), all of them being highly variable over short-time periods and having a strong seasonality.

The application of biochar—charcoal intended to be used to simultaneously mitigate climate change by contributing to carbon (C) sequestration and improving soil functions (Lehmann and Joseph, 2015) —has been suggested as a potential tool to reduce N_2O emissions from soil (Van Zwieten et al., 2015). Several laboratory and field studies have reported decreases in N_2O emissions from soil upon biochar application and attributed this to the ability of biochar to (i) modify soil physical properties and soil aeration thus changing oxygen (O_2) concentration (Case et al., 2012; L. Van Zwieten et al., 2010); (ii) reduce NH_4^+ and NO_3^- concentrations through either induced microbial immobilization or adsorption mechanisms (Nelissen et al., 2014; Thomazini et al., 2015); (iii) increase soil pH, and/or (iv) acting as "electron shuttle" (Cayuela et al., 2013). However, other studies have reported either no effect (Angst et al., 2014) or elevated N_2O emissions upon addition of biochar, the latter attributed to an enhanced N mineralization upon application (Mukome et al., 2013; Verhoeven and Six, 2014).

These mixed results could be, in part, attributed to the different experimental conditions used by the different researchers, such as the use of various types of biochar (Spokas and Reicosky, 2009), different biochar application rates (Bruun et al., 2012), or dissimilar experimental settings (field trial vs. laboratory/glasshouse experiments) (Schimmelpfennig et al., 2014). The use of different wetting and irrigation regimes may also have influenced N_2O emissions, most likely in response to changes in water-filled pore space (WFPS) and thus in soil aeration (Saarnio et al., 2013; Singh et al., 2010; Yanai et al., 2007). The simultaneous addition of biochar with other organic amendments, such as manure and poultry litter (Rose et al., 2016) and/or inorganic fertilizers, and differences in their rates of application, may also have determined the availability of labile C and N,

and thus affected N_2O production (Chen et al., 2015; Kammann et al., 2012; Zheng et al., 2012).

A more mechanistic understanding of the effect of biochar on nitrification and denitrification could help determine whether this amendment is suitable as a tool to mitigate N_2O emissions from agricultural systems, and more specifically from pastoral systems under humid-temperate climate. The few publications available in the literature on how the addition of biochar to urine patches influences N_2O emissions have reported inconsistent patterns. Clough et al. (2010) observed a temporary increase in N_2O emissions when applying a pine biochar produced at high temperature (600 °C) and of a particle size <5 mm to a silt loam soil. In contrast, Taghizadeh-Toosi et al. (2011) observed a decrease in N_2O emissions also using a pine biochar, but produced at low temperature (<400 °C) (Clough, 2018) and of a generally larger particle size to another silt loam soil. The reductions in the second study were attributed to a reduced availability of NO_3^- caused by NH_3 adsorption on biochar particles. Yet the potential role of biochar particle size on the different results obtained in N_2O emissions studies cannot be disregarded, as already highlighted by Cayuela et al. (2014).

A practical farming aspect is how the biochar amendment to soil is made, e.g., (i) surface spreading and incorporation by shallow tillage or (ii) application to depth by use of a mouldboard plough. By mouldboard ploughing, the top soil (and the biochar) becomes buried deeper in the profile, which contrasts with a top application of biochar followed by cultivation, in which the biochar remains in the topsoil without soil inversion. A recent short-term study of Calvelo Pereira et al. (unpublished) revealed that the addition of pine biochar while mouldboard-ploughing the soil (e.g., biochar and top soil placed below the

top 10 cm of soil) caused a 30% reduction in N_2O emissions following urea application compared to an inverted soil without biochar addition.

In the present soil column study, we investigated the effect of biochar particle size and the impact of soil inversion—through simulated mouldboard ploughing—on N_2O emissions from soils to which cattle urine was applied. For this, a pine biochar with a low atomic H/C_{org} ratio (and thus rich in condensed aromatic C) with a low ash content was chosen, so that the influence of labile C, nutrient content, and/or liming ability of the biochar was minimized. We hypothesized that (i) the application of biochar may affect N_2O emissions through changes in soil physical properties, specifically soil aeration and water retention; and (ii) the effects of biochar addition on these properties may differ depending on their particle size (e.g., a larger particle size may increase soil aeration whereas a smaller particle size may clog pores), and their placement in soil (e.g., the incorporation of a large particle size-biochar at depth may promote water movement from the top layer and increase the overall drainage of the soil).

5.2 Materials and methods

5.2.1 Biochar

Biochar was produced from untreated pine wood residue (*Pinus radiata* D. Don) (Foxton, New Zealand). The pine wood residue was pre-dried at 60 °C and pyrolyzed in a gas fired, rotating drum kiln (25 L) to a highest heating temperature (HHT) of 550 °C. After production, it was stored in a steel barrel for three years. The biochar was left to dry until its moisture content was reduced to ~7% before the trial was set up. Thereafter the biochar was crushed and sieved into two different particle sizes (<2 mm and >4 mm). The chemical characteristics of biochar with two different particle sizes were examined and

reported in Table 5-1. Briefly, the pH was measured at a ratio of 1:20 (*w:v*) solution of biochar:deionized water equilibrated for 1.5 h prior to measurement according to Rajkovich et al. (2012). Calcium carbonate equivalence (liming equivalence, % $CaCO_3$–eq) was determined according to IBI standards (2015), which was modified from the method proposed by Rayment and Higginson, (1992). Biochar samples were analyzed for their elemental C, H, and N composition (Elementar Analysensyteme GmbH, Hanau, Germany) and thereafter the elemental composition was recalculated on a dry-ash-free (daf) basis. Concentration of O (% daf) was then estimated by difference (100%-C%-N%-H%). Moisture, volatile matter (VM), fixed C (FC) and ash contents (wt. %) of samples was determined using a thermogravimetric analyzer (SDT Q600, TA Instruments, Melbourne, Australia) according to Calvelo Pereira et al. (2011). Total P, K, Ca and Mg were determined using Atomic Absorption Spectroscopy (AAS, GBC 904 Avanta Ver 1.33, Australia) after digestion following modified dry ashing (Enders and Lehmann, 2012). Available P was determined using formic acid extraction (Wang et al., 2012a) and available N was measured using 6 M HCl (Wang et al., 2012b). Cation exchange capacity (CEC) was measured with strontium chloride ($SrCl_2$), as described in Calvelo Pereira et al. (2015). Overall, the chemical properties of the biochar were similar for the two particle size fractions, with a high C content (>82% *w*/*w*)—mostly as condensed aromatic C, as reflected by the low atomic H/Corg ratio (≤0.5) and high fixed C content (>70% (*w*/*w*) (Wang et al., 2013) —low ash content (<3% *w*/*w*), and a pH close to neutrality. According to the classification system developed by Camps-Arbestain et al. (2015), this pine biochar had relatively low liming (class 0) and fertilizer (class 0) values.

Table 5-1. Chemical characteristics of pine biochar (feedstock source: Foxton, New Zealand) at the beginning of experiment.

Properties	Units	Biochar	
		Small	Large
Particle size	mm	<2 mm	>4 mm
pH (H_2O)	-	7.3	6.8
Liming Equivalence	% $CaCO_3$-eq	−2.2	−1.9
Bulk Density (BD)	Mg m^{-3}	0.20	0.17
Total C	g kg^{-1}	821	826
Total N	g kg^{-1}	2.9	2.5
Total H	g kg^{-1}	30.8	34.5
Total O	g kg^{-1}	146	137
C/N ratio	(*w*/*w*)	285	330
H/C_{org}	Atomic ratio	0.45	0.50
O/C_{org}	Atomic ratio	0.13	0.12
Ash	%	2.9	2.7
Volatile matter	%	18.6	17.8
Fixed C	%	74.6	76.5
CEC	$cmol_c$ kg^{-1}	1.2	1.0
Total P	g kg^{-1}	0.5	0.5
Total K	g kg^{-1}	2.6	2.4
Total Mg	g kg^{-1}	1.7	1.6
Total Ca	g kg^{-1}	5.5	5.5
Available N	mg kg^{-1}	36	40
Available P	mg kg^{-1}	84	80

Total O for biochar was determined by (100%-C%-N%-H%) and converted to g kg^{-1}.

5.2.2 Soil

The soil used in this experiment was collected from the Pasture and Crop Research Unit of Massey University at Palmerston North (40°23′20.37″ S, 175°36′32.33″ E), New Zealand. It classifies as Tokomaru silt loam Pallic soil according to the New Zealand soil classification system (Hewitt and Dymond, 2013) and Typic Fragiaqualf according to Keys to Soil Taxonomy (Soil Survey Staff, 2014). The soil was sampled at 0–10 cm (topsoil), 10–20 cm and 20–40 cm (subsoils). The physicochemical properties of the top layers are reported in Table 5-2. Soils were then thoroughly mixed, sieved to 5 mm, and stored in the cold room (temperature 4 °C) until used.

Table 5-2. Chemical characteristic of Tokomaru silt loam soil (Palmerston North, New Zealand) at the beginning of experiment.

Properties	Units	0–10 cm	10–20 cm	20–40 cm
pH (H_2O)	-	5.48	5.51	5.60
Bulk Density (BD)	Mg m^{-3}	1.05	1.29	1.43
Total C	g kg^{-1}	35.2	22.6	13.0
Total N	g kg^{-1}	3.4	2.2	1.2
C/N ratio	(*w*/*w*)	10.4	10.3	10.8
Cation Exchange Capacity (CEC)	$cmol_c$ kg^{-1}	20.0	18.0	15.0

5.2.3 Glasshouse experiment

PVC columns of 20 cm diameter and 40 cm depth attached to 1.3 m PVC drainage collection columns or Flux meters (American Society of Agronomy, 2010) were used in this soil column study. Soil columns were prepared as follows: (i) for the biochar-amended soils, the 0–10 cm soil layer was hand-mixed with either <2 mm or >4 mm biochars (2% *w*/*w* or ~20 t ha^{-1}) (Supplementary Information; Figure S5-1); (ii) the 0–10 cm soil layer of all treatments received NPK fertilizer (60 kg N ha^{-1}; 60 kg P ha^{-1} and 50 kg K ha^{-1}); (iii) soil (with or without biochar) was then repacked into the soil column either at the original 0–10 cm depth (simulating incorporation by shallow tillage) or inverting the top soil (simulating incorporation by mouldboard ploughing) and placing it at 10–20 cm depth (Supplementary Information; Figure S5-2). Soil layers without biochar amendment were repacked to the original bulk density; soil layers with biochar amendment were repacked to a recalculated bulk density (considering the bulk density of biochar particles and application rate added). Additional two columns were prepared for destructive sampling to represent time zero (soil core prior to seeding). Overall, there were 26 cores (24 + 2) from six treatments with four replicates for each treatment, and the two time zero columns. The treatments were the following: un-inverted control (UC), un-inverted small particle size biochar (US), un-inverted large particle size biochar (UL),

inverted control (IC), inverted small particle size biochar (IS), and inverted large particle size biochar (IL). The experiment was conducted in a glasshouse at the Plant and Growth unit of Massey University at Palmerston North from October 2014 to September 2015, following the time line described in Supplementary Information; Table S5-1.

Annual ryegrass (*Lolium multiflorum* L.) was seeded in all columns and thinned to 20 seedlings per column upon germination. During the experiment, ryegrass was cut nine times (four in summer and five in autumn) to five cm height to simulate cattle grazing. Urine applications were carried out in December 2014 (referred to as summer trial) and April 2015 (referred to as autumn trial) at rates of 354 kg N ha^{-1} and 563 kg N ha^{-1}, respectively, so that the N_2O measurements could reflect changes associated with seasons (Figure 5-1). Accordingly, the average WFPS of the soil was maintained at ~40–50% and ~70–80% for summer and autumn trial, respectively.

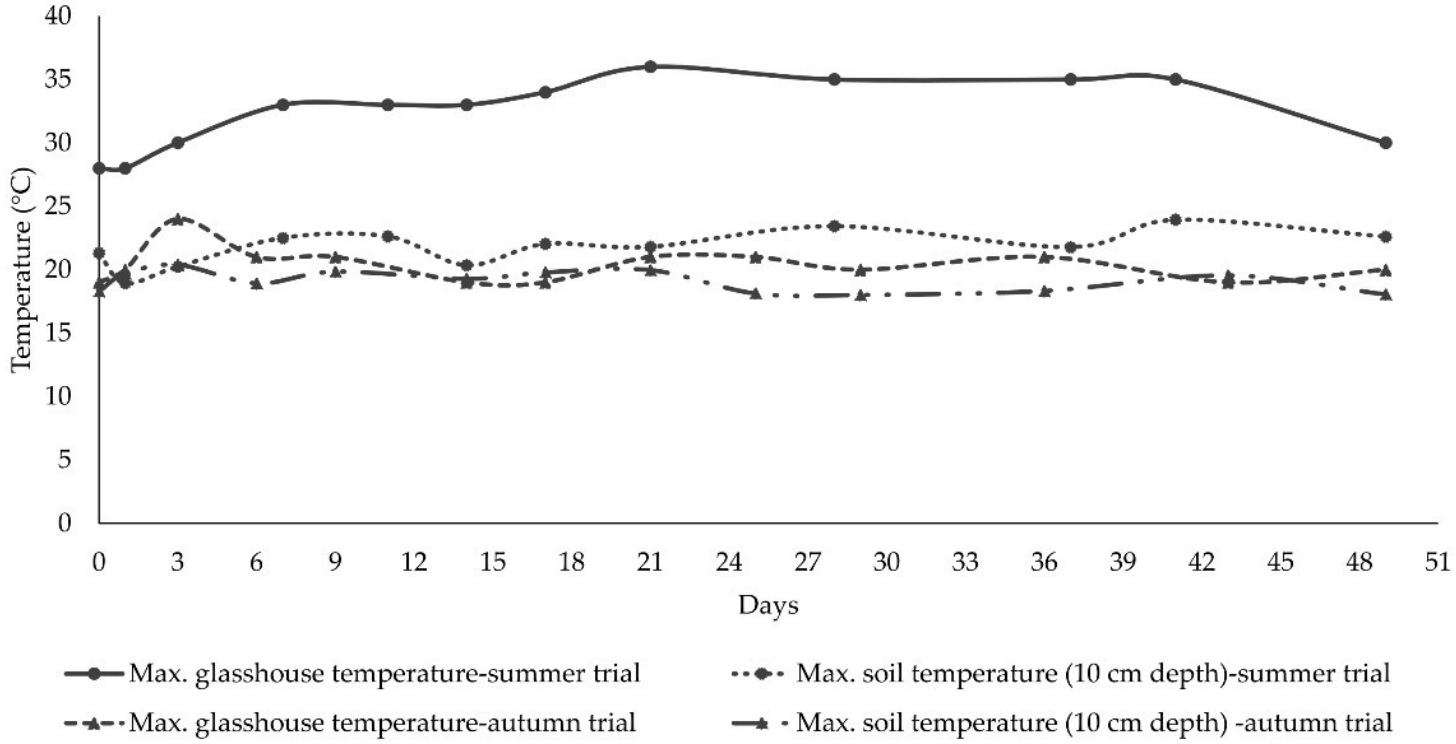

Figure 5-1. The maximum glasshouse and soil temperatures (at 10 cm depth) over the 49-day of both summer and autumn trials. In summer, cores were irrigated with 8 mm d^{-1} of deionized water to maintain initial soil WFPS% of 40–50% and the average daily evaporation rate was ~6 mm d^{-1}. In autumn, cores were irrigated with 5 mm d^{-1} of deionized water to maintain initial soil WFPS % of 70–80% and the average daily evaporation rate was ~2 mm d^{-1}. The cores were irrigated after gas measurements were taken. In summer, specific actions were taken to cool down the cores and the minimum glasshouse temperature during both summer and autumn trials was always maintained at ~17 °C.

5.2.4 Nitrous oxide emission measurement

N_2O fluxes were measured (at 0, 30, and 60 min) before urine application and then thereafter for every two to three day, up to seven week during the summer trial and measurements were repeated during the autumn trial. The gas sampling was carried out between 12 and 3 pm using a gas chamber with headspace volume of 3.4 L. Fifty ml of gas sample were collected at each sampling time using a syringe, and transferred into evacuated glass vials. In each sampling event, two ambient samples (i.e., outside the chamber) were taken to check for background emission. Concentration of N_2O was measured using gas chromatography (GC-2010 Plus, Shimadzu, Japan) with a carrier gas N_2 flow of 30 mL min^{-1}, a column temperature of 70 °C and detector temperature of 315 °C. The increase in N_2O concentration within the gas chamber headspace was calculated using linear regression and the cumulative N_2O emissions were calculated using linear integration of daily fluxes (Jones et al., 2011; Luo et al., 2008).

5.2.5 Leachate collection

During the summer trial, no leachates were produced, given the WFPS of the soils (40–50%) and the high ambient temperature. Once this ended, water was applied routinely to keep the grass growing while waiting for the autumn trial to begin. To minimize carryover N from the summer application to the autumn trial, all cores were leached twice (first and second leaching events) with copious amount of water prior to the second application of urine. This also allowed the WFPS of the soil to increase up to ≥70% as needed for the autumn trial. During the autumn trial, no leachate was collected as there were no fluctuations in the irrigation scheduled. By the end of week seven for autumn trial, all cores were leached (third leaching event) and one more N_2O fluxes measurement were

taken to check for any extended N_2O emission. Drainage water collected after each of these leaching events was measured and analyzed colorimetrically for inorganic N content (NO_3-N and NH_4-N) using a Technicon Auto Analyser (Blakemore, 1987).

5.2.6 End-of-trial sampling

All the columns were dismantled in September 2015, 327 d after the beginning of the trial. Soil cores were taken from the center of each column using slide hammer (45 mm diameter) (Supplementary Information; Figure S5-3). Each soil core was then scanned using a modified contact probe of ASD FieldSpec 3 Vis-NIR Spectrometer (Kusumo et al., 2009) to predict root density and soil C content (results not included in this study). After scanning, each 10-cm soil layer (for the 0–10 and 10–20 cm depth layers—the bottom soil was not characterized) was sliced into layers 3, 3 and 4 cm thick (Supplementary Information; Figure S5-3). Each slice was weighed, then halved evenly and re-weighed. One half was used to determine root density (mg cm^{-3}) by wet sieving (Kusumo et al., 2009); part of the other half was used to determine soil moisture and soil water holding capacity (WHC), while the rest was air-dried, homogenized, and ground for soil chemical characterization. Soil bulk density was calculated for each soil slice using the internal diameter of the corer (43.5 mm), the slicing depth, and the weight of the soil oven dried at 105 °C.

Soil total C and N were analyzed using a Vario MACRO cube CHNS elemental analyzer (Elementar Analysensyteme GmbH, Hanau, Germany). Soil pH was measured in water at a soil:water ratio of 1:2.5 (*w:v*) (Blakemore, 1987). The WHC was measured at −15, −1 and −0.3 bar matric potentials using a pressure plate (Dane and Hopmans, 2002). The moisture content was gravimetrically determined and then converted to volumetric basis

using the bulk density. The plant-available water content (AWC) was calculated as the difference in volumetric water content at −0.3 and −15 bar.

5.2.7 Other measurements

Daily soil temperature was recorded using sensors installed in randomly selected columns (Figure 5-1). The WFPS was calculated based on the ratio of the volumetric soil water content to the total pore space (particle density assumed to be 2.65 Mg m^{-3}). Each column was weighed periodically, and the amount of water added to each column and the rate at which this was evaporated—measured using evaporation pans placed inside the glasshouse—were recorded on daily basis.

Freshly harvested swards were weighed, dried at 70 °C for 48 h and re-weighed to calculate the dry matter (DM) yield. Then the dried swards were ground, acid-digested and analyzed for total N based on the colorimetric auto-analysis procedure using a Technicon Auto Analyser (Blakemore, 1987).

5.2.8 Statistical analysis

Cumulative N_2O was calculated by assuming that changes in fluxes between measurements were linear. Data were tested for normality and the homogeneity of variance using the Kolmogorov-Smirnov and Multiple Comparison test, respectively. Data that did not fulfill the assumptions were log-transformed before further statistical analysis. The effect of each treatment: (i) biochar application (control vs. small biochar particle size vs. large biochar particle size); and (ii) soil inversion (un-inverted and inverted) were assessed separately using one-way ANOVA, followed by LSD post-hoc test if significant difference were detected at $p < 0.10$. Means and standard error of the

mean (SEM) were also reported. All statistical analyses were conducted using Minitab 16 (Minitab Inc., State College, PA, USA).

5.3 Results

5.3.1 Dry matter (DM) yield, N concentrations in plant and N plant uptake

Cumulative ryegrass DM yields at the end of the summer trial (range: 374 to 401 g m^{-2}) were twice to three times larger than those of the autumn trial (range: 137 to 179 g m^{-2}) (Table 5-3). There were no significant effects of either biochar addition (regardless of particle size) or soil inversion on DM yield. This is consistent with the general lack of changes in soil chemistry (e.g., soil pH, Supplementary Information; Table S5-2) caused by the addition of biochar to the system and the lack of nutrient value of this amendment (Table 5-1). Ryegrass grown during the summer season had a lower N concentration (range: 3.2% to 3.6%–*w*/*w*) than that grown during autumn (range: 5.1% to 5.4%–*w*/*w*), yet the amount of N taken up by the swards was larger in the former (range: 11.9 to 13.5 g m^{-2}) than in the latter (range: 7.3 to 9.2 g m^{-2}). This was consistent with the higher growth of swards in the warmer season, which led to an overall greater plant N uptake. While biochar addition had no effect on plant N, soil inversion caused an increase in N plant uptake in all summer treatments, although the effect was only significant for the control (UC: 12.7 g N m^{-2}; IC: 13.4 g N m^{-2}: $p = 0.018$) (Table 5-3).

Table 5-3. Treatment and soil inversion effects on dry matter yields, plant N concentration, plant N uptake, and percentage of the total N applied taken up by plant for summer and autumn trial.

Summer Trial				
		Treatments		
Properties (Unit)	**Soil Inversion**	**Control**	**Small-Particle Size Biochar**	**Large-Particle Size Biochar**
Dry Matter (DM)	Un-inverted	374aA	350aA	351aA
($g\ m^{-2}$)	Inverted	374aA	401aA	386aA
Plant N concentration	Un-inverted	3.4aA	3.4aA	3.5aA
($g\ N\ 100\ g^{-1}$)	Inverted	3.6aA	3.2aA	3.3aA
Plant N uptake	Un-inverted	12.7aB	11.9aA	12.3aA
($g\ m^{-2}$)	Inverted	**13.5**aA	12.8aA	12.8aA
N taken up out of added N (354 kg N ha^{-1})	Un-inverted	36.0aB	33.7aA	34.7aA
(%)	Inverted	38.0aA	36.3aA	36.1aA
Autumn Trial				
		Treatments		
Properties (Unit)	**Soil Inversion**	**Control**	**Small-Particle Size Biochar**	**Large-Particle Size Biochar**
DM	Un-inverted	179aA	137aA	157aA
($g\ m^{-2}$)	Inverted	172aA	172aA	155aA
Plant N concentration	Un-inverted	5.1aA	5.3aA	5.4aA
($g\ N\ 100\ g^{-1}$)	Inverted	5.2aA	5.2aA	5.3aA
Plant N uptake	Un-inverted	9.2aA	7.3aA	8.5aA
($g\ m^{-2}$)	Inverted	8.9aA	8.9aA	8.2aA
N taken up out of added N (563 kg N ha^{-1})	Un-inverted	16.2aA	13.0aA	15.1aA
(%)	Inverted	15.9aA	15.9aA	14.6aA

Within a specific season, (i) different small letters within a row indicate differences between biochar treatments (n = 4) and $p < 0.10$), and (ii) different uppercase letters within a column indicate differences between un-inverted and inverted treatments (n = 4 and $p < 0.10$).

5.3.2 N_2O emissions fluxes

During both summer and autumn, the average N_2O emission prior to urine application from un-inverted cores (summer: 0.1 to 1.5 N_2O-N g ha^{-1} day^{-1}; autumn: 0.8 to 4.6 N_2O-N g ha^{-1} day^{-1}) were lower than those from the inverted cores (summer: 1.6 to 2.1 N_2O-N g ha^{-1} day^{-1}; autumn: 4.4 to 24.8 N_2O-N g ha^{-1} day^{-1}), with differences being significant between the un-inverted and inverted controls of both seasons, and also for the treatment with large particle biochar run during autumn (Figure 5-2, Supplementary Information; Table S5-3).

Shortly after the application of urine, all treatments displayed a peak in N_2O emissions (Figure 5-2), these being generally higher in biochar-amended treatments (US, UL, IS, IL) compared to their respective controls (UC, IC), although differences were not significant. The time at which the peak occurred was influenced by (i) the season under consideration, and (ii) whether the soils were inverted or not. During summer, N_2O emissions from the un-inverted soils always peaked (30.5 to 60.7 N_2O-N g ha^{-1} day^{-1}) within the first five day after urine application, whereas when inverted, peaks were smaller (13.9 to 29.1 N_2O-N g ha^{-1} day^{-1}), and displaced to day seven. During autumn, both un-inverted and inverted treatments showed a first peak within the first five day after urine application (40.7 to 93.8 N_2O-N g ha^{-1} day^{-1}), and a second and smaller peak by day 10 (9.4 to 28.6 N_2O-N g ha^{-1} day^{-1}), but no significant differences detected between treatments for both un-inverted and inverted soils (Figure 5-2, Supplementary Information; Table S5-3). Also, for the inverted soil, both treatments with biochar had an extended duration of N_2O emission (21 days in summer and 25 days in autumn) compared with controls, which subsided after 11 days in summer and 17 days in autumn, while for

un-inverted soils, all treatments including controls have similar duration of N_2O emission in both seasons (14 days in summer and 17 days in autumn).

When comparing between seasons, N_2O emissions were always higher in autumn than in summer from all treatments for both un-inverted and inverted cores, as expected, given the higher WFPS and higher amount of N added in autumn than in summer. However, when N_2O emissions were reported as percentage of added N emitted as N_2O, no significant differences were found between seasons.

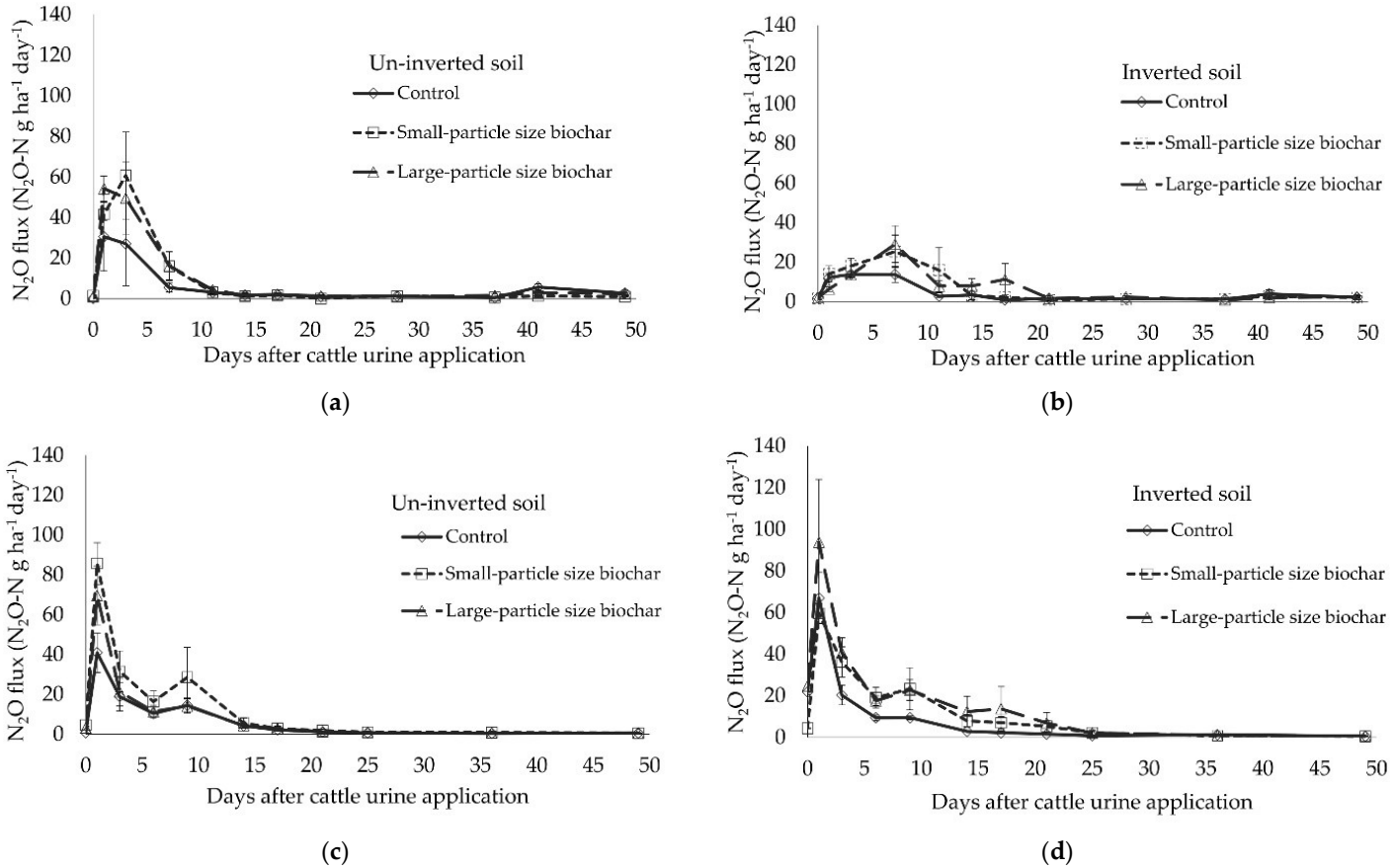

Figure 5-2. Average N_2O-fluxes (SEM (n = 4)) by day from soil columns after cattle urine application for summer (**a**,**b**), and autumn trials (**c**,**d**).

5.3.3 Cumulative N_2O emissions

For the summer trial, the average cumulative N_2O emissions from all treatments ranged from 200 to 372 N_2O-N g ha^{-1} (Figure 5-3a), which accounted for 0.06% to 0.11% of applied N (354 kg N ha^{-1}). The addition of biochar (regardless of particle size) caused a consistently higher cumulative N_2O emission than the corresponding controls in both un-inverted and inverted treatments, although the differences were not significant. Soil inversion did not have a significant effect on cumulative N_2O emissions either.

For the autumn trial, the average cumulative N_2O emissions from all treatments ranged from 239 to 558 N_2O-N g ha^{-1}, which accounted for 0.04% to 0.10% of applied N (563 kg N ha^{-1}) (Figure 5-3b). Here, variability between replicates was larger than during summer, which made difficult the detection of significant differences between treatments. However, the combined effect of biochar (of large particle size) addition and soil inversion, IL, did cause a significant increase in N_2O emissions, compared with the un-inverted soil, UL. No significant differences were detected between seasons when comparing the cumulative N_2O emissions out of total N added for each treatment.

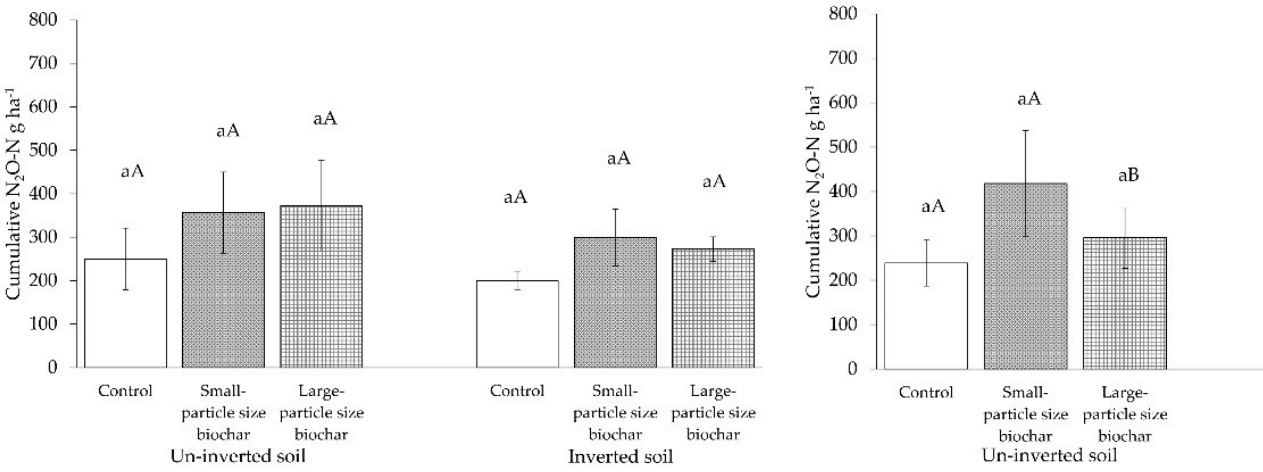

Figure 5-3. Cumulative N_2O emissions from soil columns after cattle urine application for summer
Within a specific season and specific soil inversion treatment, different small letters indicate dif
treatments (SEM (n = 4) and $p < 0.10$). Within a specific season and specific biochar treatment, c
indicate differences between un-inverted and inverted treatments (SEM (n = 4) and $p < 0.10$).

5.3.4 Leachate volume and soil water holding capacity

The volume of leachates after the first leaching event was smaller in the biochar-treated soils than in the non-treated (UC: 41, US: 17 and UL: 23 mm; $p = 0.017$; IC: 27, IS: 10 and IL: 13 mm; $p = 0.062$) (Table 5-4). Differences in leachate volume between biochar-amended and non-amended soils were still evident for the inverted treatments after the second leaching event (IC: 27, IS: 20 and IL: 14 mm; $p = 0.060$), but not for the un-inverted ones. After the third leaching event, no significant differences were observed between biochar-amended and un-amended treatments (Table 5-4). Overall, out of the total N applied, ≤0.2% was lost as mineral N in the form of NO_3^- (NH_4^+ concentrations in leachates were negligible) with no significant differences between treatments (Supplementary Information; Table S5-4).

Table 5-4. Treatment effects on the amount of drainage collected for every leaching event including cumulative drainage volumes.

Leaching Event	Leaching Volume (mm) between Treatments							
	UC	**US**	**UL**	***p*-Value**	**IC**	**IS**	**IL**	***p*-Value**
1st	41a	17b	23b	**0.017**	27a	10b	13b	**0.062**
2nd	24a	26a	26a	0.939	27a	20ab	14b	**0.060**
3rd	35a	38a	32a	0.750	39a	42a	52a	0.335
Cumulative	101a	81a	80a	0.109	92a	71.4a	80a	0.378

UC—control un-inverted; US—Un-inverted 0–10 cm with <2 mm biochar; UL—un-inverted 0–10 cm with >4 mm biochar; IC—control inverted; IS—inverted 0–10 cm with <2 mm biochar; IL—inverted 0–10 cm with >4 mm biochar. Different letters denote significant differences at $p < 0.10$ between treatments at each leaching event ($n = 4$).

At the end of the experiment, there were no significant differences in soil bulk densities between treatments (Supplementary Information; Table S5-5). The same was so for the volumetric soil moisture content at the different water potential tested (−0.3, 1 and 15 bar; Supplementary Information; Table S5-6) with the exception of the 6–10 cm layer, in the

un-inverted soil, and the 10–13 cm layer, in the inverted one at three matric potentials (Figure 5-4). Interestingly, these layers corresponded to those of biochar-amended soils that were at the boundary with the non-biochar soil, and the effect was particle size-dependent (Figure 5-4; Supplementary information; Figure S5-2). Specifically, in the un-inverted soil, it was the small particle size biochar that significantly retained the highest amount of water at −0.3 and −1 bar. In the inverted soil, it was the large particle size biochar that caused the largest water retention at the 10–13 cm depth, this difference being significant at all moisture tensions. The control soil always had the smallest water content at the different tensions studied (Figure 5-4).

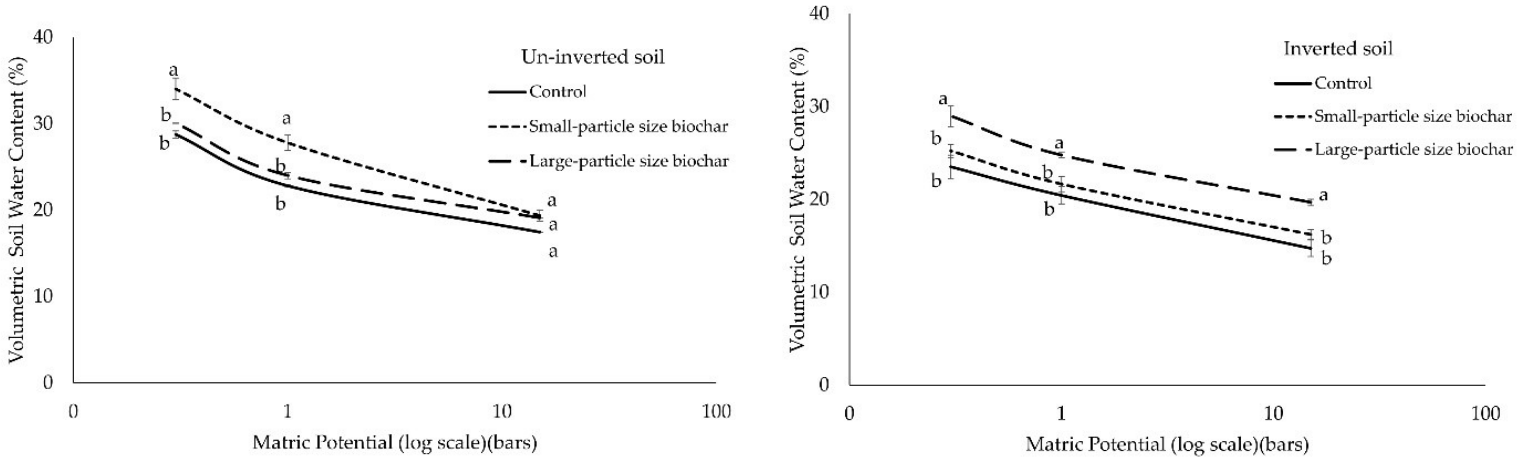

(**a**) (**b**)

Figure 5-4. Volumetric soil moisture contents (%) at different matric potentials; −15, −1 and −0.3 bar (in log scale) at (a) 6–10 cm depth (un-inverted soil) and (b) 10–13 cm depth (inverted soil) measured after the end of the experiment. Within a specific matric potential, different small letters indicate differences at $p < 0.10$ between treatments (SEM (n = 4)). In the un-inverted soil, biochar was at 0–10 cm depth; in the inverted soil biochar was at 10–20 cm depth.

5.3.5 Nitrogen mass balance

A mass balance indicated the amount of urine-N taken up by ryegrass plants was <40% in summer and <20% in autumn, the amount of urine-N lost as N_2O was 0.7% to 0.13% of the N applied for both trials.

5.4 Discussion

5.4.1 Dry matter yield (DM), N concentrations in plant and N plant uptake

The apparent differences in the growth of swards during the summer period compared to that during the autumn was mostly attributed to differences in temperature (summer mean = 32.5 ± 2.8 °C; autumn mean = 20.4 ± 1.4 °C). Although annual ryegrass is a cool-season grass (Charlton and Stewart, 1999), the low total DM from autumn trial may also have been caused by the lack of fertilizer use over the course of this trial and in addition pasture scorching, caused by the high concentration urine applied, inhibited early growth (Baral et al., 2014; Selbie et al., 2015). The addition of biochar did not cause differences in plant growth or N uptake, as expected, given the low fertility value of the biochar and high stability of the C in biochar, which minimized N immobilization. Also, the relatively low CEC (~1.12 $cmol_c\ kg^{-1}$ at the beginning of the experiment) of biochar would make any possible additional retention of NH_4^+ to be negligible. Soil inversion, on the other hand, did have an effect causing a greater N plant uptake compared to the un-inverted soil during summer. This could be attributed to the fact that the new top horizon—being impoverished in soil C—there was less urine N immobilization than in the un-inverted soil, and thus increased the short-term N availability to plants.

5.4.2 N_2O emissions

5.4.2.1 N_2O Emissions during the summer trial

Denitrification is expected to be the dominant N_2O formation pathway in soil with WFPS >60% (Bateman and Baggs, 2005), which were the moisture conditions of the soils during autumn (70–80%). The WFPS during summer was considerably smaller (40–50%), but still the percentage of N_2O-N loss out of urine-N added was similar during both seasons. Denitrification may have also contributed to N_2O emissions during summer, in addition to nitrification—given that anaerobic microsites have been shown to be also present at WFPS ~45% (Carter, 2007). In the inverted soils though, denitrification was probably less favored at the early stages of the experiment (i.e., summer), as the top layer of the inverted soils had small organic matter content. This was to some extent supported by the different pattern in the daily N_2O emissions—with a delayed and broader peak—that these soils had compared with the un-inverted ones.

During summer, biochar addition to soil had no significant effect on N_2O emissions. Yet N_2O emissions from biochar-amended and inverted soils showed a larger and delayed larger peak compared with just inverted soils, which could be attributed, at least in part, to denitrification occurring once the urine reached the organic matter-rich and biochar-amended layer, as favored by a larger retention of water in it (Barnes et al., 2014; Basso et al., 2013). The greater water retention in biochar layers was supported by the fact that, in the first leaching events, biochar-amended soils drained a smaller amount of water than the non-biochar treatments, and this was more accentuated in the inverted treatments. Volumetric soil moisture contents measured in biochar-amended soils also showed significant greater values ($p < 0.05$) compared to un-amended ones but only at the boundary soil layers (Supplementary Information; Table S5-6), as discussed in Section 4.2.3.

5.4.2.2 N_2O Emissions during the autumn trial

Emissions of N_2O during autumn were generally larger than those during summer, which was attributed to the larger urine application, greater water content of the soil, and the smaller N uptake by the plants. In contrast to summer time, soil inversion did not have an effect on the shape of the curve of daily N_2O emissions. This could be explained by the fact that by that time, ryegrass roots had already contributed to increase soil organic matter content (Supplementary Information; Table S5-7 and S5-8), along with the fact that WFPS during autumn was larger, conditions that favored denitrification as soon as nitrate was made available. The immediate N_2O emission after urine application suggests that this was mainly produced through denitrification (de Klein and Logtesjin, 1994).

The cumulative effect of the inversion treatment on N_2O emissions only caused significant differences when in combination with large particle size biochar and during this wet season. In fact, this was the only treatment combination in which biochar amendment had a significant effect on N_2O emissions, although overall, biochar-amended soils consistently generated greater N_2O emissions compared with the treatments without biochar.

5.4.2.3 Effect of biochar particle-size and soil inversion on soil moisture: implications on N_2O emissions

The differences in water retention encountered at the boundary layers of soils amended with biochar suggests that, the effect of biochar on soil water retention was not only on the amount of water retained within biochar porosity, but also on the water hydraulic conductivity of the soil column. Soil inversion *per se* had an effect on water hydraulic conductivity, as noted during the first leaching events, in which the collected water was

considerably smaller than the un-inverted soils. Burying the organic matter-rich surface horizons might have slowed down the flow of water due to hydrophobicity effects caused by organic molecules and produced a transient perched water layer during the autumn experiment. Moreover, biochar seemed to have caused a boundary effect in the un-inverted soil mixed with biochar of small particle size (US treatment) and in the inverted soil mixed with biochar of large particle size (IL treatment). The accumulation of water at the boundaries of these soil layers (Supplementary Information; Figure S5-2) may explain the higher volumetric moisture content of those specific biochar layers, as that may have caused an impregnation of biochar pores with water (to a larger extent than the operational wetting of soil samples prior to the use of the pressure plate). This may in turn explain that, in autumn, the US treatment was the un-inverted treatment with the largest N_2O emissions, and the IL was the inverted treatment with the largest N_2O emissions, yet only in the latter differences were significantly different. While a priori, the presence of a large biochar particle size would be thought to facilitate water drainage through this buried soil layer in the IL treatment, it is probable that in this study it had the opposite effect. The presence of a subsurface soil layer with large particle size biochar and greater aggregation may have caused a need for a larger water potential at the contact zone between the two soil layers in order to drain through the subsurface layer. It has been reported that when a fine-textured layer overlaying a coarse-textured one, the water movement in the profile is hindered i.e., the infiltration rate decreased when the water reached the interface between layers, allowing water to be stored in the fine-textured layer for a longer time (Hillel, 1998; Si et al., 2011). Overall, the results highlights the important

effect that biochar particle size has on soil physical properties as already reported by Lim et al. (2016).

5.5 Conclusion

This soil column study has shown that, compared to a simulated standard re-grassing of soil using a shallow cultivation technique, the combination of soil inversion and addition of biochar to a soil had no major impact on ryegrass growth and N recovery from soil. However, these treatments caused changes in soil physical properties that were associated with higher N_2O emissions after the application of cattle urine, specifically in the treatment in which a larger particle size biochar was used in combination with soil inversion. Field experiments with longer duration are needed to evaluate to what extent the changes in soil physical properties caused by soil inversion and application of biochar (with special attention to particle size) may affect the N_2O emissions from soil in the long term.

CHAPTER 6. INVESTIGATING THE INFLUENCE OF BIOCHAR PARTICLE SIZE AND DEPTH OF PLACEMENT ON SOIL ORGANIC C STOCKS AND THEIR PREDICTION USING NEAR-INFRARED (NIR) SPECTROSCOPY

Studies presented in Chapters 5 and 6 were based on the same glasshouse experiment. In this chapter, the effect of biochar particle size and depth of placement was evaluated in relation to soil organic C. Also, following the use of NIR spectroscopy on biochar presented in Chapters 3 and 4, the use of NIR spectroscopy was expanded to estimate the soil C concentration and SOC stocks in biochar-amended soil.

Abstract

Biochar can either enhance or slow down the decomposition of native organic matter – the so-called priming effect. Studies have commonly assessed the priming effect of biochar on soil organic C decomposition in relation to the type of feedstock and pyrolysis temperature. However, other biochar properties, such as its particle size and method of incorporation into the soil have received little attention. The objective of this study was to investigate the effect of (i) biochar particle size, and (ii) the biochar incorporation technique (through soil inversion simulating mouldboard ploughing) on soil organic C in the presence of annual ryegrass under glasshouse conditions. Pine biochar (550 °C) of two different particle sizes (<2 mm and >4 mm) was mixed either with the top soil layer at the original 0–10 cm depth of the soil column or with the 10–20 cm depth layer by inverting the top soil to simulate ploughing. Carbon stocks were estimated using NIR spectroscopy coupled with partial least-squares regression analysis (NIR/PLSR) and direct organic C measurements using an elemental analyzer. We found that the application of large-particle size biochar at depth induced significant C loss (9.20 Mg C ha^{-1} ($P < 0.05$), possibly through the combination of enhanced soil aeration, limited soil particles and biochar interactions due to its lower surface area (compared with the small-particle size biochar), and the interrupted C supply from new plant inputs at that depth due to soil inversion. This study highlights the role of biochar particle size and the method of biochar placement on soil organic C stocks, and also shows the potential of using NIR spectroscopy technique to predict the soil C concentration and soil C stocks.

Keywords

Biochar; biochar particle size; soil inversion; soil C stocks; near-infrared spectroscopy

6.1 Introduction

Soil carbon (C) has a key role in the fulfillment of soil functions (e.g., biomass production; storage and transformations of nutrients; storage of water; biodiversity pool; carbon pool) and the provision of ecosystem services (e.g., food security, water security, climate regulation) (FAO, 2015). Soils are the largest terrestrial C pool and changes in their stocks can have key implications in our climate (Lal, 2008), as even small gains in soil organic C can result in a considerable reduction in atmospheric CO_2 concentrations (4 Per 1000, 2015). Human activity has caused the loss of organic matter from soils through unsustainable agricultural practices and reduced C stocks in the top 2 m of agricultural soils by ~133 Pg C (Sanderman et al., 2018). Increases in soil C stocks can be attained by (i) the addition of organic C amendments (e.g., manure, biochar), (ii) the use of farm operations for soil management that minimize soil disturbance (e.g., minimum tillage), and/or (iii) the selection of deep-rooted species, among others (Whitehead et al., 2018). The use of biochar has not only been promoted as a strategy for C sequestration (Criscuoli et al., 2014; Woolf et al., 2018a) but also as an agricultural management practice aimed at improving soil properties (Ye et al., 2019). These include (i) the addition of plant-available nutrients (Camps-Arbestain et al., 2015; Wang et al., 2012a), (ii) the reduced loss of nutrients through leaching (Borchard et al., 2019; Laird et al., 2010), (iii) the effects on soil physical properties (Blanco-Canqui, 2017; Herath et al., 2013), and (iv) its liming properties (Singh et al., 2017). However, the effect of biochar on the native organic matter can vary widely (Zimmerman and Ouyang, 2018), as expected, given the broad array of biochars and soils (and the quality and quantity of the organic matter that soils contain). Proposed mechanisms for a decrease in the mineralization rate of soil organic C

due to biochar-soil interactions (i.e., negative priming) are (i) increased physical protection through soil aggregation (Weng et al., 2017), (ii) formation of mineral-organic associations via adsorption of soil organic C ligands on biochar surface particles (Keith et al., 2015) and/or (iii) the inhibition of microbial activity due to toxicity (Whitman et al., 2015), whereas (i) an amelioration of soil pH, (ii) the addition of a limiting nutrient, and/or (ii) the addition of labile C in biochar can accelerate the decomposition of native organic matter (i.e., positive priming) (Whitman et al., 2015). Moreover, the effect of biochar on native organic matter cycling has been commonly assessed in relation to certain biochar properties i.e. type of feedstock and pyrolysis temperature (Zimmerman et al., 2011), whereas other biochar properties, such as its particle size and the method of incorporation into the soil (e.g., whether the biochar is spread on the soil surface, uniformly mixed into the topsoil or incorporated at certain soil depth), have received little attention (Blackwell et al., 2009; Liang et al., 2016). This has resulted in the lack of guidelines to identify the suitable particle size and incorporation technique for a particular biochar use. Biochars with small particle size (< 2 mm) have greater surface contact with soil particles, mix better with soil, and may be able to become incorporated into soil aggregates and even promote soil aggregation (Brodowski et al., 2006), which would contribute to biochar and the organic matter preservation. However, biochars with small particle size may decompose faster due to their larger surface area (Sigua et al., 2014) and thus increase the overall soil C mineralization (Liang et al., 2016). Also, the generation of dust resultant from biochar application is also greater as particle size decreases, whereas the use of biochar of large particle size requires less processing and is easier to handle.

The method chosen for the incorporation of biochar determines its placement in the soil and therefore it also affects the biochar decomposition rate. Most of the studies on biochar involve the mixing of biochar into the topsoil probably because this application technique is relatively easy and straightforward. However, the incorporation of biochar at a certain depth as with the use of mouldboard ploughing, although less common, has also been adopted to reduce biochar susceptibility to erosion along with its potential benefit for root growth (Graves, 2013). In fact, the incorporation of biochar at depth has been shown to influence soil water infiltration and retention, and this may indirectly affect the decomposition of soil organic C (Z. Liu et al., 2016). Therefore, understanding the effect of biochar particle size and method of incorporation on soil organic C is essential for assessing the potential of using biochar as a C sequestration tool.

The present glasshouse study, investigated the effect of biochar particle size and the incorporation technique (in this case through soil inversion simulating mouldboard ploughing) on soil organic C in a soil column under annual ryegrass. For this, pine biochar with a low atomic H/Corg ratio (i.e., rich in condensed aromatic C) and a low ash content was chosen, so that the influence of labile C, nutrient content, and/or the liming ability of the biochar was minimized. The primary hypothesis was that, compared with small-particle size biochar, the application of large-particle size biochar may affect soil aeration to a greater degree and thus further accelerate soil C decomposition rate with increased oxygen availability and this effect is greater when the biochar was incorporated at depth due to the more compacted soil at deeper layer with poorer aeration compared to the surface layer. Carbon stocks were estimated using two methodologies: NIR spectroscopy coupled with partial least-squares regression analysis (NIR/PLSR) and direct organic C

measurements using an elemental analyzer. This tested the secondary hypothesis that the NIR spectroscopy can be used to predict the SOC concentration and SOC stocks in biochar-amended soil.

6.2 Materials and methods

6.2.1 Biochar

Biochar was produced from untreated pine wood residue (*Pinus radiata* D. Don) (Foxton, New Zealand) at a maximum temperature of 550 °C. After production, it was stored in a steel barrel for three years and later was crushed and sieved into two different particle sizes (<2 mm and >4 mm) before usage. The selected properties of the biochar at the beginning of the experiment are given in Table 6-1. Briefly, biochar elemental C, H, and N composition were determined using Vario MACRO cube CHNS elemental analyzer (Elementar Analysensysteme GmbH, Hanau, Germany), while moisture, volatile matter (VM), fixed C (FC) and ash contents (wt. %) of samples were determined using a thermogravimetric analyzer (SDT Q600, TA Instruments, Melbourne, Australia) according to Calvelo Pereira et al. (2011). Overall, the biochar of both particle size fractions had low ash content (<3% w/w) and high C content (>82% w/w) – mostly as condensed aromatic C, as reflected by the low atomic H/C_{org} ratio (≤0.5) and high fixed C content (>70% w/w). Details on biochar characterization and methodologies have been described in Mahmud et al. (2018).

Table 6-1. Chemical characteristics of pine biochar (feedstock source: Foxton, New Zealand) at the beginning of the experiment.

Properties	Units	Biochar	
		Small	Large
Particle size	Mm	<2 mm	>4 mm
Bulk Density (BD)	Mg m^{-3}	0.20	0.17
Total C	g kg^{-1}	821	826
Total N	g kg^{-1}	2.9	2.5
Total H	g kg^{-1}	30.8	34.5
Total O	g kg^{-1}	146	137
C/N ratio	(*w*/*w*)	285	330
H/C_{org}	Atomic ratio	0.45	0.50
O/C_{org}	Atomic ratio	0.13	0.12
Ash	%	2.9	2.7
Volatile matter	%	18.6	17.8
Fixed C	%	74.6	76.5

6.2.2 Soil collection and glasshouse experiment

The detailed description of the soil collection and experiment setup is provided in Mahmud et al. (2018) (Table 6-2). Briefly, a Tokomaru silt loam Pallic soil (Typic Fragiaqualf) (Hewitt and Dymond, 2013; Soil Survey Staff, 2014), sampled at 0–10 cm (topsoil), 10–20 cm and 20–40 cm (subsoils) was collected from the Pasture and Crop Research Unit of Massey University at Palmerston North (40°23′20.37″ S, 175°36′32.33″ E), New Zealand. Soil amended with either < 2 mm or > 4 mm particle size biochar (2% *w*/*w* or ~20 t ha^{-1}) was repacked into the soil column either at the original 0–10 cm depth (simulating incorporation by shallow tillage) or inverting the topsoil (simulating incorporation by mouldboard ploughing) and placing it at 10–20 cm depth. Overall, there were 26 columns (24 + 2) from six treatments with four replicates for each treatment, and the two time zero columns. The treatments were the following: un-inverted control (UC), un-inverted small particle size biochar (US), un-inverted large particle size biochar (UL),

inverted control (IC), inverted small particle size biochar (IS), and inverted large particle size biochar (IL). All soil columns were planted with annual ryegrass (*Lolium multiflorum* L.) and its height was kept to 5 cm. The experiment was conducted in a glasshouse at the Plant and Growth unit of Massey University at Palmerston North from October 2014 to September 2015, which simulated summer and autumn conditions with the average water-filled pore space (WFPS) of the soil was maintained at ~40–50% and ~70–80%, respectively.

Table 6-2. Chemical characteristic of Tokomaru silt loam soil (Palmerston North, New Zealand) at the beginning of the experiment.

Properties	Units	0–10 cm	10–20 cm	20–40 cm
pH (H_2O)	-	5.48	5.51	5.60
Bulk Density (BD)	Mg m^{-3}	1.05	1.29	1.43
Total C	g kg^{-1}	35.2	22.6	13.0
Total N	g kg^{-1}	3.4	2.2	1.2
C/N ratio	(*w*/*w*)	10.4	10.3	10.8
Cation Exchange Capacity (CEC)	$cmol_c$ kg^{-1}	20.0	18.0	15.0

6.2.3 Soil sampling and analysis

At the end of the experiment, all columns were dismantled and soil cores were taken from the center of each column using slide hammer (45 mm diameter). Each soil core was then scanned using a modified contact probe of ASD FieldSpec 3 Vis-NIR Spectrometer (Kusumo et al., 2009) to collect the UV-Visible NIR spectral reflectance at 1-cm intervals between 0 and 20 cm (Figure S6-1). The spectrometer provides spectra from 350 nm to 2500 nm with 1 nm resolution. One spectrum recorded per sample was the average of 30 spectra acquisitions. After scanning, each 10-cm soil layer (for the 0–10 and 10–20 cm depth layers; the bottom soil was not characterized) was sliced into layers 3, 3, and 4 cm thick. Each slice was weighed, then halved evenly and re-weighed for further analysis as described in Mahmud et al. (2018). Root density (mg cm^{-3}) was determined by wet sieving

(Kusumo et al., 2009). Soil total C and N were analyzed using a Vario MACRO cube CHNS elemental analyzer (Elementar Analysensyteme GmbH, Hanau, Germany) and total C was assumed to equal SOC because this soil contained no inorganic C (pH < 6), while non-oxidizable soil organic C ($OC_{non\text{-}ox}$) fraction was determined using potassium dichromate (Herath et al., 2015). Soil bulk density was calculated for each soil slice using the internal diameter of the corer (43.5 mm), the slicing depth, and the weight of the soil oven-dried at 105 °C.

It is worth mentioning that there were no differences in dry matter between treatments (Mahmud et al., 2018). Hence, the amount of plant materials deposited onto the soil surface of each treatment was assumed to be similar for all treatments. Also, based on the data obtained for the root contents (Table S6-1), the root growth in the soil columns was not affected by either biochar addition or soil inversion.

6.2.4 Soil carbon and nitrogen calculation

The calculation for C and N stocks were made based on studies done by Ellert & Bettany (1995) and Ellert et al. (2007). Briefly, C and N concentration, soil bulk density, and the thickness of each section sampled were used to calculate the C and N stocks for each depth interval (0-3, 3-6, 6-10, 10-13, 13-16, 16-20 cm) (Eqn. 1) followed by the sums of all these sections to get the total C and N stocks to a fixed depth of every 10 cm for both topsoil and subsoil layers. Soil C and N data were then recalculated further for equivalent soil mass for both topsoil and subsoil layers, a slight change from Ellert et al. (2007) method in which they calculate the equivalent mass using the soil mass from the deepest core segment only, to account for the dissimilarities in soil masses at fixed depth caused by small differences in soil bulk density between treatments/columns at the end of the

experiment. To achieve this, the average soil mass of topsoil and subsoil layers were used to calculate the soil C and N stocks of each respective layer for each soil column (Eqn 2.1 and 2.2) and then the soil C and N stocks of the full profile (0-20 cm depth) were obtained based on the sums of the C and N stocks of both topsoil and subsoil layers. For the comparison between measured and predicted soil C stocks, the calculation was repeated using NIR/PLSR predicted soil carbon concentration.

Soil C content at a fixed depth (C_{fd}, Mg C ha^{-1}) is calculated as:

$$C_{fd} = C \times BD \times T \times 0.1 \quad (1)$$

where C is the soil carbon concentration (g kg^{-1}), BD is bulk density (g cm^{-3}), T is the thickness of soil layer (cm), and 0.1 is a unit conversion factor.

Soil C content at equivalent mass (C_{em}, Mg C ha^{-1}) is calculated using the following equations:

$$C_{em} = C_{fd} - M_x \times C_{dn}/1000 \quad (2.1)$$

$$M_x = M_{fd} - M_{average} \quad (2.2)$$

where C_{fd} is the soil C content at a fixed depth (Mg C ha^{-1}) and C_{dn} is soil C concentration at the deepest layer (g kg^{-1}), while, M_x is the soil mass to be used to attain the equivalent soil mass (Mg ha^{-1}), M_{fd} is the mass of soil at the selected fixed depth (Mg ha^{-1}), and $M_{average}$ is the average soil mass at the selected fixed depth of all soil columns (Mg ha^{-1}).

We had used two different values for $M_{average}$, depending on whether it was the original topsoil or subsoil: 948 and 1107 Mg ha^{-1}, respectively. $M_{average}$ = 948 Mg ha^{-1} was used in the calculation for the un-inverted and inverted topsoil (the inverted topsoil was the new

subsoil), while $M_{average}$ = 1107 Mg ha^{-1} was used in the calculation for the un-inverted and inverted subsoil (the inverted subsoil was the new topsoil).

6.2.5 NIR data treatments and pre-processing

Indico Pro (Ver. 6.0) was used to correct the splice in the spectrum and all the data collected were saved in an ASCII text file. A chemometric analysis software-ParLeS (Viscarra Rossel, 2008) was used to pre-process the spectral data as follows: data were transformed from reflectance (R) to log (1/R) and were pre-processed using standard normal variate (SNV) with wavelet detrending (0.2 and 5, trend and decomposition level, respectively). A Savitzky–Golay filter with a second-order polynomial algorithm and a window size of 11 nm was used to reduce the noise. The smoothed data were thereafter processed into the first derivative, and then finally treated using mean centering (Savitzky and Golay, 1964). Rather than using the full recorded bands of 350-2500 nm, only 780-2450 nm bands located in the near-infrared region were used. This region corresponds to the most significant wavelength range for soil C content estimation (Chen et al., 2011; Peng et al., 2014). This step also excludes noise at shorter wavelengths and reduce the complexity of the model.

6.2.6 NIR data analysis

6.2.6.1 Principal component analysis (PCA)

Principal component analysis (PCA) was run prior to any other multivariate technique using the pre-processed NIRS data to check for outliers or any discernable pattern from sample distribution shown in the scores plot (Esbensen et al., 2002).

6.2.6.2 Partial least square regression (PLSR)

Following the PCA analysis, partial least square regression (PLSR) was carried out to build the calibration models using the 144 soil samples by correlating the pre-processed NIR spectral data at selected wavelength ranges of 780-2450 nm with the reference data i.e. total C (%). The optimum number of factors that produce low root mean square error (RMSE) and low Akaike Information Criterion (Viscarra Rossel et al., 2006) were used in the calibration model. The model was validated using leave-one-out cross-validation (LOO-CV) due to the limited number of samples. The accuracy of the established model was determined based on the root mean square error of LOO-CV (RMSECV), the coefficient determination (R^2) and RPD (ratio of prediction to deviation); RPD is the standard deviation of the reference data divided by the root mean square error (SD/RMSE) (Kusumo et al., 2011). Due to differences in treatments i.e. the addition of biochar with different particle sizes and soil inversion in this trial, attempts were also made to see whether the prediction ability of the calibration model can be improved by (i) separately using samples from treatments with either small or large particle size biochar from both inverted and un-inverted soils (Calibration model 2; n=96 and model 3; n=96, respectively), and (ii) separately using samples from either un-inverted (Calibration model 4; n=72) or inverted treatments (Calibration model 5; n=72), regardless of differences in biochar particle sizes. This attempts yielded the other four calibration models validated using cross-validation for soil C prediction.

6.2.7 Data harmonization

Originally, 480 NIR spectra were collected from 24 soil cores at 1-cm intervals between 0 and 20 cm. However, the laboratory measurement of total C was done according to sliced soil layers at 3, 3, and 4 cm for each 0-10 and 10- 20 cm soil depth. Therefore, prior

to any data treatments or analysis, spectra recorded at every centimeter were averaged to match the depth intervals at which soil samples were collected for laboratory analysis. The final number of aggregated spectra was 144.

6.2.8 Statistical analysis

The effect of each treatment: (i) biochar application (control vs small particle size biochar vs large particle size biochar), and (ii) soil inversion (un-inverted vs inverted) were assessed separately using one-way ANOVA for total soil C and N concentrations, non-oxidizable C fraction, soil bulk density, and total soil C and N stocks according to assigned soil depths. This was followed by LSD post-hoc test when significant difference were detected at $P < 0.10$. Means and standard error of the mean (SEM) were also calculated. Mean 0–20-cm SOC stocks calculated using measured or NIR/PLSR predicted soil carbon contents were compared using paired t-test ($\alpha = 0.05$). All statistical analyses, other than NIR data treatments and PLSR, were conducted using Minitab 16 (Minitab Inc., State College, Pennsylvania).

6.3 Results

6.3.1 Changes in soil C and N concentrations (including soil non-oxidizable C) and soil bulk density by the end of the trial.

As expected, biochar addition to the un-inverted topsoil (at 0-10 cm depth) (Figure 6-1a; Tables S6-2 to S6-4) increased the average soil C concentrations up to 13 and 16 g kg^{-1} soil (and that of non-oxidizable C for up to 10 and 13 g kg^{-1} soil) for the UL and US treatments, respectively, compared with the corresponding control treatment ($P < 0.01$). No significant differences in soil C concentrations between the two biochar particle size treatments were found, except at 3-6 cm depth, where the average non-oxidizable soil C

fraction in UL was significantly lower than the corresponding US layer ($P < 0.001$) (Figure 6-1a and Table S6-4). In this un-inverted topsoil (0-10 cm), there was a trend towards decreasing total soil C at depth for all treatments, with soil C concentration values being highest in the top 0-3 cm yet differences were not significant. Biochar addition has no significant effect on soil C concentrations of the un-inverted subsoils (at 10-20 cm depth) (Figure 6-1a).

For the inverted topsoil (at 10-20 cm depth) (Figure 6-1b), the average soil C concentration increase were 11 and 17 g kg^{-1} soil (and those of non-oxidizable C for up to 10 and 16 g kg^{-1} soil) for the IL and IS treatments, respectively ($P < 0.01$) compared to the corresponding control treatment (Table S6-2). No significant differences in soil C concentrations between the two biochar treatments were found, except at 13-16 and 16-20 cm depth, where means of both total C concentration and the non-oxidizable C fraction in IL were significantly lower than the corresponding IS layers ($P < 0.001$) (Figure 6-1b and Table S6-4). Only soil layers with large biochar particles (IL treatment) showed a decreasing trend in soil C concentration at depth although this was not significant, while there was no consistent trend in the other two treatments (IC and IS) (Figure 6-1b). Biochar addition has no significant effect on soil C concentrations of the inverted subsoils (at 0-10 cm depth) (Figure 6-1b).

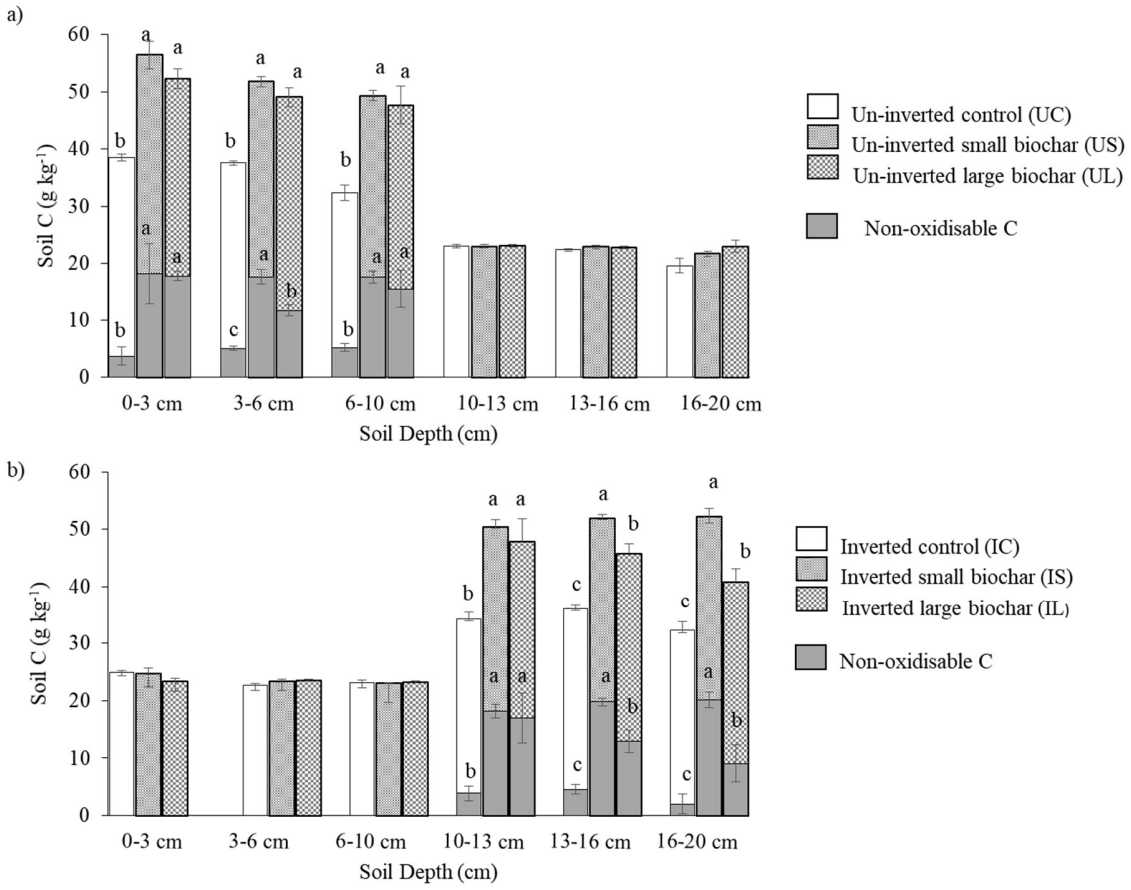

Figure 6-1. Soil C and non-oxidizable C concentration of topsoil and inverted topsoil with depth at the end of the trial for (a) un-inverted soil and (b) inverted soil. Different letters indicate significant differences between treatments for each soil depth ($p < 0.10$). Error bars indicate the standard error of the mean (SEM) ($n = 4$).

The effect of soil inversion on the average soil C concentration of the topsoil was only significant for treatments with large biochar particles, with inverted topsoil amended with large biochar (IL) having significantly lower soil C concentration than the un-inverted topsoil with similar biochar treatment (UL) ($P< 0.05$) (Table S6-2). This is opposed to the pattern observed in the average soil C concentration of the original subsoil layers of controls (UC, IC) and small-particle size treatments (US, IS), as this was higher ($P< 0.05$) when the layers were inverted (i.e., they became topsoil, as in IC and IS treatments) (Table S6-2). Also, for the N concentration and bulk density of the soil, there were no significant

differences detected regardless of soil inversion or the addition of biochar with different particle sizes (Figure S6-2 and Table S6-5). However, the fact that for a specific soil layer, e.g., un-inverted and inverted top soil, bulk density ranged between 0.84 to 1.00 g cm^{-3}, justified the need to calculate the C and N stocks on equivalent soil mass basis.

6.3.2 Changes in soil C and N stocks calculated at an equivalent soil mass by the end of the trial

The changes over time in soil C stocks (0-20 cm) calculated at an equivalent soil mass were shown in Figure 6-2. Prior to plant growth (T0), the soil C stock of the control treatments (UC and IC) was 61.7 Mg C ha^{-1}, with 59 and 41% of it being distributed in the 0–10 and 10–20 cm depth, respectively. At the end of the experiment, the non-amended treatments (UC and IC) lost 3.8 and 3.4 Mg C ha^{-1} (6.1 and 5.5% of the initial C stocks), respectively (significant at $P < 0.10$).

At T0, soil C stocks of biochar-amended soils increased from 61.7 to 77.3 Mg C ha^{-1}. By the end of the experiment, the US and UL treatments lost 2.90 (3.8%) and 5.10 (6.6%) Mg C ha^{-1} (significant at $P < 0.10$ for UL), respectively, and the IS and IL treatments lost 1.91 (2.5 %) and 9.20 (11.9%) Mg C ha^{-1} (significant $P < 0.05$ for IL), respectively.

The effect of biochar addition on the soil C stocks calculated at an equivalent soil mass of the overall 0-20 cm soil depth was, as expected, significant ($P< 0.001$) for all treatments when compared with the corresponding un-amended controls. However, the effect of biochar particle size on soil C stocks was only significant ($P < 0.05$) for the inverted soils, these being lower in the IL treatment than in the IS treatment. The effect of soil inversion when comparing between un-inverted soil and inverted soil amended, was also only

significant between treatments that received biochar with large particle size (UL vs IL) (P < 0.10) (Figure 6-2 and Table S6-6).

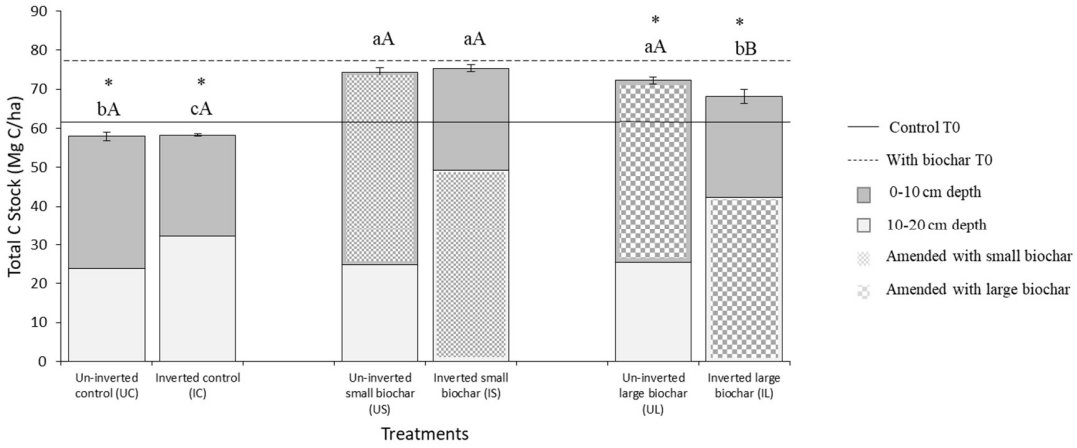

Figure 6-2. Soil C stocks calculated at an equivalent soil mass for the overall depth of 0 to 20 cm. Error bars indicate the standard error of the mean (SEM). The asterisk indicates significant differences between soil C stock measured at 0-20 cm by the end of the trial and their corresponding measurement at T0 ($p < 0.10$). Within a specific soil inversion, different small letters indicate differences in soil C stock between treatments ($n = 4$ and $p < 0.10$) while, within specific biochar treatment, different uppercase letters indicate differences between un-inverted and inverted treatments ($n = 4$ and $p < 0.10$).

The results on soil C stocks at an equivalent soil mass obtained separately according to layers (the topsoil or subsoil) are also provided (Table 6-3). The soil C stocks of both un-inverted and inverted topsoils amended with biochar were significantly higher ($P < 0.001$) than their respective controls. By inverting the topsoil, significantly lower soil C stocks ($P<0.10$) were measured for control (IC) and treatment with large biochar (IL) ($P<0.05$) than the un-inverted topsoil. The un-inverted subsoil from the treatment with large biochar (UL) was found to have significantly higher soil C stocks than the corresponding control (UC) ($P<0.10$), despite not having received any organic C amendment. The inverted subsoil from control (IC) and treatment with small biochar (IS) has significantly higher soil C stocks ($P<0.05$) than the un-inverted subsoil from the respective treatments (Table

6-3). For both un-inverted and inverted soils, no significant differences in total soil N stocks were found between treatments when calculated on an equivalent soil mass basis (Figure S6-3). This was expected given the low N content of the biochar.

Table 6-3. Soil C stock (Mg ha^{-1}) calculated at equivalent soil mass measured at 0-10 and 10-20 cm depth by the end of the experiment, with treatment or soil inversion as the factor.

	Treatments		
Soil Inversion (depth in the soil column)	Control	Small-particle size biochar	Large-particle size biochar
Un-inverted topsoil (at 0-10 cm depth)	34.0cA	49.5aA	46.7bA
Inverted topsoil (at 10-20 cm depth)	32.2cB	49.2aA	42.3bB
Un-inverted subsoil (at 10-20 cm depth)	23.9bB	24.9abB	25.5aA
Inverted subsoil (at 0-10 cm depth)	26.1aA	26.2aA	25.8aA

Different small letters within a row indicate differences between biochar treatments ($n = 4$) and $p < 0.10$), and (ii) different uppercase letters within a column indicate differences between un-inverted and inverted treatments ($n = 4$ and $p < 0.10$). In the un-inverted soil, biochar was at 0-10 cm depth while in the inverted soil biochar was at 10-20 cm depth.

6.3.3 NIR data

6.3.3.1 NIR spectra and PCA

Figure S6-4 (a) showed the averaged pre-processed NIR reflectance of un-inverted and inverted topsoil layers (at 0-10 cm depth for un-inverted treatments or 10-20 cm depth for inverted treatments). The un-inverted topsoil had overall lower spectral reflectance compared to the inverted topsoil, with soil layers amended with biochar having always a lower spectral reflectance than their respective controls, regardless of biochar particle size. The shape of the spectra was generally similar for all samples, with strong absorption bands around 1400 nm and 1900 nm, while weak yet noticeable bands around 1800 and

2200 nm (Figure S6-4a). Bands around 1400 nm can be attributed to overtones of O-H stretching bond, while around 1900 nm is the combination of H-O-H bend with O-H stretching (Clark, 1999). Both of these bands are associated with free water, as well as water contained in the lattice of various clay minerals or adsorbed to soil particle surfaces, either organic or inorganic (Clark et al., 1990). Small absorption peaks around 1800 and 2200 nm may be due to O-H bonds in clay minerals and organic compounds (Ben-Dor and Banin, 1995; Dalal and Henry, 1986).

A principal component analysis (PCA) of the pre-processed spectra was carried out (Figure S6-4b) and the first two principal components (PC1 and PC2) obtained accounted for around 89 and 5% of the total variance, respectively. Only samples amended with small-particle size biochar showed a clear different trend plotting in the upper right side of Quadrant I away from the rest of the samples, with clusters of samples from inverted soils plotting towards the lower right of Quadrant I. The separation between samples with the large particle size of biochar and controls was less distinct regardless of soil inversion, all plotting in the lower left side of the plot.

6.3.3.2 PLSR analysis for soil C concentration

Figure S6-4 (a) presents a summary of the statistics of soil organic C concentration for all soil layers from all treatments (n=144). The content of soil organic C ranges from a minimum of 1.68% to a maximum of 6.14% with a mean value of 3.39% and the median value of 2.75%. The soil C dataset was characterized by a positively skewed distribution (0.55). The calibration model obtained using the pre-processed NIR spectral data of all 144 samples (Calibration model 1; n=144) at wavelengths ranging between 780 to 2450 nm rendered a relatively good ability to predict the soil C concentration (%) with the

RMSE values of cross-validation being 0.56 % and the RPD values of 2.25 (Table 6-5). Models with RPD values > 2 are considered to be sufficient for quantitative prediction depending on the intended application of the model (Chang et al., 2001; Dunn et al., 2002; Viscarra Rossel et al., 2006). All other calibration models also have RPD values higher than 2, except for the model built using samples from treatments with large particle sizes biochar of both un-inverted and inverted soils (Calibration model 3; n=96; RPD=1.95; RMSEcv=0.55%). The calibration model 2 (n=96) built using samples from only small biochar of both un-inverted and inverted soil had the highest RPD (2.47) and the RMSEcv values (0.49%). This was followed by a model based on samples from inverted soils only (calibration model 5; n=72; RPD=2.42; RMSEcv=0.48%) and from un-inverted soils only (Calibration model 4; n=72; RPD=2.16; RMSEcv=0.62%).

Table 6-4. Statistical summary of the soil organic C concentration for all soil layers from all treatments**.**

Statistic	Data
Count	144
Minimum (%)	1.68
Maximum (%)	6.14
Mean (%)	3.39
Median (%)	2.75
Standard Deviation (%)	1.25
Skewness	0.55
Kurtosis	-1.25

Table 6-5. Partial least square regression (PLSR) calibration models for the prediction of soil C concentration (%).

Calibration model	Cores	No. of samples (samples with biochar)	No. of Factors for PLSR model	Leave-one-out-cross-validation (LOO-CV)		
				R^2	RMSECV (%)	RPD
1	All	144 (48)	6	0.803	0.556	2.25
2	Small biochar, both un-inverted and inverted soil	96 (24)	3	0.835	0.499	2.47
3	Large biochar, both un-inverted and inverted soil	96 (24)	3	0.736	0.549	1.95
4	Un-inverted	72 (24)	3	0.783	0.617	2.16
5	Inverted	72 (24)	4	0.827	0.485	2.42

*R^2: the coefficient of determination; RMSECV: root mean square error of LOO-CV; RPD: the ratio of prediction to deviation.

6.3.4 Comparison between measured and NIR/PLSR predicted soil C stock

The significant relationship between measured and NIR/PLSR predicted soil C stocks at equivalent soil mass of both topsoil and subsoil layers for each soil column (n=48) was shown using linear regression (R^2= 0.84; P= 0.013) (Figure 6-3a). Measured soil C stock values of each topsoil and subsoil layers were calculated using laboratory-measured soil C concentration, while the NIR/PLSR predicted soil C stock values were calculated using predicted C concentration obtained from Calibration Model 1. The sums of soil C stocks for both topsoil and subsoil layers for each soil column were used to calculate the overall

soil C stock at 0 to 20 cm depth. Both measured and NIR/PLSR predicted means of soil C stock (0-20 cm) for each treatment were shown in Figure 6-3b (and Table S6-7). None of the treatments showed significant differences between measured and predicted means, except for treatments of un-inverted soils amended with large particle size biochar (UL). The NIR/PLSR predicted mean for UL was significantly lower than the mean calculated using soil C data from laboratory analysis ($UL_{measured}$ = 72.2 Mg C ha^{-1}; $UL_{predicted}$ = 66.2 Mg C ha^{-1}; P=0.008). Prediction of soil C stock means for treatments amended with large-particle biochar were significantly lower compared to treatments with small particle biochar for both un-inverted and inverted soils (UL vs US; IL vs IS) (Figure 6-3b and Table S6-8). These results were slightly different from those obtained for soil C stocks calculated using laboratory-measured data, which showed that the effect of biochar particle size was only significant for treatments with inverted soils (Figure 6-2). Also, based on these predicted soil C stock values, the application of soil inversion had no significant effect across all treatments (Table S6-8).

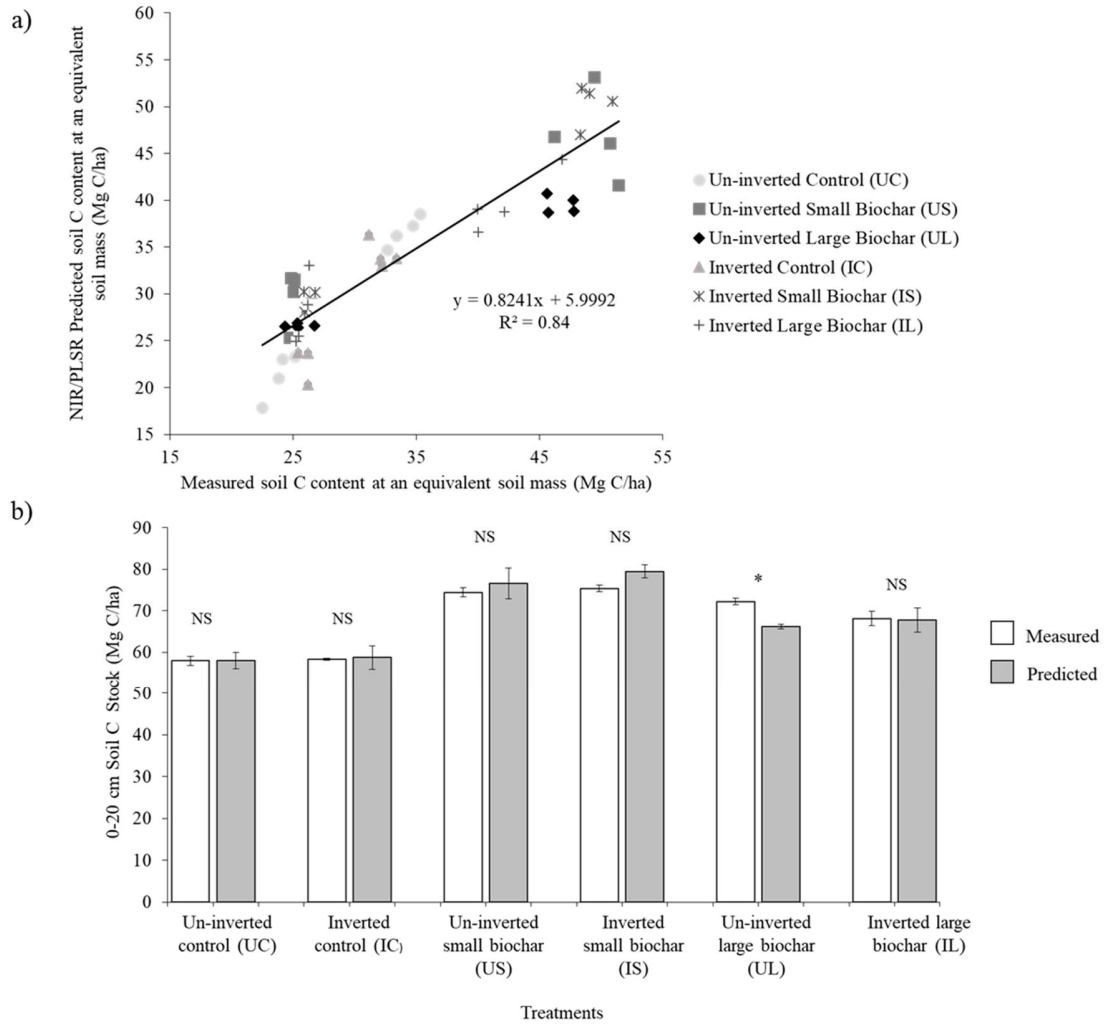

Figure 6-3. a) Relationship between measured and NIRS/PLSR predicted C stock calculated at equivalent soil mass for both topsoil and subsoil layers for each column (n=48); b) Comparison between measured and NIR/PLSR predicted means soil C stock (0-20 cm) for each treatment (n = 4 and $p < 0.05$). Error bars indicate the standard error of the mean (SEM).

6.4 Discussion

6.4.1 On changes in soil C (including soil non-oxidizable C) and soil N

The organic C lost by the end of the experiment observed in all treatments except for treatments with small-particle biochar (US & IS) (Figure 6-2) could be attributed to the

disturbance of the soil upon preparation of the columns (Franzluebbers, 1999; Kainiemi et al., 2016). The fact that there were greater losses in the treatment that received biochar of large particle size could be related to the fact that this is a heavy soil and the addition of a bulking agent increased aeration and accelerated the decomposition of available C (Dong et al., 2018; Mukherjee and Lal, 2013). The high soil organic C loss that occurred in the treatment with large biochar may also be caused by the constrained formation of soil aggregates due to the lower surface area of large particle biochar for soil-biochar interaction (Brodowski et al., 2006; Herath et al., 2013).

None of the treatments with small-particle biochar, either with or without inverted soil (IS and US, respectively) had a significant C loss over time, even when being compared with other treatments. The use of small-particle biochar could have affected soil aeration to a smaller extent, and thus the soil C decomposition in these treatments would have been lower than in the treatments that received large-particle biochar. Small-particle biochar might also have offered more sites for sorption of organic ligands due to its larger surface area compared to the large-particle biochar, which may have enhanced organic matter preservation in soil (Joseph et al., 2010; Liang et al., 2016; Singh and Cowie, 2014; Zimmerman et al., 2011). The use of large-particle biochar may have produced the opposite situation, which might explain the significant C loss observed from the treatment with inverted soil and amended with large particle biochar (IL) as compared with its corresponding treatment with small biochar (IS). The increased aeration from the addition of large biochar may lead to a higher C decomposition rate in biochar amended layers of IL at 13-16 and 16-20 cm depth. However, At the 10-13 cm layer, we suggest that there was a “boundary effect” causing the biochar layer located at the boundary with the non-

biochar soil to have higher water retention due to the changes in the water hydraulic conductivity of the soil column from the presence of biochar at depth (from soil inversion) (Mahmud et al., 2018; Yan et al., 2018). As a result, organic C decomposition in this 10-13 cm layer was possibly restricted due to the existence of anoxic conditions. Although in the previous finding of Mahmud et al. (2018), the accumulation of water at the contact zone was also found to be significant for the boundary layer of the US treatment (6-10 cm), the fact that no significant differences in soil C concentration were observed between biochar treatments at this particular layer (Figure 6-1a) suggests that the boundary effect from the addition of small-particle biochar was less pronounced. Therefore, despite the increase in water retention at the boundary layer, it had less impact on the existing soil C decomposition rate.

Interestingly, not only total soil organic C but also the non-oxidizable organic C concentrations of biochar layers at 13-16 and 16-20 cm depth in IL were significantly lower than their corresponding layers in IS. The non-oxidizable C concentration is the C fraction that is not oxidized by potassium dichromate ($K_2Cr_2O_7$) and commonly attributed to the recalcitrant fractions of biochar-C, although a fraction of native soil C can also be non-oxidizable with potassium dichromate, as it is the case of the soil under study here. The oxidizable C is associated with labile organic matter, including labile C in biochar (Leng et al., 2019). While it is possible that part of the non-oxidizable C of native organic matter decomposed over time, a non-oxidizable fraction of C in biochar might also have been lost – overall, this might explain the lower non-oxidizable C concentrations in the inverted soil layer with large-particle biochar compared with the corresponding treatment with small-particle biochar. Although it has been well accepted that biochar produced at

higher temperature has greater stability due to its highly condensed aromatic molecular structure, knowledge on its resistance toward chemical and biological degradation as a function of varying environment exposures, including biochar particle size, needs further study (Lehmann and Joseph, 2015). Other than the increased formation of oxygen-containing surface functional groups such as carboxyl and carbonyl groups over time as biochar weathers (Mia et al., 2017), the degradation of condensed aromatic C in biochar due to the environmental exposure has been observed and attributed to the increased rate of oxidation from higher oxygen availability (Ascough et al., 2018; Bird et al., 2017; Zimmermann et al., 2012). It is also worth mentioning that the biochar used in this study has been kept in a steel barrel for three years and moved to several locations after its production. Thus, it was expected that this biochar has been somewhat oxidized from the exposure to moisture from its varying surrounding areas prior to its application which possibly contributed further to its reduced resistance toward dichromate oxidation once exposed to the soil environment.

The C loss in IL treatment was also significantly higher than its corresponding un-inverted treatment (UL) (Figure 6-2). The fact that soil inversion had, in general, no effect when looking at the overall C stock (Figure 6-2) but when looking at the different layers (Table 6-3), the data shows that the new topsoil was gaining steady C input from growing plants while the new subsoil was losing probably the easily decomposable unprotected C (Mitchell et al., 2018; Six et al., 2002) which was in a steady condition when being in the topsoil from continuous new plant input but was disturbed once buried. This event was more pronounced when a bulking agent was added and further increase the C decomposition from greater soil aeration as suggested from the significantly greater C

loss in IL treatment. It was also possible that in biochar treatments with un-inverted soils (US and UL), the interactions between the new C inputs (from plant materials) with biochar particle promotes stabilization of the new C (Herath et al., 2014) whereas, this interaction was hindered in treatments with inverted soils (IS and IL).

Although we observed a trend of reduced bulk density with biochar application, the differences between biochar-amended and un-amended treatments were not significant. Therefore, we suggest that the significant C loss observed in the inverted soil amended with large biochar in this study was not solely due to greater soil aeration, as hypothesized earlier, but also to other factors such as the limited protective soil-biochar interactions associated with the lower surface area of large particle biochar and the interrupted C supply from new plant inputs due to soil inversion.

6.4.2 On NIR and further comparison between measured and NIR/PLSR predicted soil C stock

The lower reflectance (higher absorbance) of the un-inverted topsoil layers (from UC, US, and UL) compared with the inverted topsoil layers (from IC, IS, and IL) (Figure S6-4a) was attributed to the higher soil C content of the topsoil that kept receiving C input from plants and had high root density (Kusumo et al., 2011; Rodionov et al., 2016) as opposed to the inverted topsoil. In addition to the higher soil C content from direct plant input, biochar application further contributed to the reduced reflectance of the spectra (Kusumo et al., 2014). The distinct behavior of the small particle size treatments with regards to the NIR reflectance spectra compared with the rest of the treatments could be attributed to several factors. On one hand, the small-particle biochar allowed a good mixing with soil particles and thus other signals in the spectra of this soil layer were masked by the

presence of this biochar. This might explain the relatively flat spectra in the wavelength range of 780-1400 nm. Yet differences between US and IS treatments were also detected in the PCA plot (Figure S6-4b) and could reflect differences in fresh organic detritus, as the US treatment continued receiving plant C input (Viscarra Rossel and Webster, 2011).

Overall, the prediction accuracy obtained in this study were comparable with those reported in the literature on the prediction of soil C concentration using cross-validated NIR/PLSR model from fresh soil samples but done without biochar application (Kusumo et al., 2011; Ladoni et al., 2010; Roudier et al., 2015). We did not find published literature on the use of NIR spectroscopy on soil amended with biochar except by (i) Reeves et al. (2010) showed that the addition of biochar to soil may affect the NIR spectral signature of the original soil C, (ii) Allen & Laird (2013) and (iii) Uchimiya et al. (2019) who showed that NIRS combined with PLSR can be used to predict the total C of soils amended with biochar. In both studies done by Allen and Laird (2013) and Uchimiya et al. (2019), soil samples were air-dried and sieved prior to NIRS scanning and the range of NIR wavelength used was between 1100 to 2500 nm. Based on their cross-validated models, the RPD obtained in the study done by Allen and Laird (2013) for the prediction of organic C for soils collected from the field and the incubated soil columns without plants were 2.4 (RMSECV=0.23%) and 5.6 (RMSECV=0.10%), respectively, while in Uchimiya et al. (2019), the RMSECV was 0.14% and no RPD was given. Our results (Table 6-5) suggest that reliable predictions of C concentration for soils amended with biochar can be achieved even though the NIR spectra were recorded from fresh soil cores. However, the prediction accuracy may be negatively affected by an increasing biochar particle size. The larger the size the less evenly the biochar can be distributed in the soil

compared to the small particle size biochar, and this was not accurately "captured" by NIR. The prediction obtained from un-inverted soil samples (Calibration model 4), was also found to be lower than treatments with inverted soils. This may be caused by the higher presence of plant residues and roots in the un-inverted topsoil layers affected the spectral signal acquisition and increases the prediction uncertainty (Bellon-Maurel and McBratney, 2011). It was also possible that due to the similarity of some functional groups found in biochar C and in the soil organic matter (Reeves et al., 2008), the biochar C was being under-detected when it was present in the un-inverted soil with higher C content.

The above-mentioned reasons for decreased prediction accuracy may also explain the differences observed in soil C stocks estimates between the methods used (laboratory measurement vs. NIR/PLSR prediction). Particularly, the underestimation of C stocks in the UL treatment, where there was the co-existence of high plant residues, roots, and large particle size biochar (> 4 mm) Therefore, even if the organic C concentration of a given soil may be predicted using NIR with good accuracy, the need for this technique to be tested prior to an eventual determination of soil C stock is warranted. To our knowledge, only a few studies have used the NIR predicted soil C concentration to calculate the soil C stocks at a given depth. While none of these studies involves biochar-amended soil, our results are still comparable. A study by Roudier et al. (2015) – in which fresh soil cores were also extracted and scanned directly along the vertical side of the core – reported the feasibility of using NIR for *in-situ* measurement of soil C and the subsequent prediction of soil C stocks, yet they noted that the good performance of their model was due to the limited variability of their samples. Two recent studies by Guo et al. (2019) and Segnini

et al. (2019) also obtained good results, however, they both used dried, finely-ground, and sieved soil samples.

6.5 Conclusion

This study shows that biochar particle size and place of application can affect the decomposition rate of soil organic matter and therefore adequate information is needed prior to the use of this amendment. In this study, we observed that the combined effect of relatively large particle size (>4 mm) biochar and depth application via soil inversion accelerated the decomposition of native organic matter of a Pallic soil, which is characterized by having poor drainage. On the contrary, the surface application of the same biochar but with smaller particle size (<2 mm) did not prime the decomposition of native organic matter. Soil inversion *per se* did not seem to increase the rate of soil C loss in this study.

This study also showed the potential of using NIR spectroscopy technique to accurately predict the organic C concentration of a soil amended with biochar from intact soil cores, which would be both time- and cost-effective. We also explored the outcomes of using NIR predicted soil C concentration values to estimate soil C stocks. We found that although a good prediction accuracy for soil C concentration was achieved (Calibration model 1; n=144; RPD= 2.25; R^2 =0.803; RMSECV=0.56%), the errors introduced from the variations in treatment may propagate into the subsequent determination of soil C stocks resulting in slightly different conclusions than when laboratory-measured values were used. Further research especially in the field setting is needed to validate our findings.

CHAPTER 7. OVERALL SUMMARY AND RECOMMENDATIONS FOR FUTURE RESEARCH

7.1 Summary

Extensive research has been done to evaluate the use of biochar for C sequestration-climate mitigation and soil improvement. Yet, the outcomes are mixed and understanding of its mechanisms and factors is still lacking. The variability in the impact of biochar addition does not only depend on biochar properties (which is influenced by both feedstock and production conditions), but also on soil properties, presence of plants, application rate, land-use, including interactions between various factors and mechanisms (Woolf et al., 2018b). While several biochar-related properties (e.g. feedstock type, production temperature, application rate) and their interactions with other external factors (e.g. experiment setting, soil properties, plant inputs) have been given more attention in research, others possibly important parameters were often overlooked and insufficiently addressed (Cayuela et al., 2014; Lehmann and Joseph, 2015).

The increasingly widespread use of biochar also calls for better tools either to characterize biochar for standardization purposes or to measure the impact of its application to the soils. Near-infrared (NIR) spectroscopy is known as a rapid, cost-effective, non-destructive technique and can be used in both laboratory and on-site (Nocita et al., 2015a). Since NIR spectroscopy works well for soil and organic matter analysis, it would also be suitable for biochar-related studies.

This thesis highlights the importance of biochar particle size and application depth pertaining to the impact of biochar application to soil (i.e on N_2O soil emission and SOC stocks), including the use of NIR spectroscopy for predicting the maximum pyrolysis temperature of biochar and for SOC stock assessment.

7.1.1 The use of NIR model for predicting the maximum pyrolysis temperature of biochar (Chapter 3)

The hypothesis of this initial experiment was that the NIR spectroscopy can be used to predict the highest heating temperature achieved during biochar production. Eighty-two biochars have been used to build the NIR calibration model for predicting the highest heating temperature (HHT) during biochar production. These biochars were produced from animal manures, crop residues, nutshells, mixed waste, woody materials, and yard waste, at pyrolysis temperatures ranging between 220 to 800 °C. Sixty-eight biochars were produced using the slow pyrolysis technique, while the rest of them (n=14) were produced using other production techniques (ablative updraft pyrolysis, fast pyrolysis, intermediate pyrolysis, fixed bed gasification, torrefaction, and updraft pyrolysis). The partial least square regression (PLSR) analysis was carried out to build the calibration model by correlating the pre-processed NIR spectral data of 82 biochar with their reported HHT. A separate prediction set was prepared from twenty biochars produced from pine wood at HHT ranged from 325 to 723 °C using the slow pyrolysis technique in a small laboratory kiln, and were pyrolyzed in three different feedstock sizes. Both validations of calibration model using leave-one-out cross-validation (LOO-CV) and the prediction set yielded good accuracy (LOO-CV: r^2=0.80 and RMSECV:48.8 °C; prediction: r^2=0.82 and RMSEP: 57.7 °C; RMSE is the root mean square error). In this chapter, the ability of the NIR model to give good prediction despite the possible existence of temperature gradients attributed to the use of feedstock with different particle sizes was highlighted. These results indicate that NIR spectroscopy has the potential to be used as a monitoring and quality control tool for biochar production and thus confirmed the hypothesis that NIR

spectroscopy can be used to predict the highest heating temperature achieved during biochar production.

7.1.2 The effect of feedstock types and pyrolysis conditions on the predictive ability of NIR models (Chapter 4)

Three calibration models were developed in this chapter using three sample sets (A, B, and C) for predicting the highest heating temperature (HHT) during biochar production. We hypothesized that the varying feedstock types and pyrolysis conditions used for biochar production may decrease the performance of NIR prediction model due to the presence of data variability. Therefore, the performance of these calibration models was evaluated and compared to examine how feedstock types and pyrolysis conditions affect the efficiency of the NIR model.

Samples in set A includes the same 82 biochar samples described in Chapter 3. A subset of these 82 samples was selected as Set B (n=68) – these were all produced by slow pyrolysis and using the same pyrolyzer unit – in order to determine whether the prediction ability could be improved by reducing the variability of production conditions. Set C (n=48) is a subset of set B and was compiled by eliminating those biochar produced from "processed feedstocks" i.e. the type of feedstock that has been chemically or biologically treated thus the original composition of feedstock were changed such as food, paper, and the digested manure. This was done in order to determine whether the prediction ability could be improved by reducing the variability of production conditions. A separate sample set (n=18) was used as the prediction set. They were produced from animal manure (including mixtures of eucalyptus wood chips with either biosolids or cattle manure), crop

residue (corn stover), and woody materials (pine, poplar, and willow woodchips). The pyrolysis temperatures used ranged from 250 to 550 °C.

All three calibration models rendered a relatively good prediction ability with the overall RMSE values of cross-validation (RMSECV) being below 50 °C, whereas, when tested using the prediction set, calibration model based on set C gave the best prediction (R^2: 0.941; RMSEP: 27.3 °C), followed by the model based on set A (R^2: 0.896; RMSEP: 35.6 °C), and set B (R^2: 0.928; RMSEP: 37.3 °C). Based on the result, feedstock types have a substantial effect on the performance of the NIR model while the effect of pyrolysis conditions was less pronounced, and thus the hypothesis was confirmed.

7.1.3 The effect of soil inversion and the application of biochar with different particle sizes on soil N_2O emission

A paper from this study (Chapter 5) has been published: Mahmud, A. F., Camps-Arbestain, M., & Hedley, M. (2018). Investigating the Influence of Biochar Particle Size and Depth of Placement on Nitrous Oxide (N_2O) Emissions from Simulated Urine Patches. Agriculture, 8(11), 175.

In this glasshouse study, we investigate the effect of biochar particle size and the impact of soil inversion (through simulated mouldboard ploughing) on N_2O emissions from soils to which cattle urine was applied. We hypothesized that (i) the application of biochar may affect N_2O emissions through changes in soil physical properties, specifically soil aeration and water retention; and (ii) the effects of biochar addition on these properties may differ depending on their particle size (e.g., a larger particle size may increase soil aeration whereas a smaller particle size may clog pores), and their placement in soil (e.g., the incorporation of a large particle size-biochar at depth may promote aeration, drainage, and increase the depth of the plant rooting zone).

Pine wood biochar produced at HHT of 550 °C, crushed and sieved into two different particle sizes (<2 mm and >4 mm), were mixed into the 0-10 cm topsoil of Tokomaru silt loam (2% w/w or ~20 t ha^{-1}) and repacked into the soil column either at the original 0–10 cm depth (simulating incorporation by shallow tillage) or inverting the topsoil (simulating incorporation by mouldboard ploughing) and placing it at 10–20 cm depth. Overall, there were six treatments (2 control treatments) with four replicates for each treatment in this study. Annual ryegrass (*Lolium multiflorum* L.) was grown and was cut repeatedly to simulate cattle grazing and cattle urine was applied at the beginning of each trial (summer and autumn). Nitrous oxide emissions were monitored for every two to three days, up to seven weeks during the summer trial and measurements were repeated during the autumn trial. Based on the results, biochar addition did not cause significant differences in plant growth, N uptake, and soil bulk density, regardless of particle size or soil inversion. Also, no significant effect on N_2O emissions was observed in summer trial, whereas, the use of large particle size biochar in the inverted soil had a significant impact on increasing the cumulative N_2O emissions in the autumn trial, possibly through changes in the water hydraulic conductivity of the soil column and increased water retention at the boundary between soil layers. For the first part of the hypothesis, it was confirmed that the application of biochar affected the N_2O emissions through changes in soil physical properties i.e., soil aeration and water retention, however, the use of large particle biochar at depth provided opposite findings which were in contrast with the second part of the hypothesis.

In this study the importance of the role of biochar particle size and the method of biochar placement on soil physical properties and the implications of these on N_2O emissions was highlighted.

7.1.4 The effect of biochar particle size and placement on the decomposition rate of soil organic matter and the use of the NIR spectroscopy technique for soil C assessment.

In this study, we investigate the effect of biochar particle size and method of incorporation on SOC stocks. This study was done on the same experiment setup used in Chapter 5. We hypothesized that (i) the large-particle size biochar may affect soil aeration and accelerate soil C decomposition rate with increased oxygen availability, and this effect is greater when biochar is incorporated at depth; (ii) the NIR spectroscopy can be used to predict SOC concentration and SOC stocks in biochar-amended soil.

SOC stocks were estimated using two methodologies: direct SOC measurements using an elemental analyzer and NIR spectroscopy coupled with partial least-squares regression analysis (NIR/PLSR). The NIR spectra of soil were acquired by scanning intact soil cores using the NIR spectrometer. By the end of the experiment, significant C loss was observed in the treatment with inverted soil and amended with large-particle biochar (>4 mm), whereas none of the treatments with small-particle biochar (<2 mm), either with or without inverted soil had a significant C loss over time. We suggest that the combination of (i) greater soil aeration, (ii) the limited protective soil-biochar interactions associated with the lower surface area of large particle biochar, and (iii) the interrupted C supply from new plant inputs due to soil inversion, were the factors contributed to the significant C loss observed in the inverted soil amended with large biochar in this study. Soil

inversion *per se* did not seem to increase the rate of soil C loss in this study. Also, as expected, no significant differences in soil N were found between treatments given the low N content of the biochar.

Based on the result on the use of NIR-measured SOC concentration for estimating SOC stocks in the samples from the column experiment, reliable predictions of C concentration for soils amended with biochar can be achieved even though the NIR spectra were recorded from fresh soil cores (R^2 =0.803; RMSECV=0.56%). However, the prediction accuracy may be negatively affected by an increasing biochar particle size and soil inversion and thus may affect the subsequent SOC estimates. This study showed the potential of using NIR spectroscopy technique to accurately predict the SOC concentration of a soil amended with biochar from intact soil cores, which would be both time- and cost-effective.

The findings in this study support both hypotheses, however, further research especially in the field setting is needed to validate our findings.

The highlights of the thesis:

1) A calibration model was developed using NIR spectroscopy and PLSR to predict the maximum pyrolysis temperature of biochar (Chapter 3).
2) Feedstock types and pyrolysis conditions were shown to affect the predictive ability of NIR models for predicting the maximum pyrolysis temperature of biochar (Chapter 4).

3) A combination of large biochar and soil inversion was found to increase the cumulative N_2O emission from soils to which cattle urine was applied (Chapter 5).
4) The combined effect of using relatively large particle size (>4 mm) biochar and depth application via soil inversion accelerated the decomposition of native organic matter of Tokomaru soil (Chapter 6).
5) NIR spectroscopy technique can be used to predict SOC concentration of biochar-amended soil and has the potential to be used to estimate SOC stock (Chapter 6).

7.2 Recommendations for future research

1) The uncertainties associated with the use of diverse feedstocks types and production processes for biochar production may contribute to the conflicting impacts of biochar application to soil. Thus, there is a need for a feasible tool to control the quality and identify the suitability of biochar produced. The near-infrared (NIR) spectroscopy method proposed here has the potential to be integrated into biochar-related studies as it is a flexible yet reliable and rapid technique for biochar analysis, thus its uses should be further explored.
2) Information on every biochar parameter present in the study should be made available, so a comparison between studies can be made and the inconsistent effects of biochar can be addressed.
3) Many studies on the effect of biochar on N_2O emissions are done in the laboratory and in artificial conditions that do not consider the impact of biochar on soil drainage – as observed in this study. Future studies would need to take into account these changes and prioritise field measurements over laboratory incubations.

4) The manipulation of biochar properties post-production such as the crushing of biochar to produce the desired particle size prior to application and varying mixing depth into the soil are common and yet, its effect is rarely examined and thus should be given more attention.

References

4 per 1000 Initiative, 2015. The 4 per 1000 Initiative [WWW Document]. URL https://www.4p1000.org/ (accessed 4.26.19).

Abbruzzini, T.F., Moreira, M.Z., de Camargo, P.B., Conz, R.F., Cerri, C.E.P., 2017. Increasing Rates of Biochar Application to Soil Induce Stronger Negative Priming Effect on Soil Organic Carbon Decomposition. Agricultural Research. doi:10.1007/s40003-017-0281-7

Abella, S.R., Zimmer, B.W., 2007. Estimating Organic Carbon from Loss-On-Ignition in Northern Arizona Forest Soils. Soil Science Society of America Journal 71, 545–550. doi:10.2136/sssaj2006.0136

Aguiar, L., Márquez-Montesinos, F., Gonzalo, A., Sánchez, J.L., Arauzo, J., 2008. Influence of temperature and particle size on the fixed bed pyrolysis of orange peel residues. Journal of Analytical and Applied Pyrolysis 83, 124–130. doi:10.1016/j.jaap.2008.06.009

Allen, R.M., Laird, D.A., 2013. Quantitative Prediction of Biochar Soil Amendments by Near-Infrared Reflectance Spectroscopy. Soil Science Society of America Journal 77, 1784–1794. doi:DOI 10.2136/sssaj2013.03.0118

American Society of Agronomy, 2010. Self-Study Course Soil Science Step-by-Step Field Analysis Infiltration Rate , Hydraulic Conductivity , Preferential Flow. Crops and Soils Magazine 24–38.

Anca-Couce, A., 2016. Reaction mechanisms and multi-scale modelling of lignocellulosic biomass pyrolysis. Progress in Energy and Combustion Science 53, 41–79. doi:10.1016/j.pecs.2015.10.002

Andrade, C.R., Trugilho, P.F., Hein, P.R.G., Lima, J.T., Napoli, A., 2012. Near infrared spectroscopy for estimating eucalyptus charcoal properties. Journal of Near Infrared Spectroscopy 20, 657–666. doi:10.1255/jnirs.1028

Angst, T.E., Six, J., Reay, D.S., Sohi, S.P., 2014. Impact of pine chip biochar on trace greenhouse gas emissions and soil nutrient dynamics in an annual ryegrass system in California. Agriculture, Ecosystems and Environment 191, 17–26. doi:10.1016/j.agee.2014.03.009

Antal, M.J., Grønli, M., 2003. The Art, Science, and Technology of Charcoal Production. Industrial & Engineering Chemistry Research 42, 1619–1640. doi:10.1021/ie0207919

Ascough, P.L., Bird, M.I., Meredith, W., Snape, C., Large, D., Tilston, E., Apperley, D., Bernabé, A., Shen, L., 2018. Dynamics of Charcoal Alteration in a Tropical Biome: A Biochar-Based Study. Frontiers in Earth Science 6. doi:10.3389/feart.2018.00061

Ascough, P.L., Bird, M.I., Wormald, P., Snape, C.E., Apperley, D., 2008. Influence of production variables and starting material on charcoal stable isotopic and molecular characteristics. Geochimica et Cosmochimica Acta 72, 6090–6102. doi:10.1016/j.gca.2008.10.009

Atreya, A., Olszewski, P., Chen, Y., Baum, H.R., 2017. The effect of size, shape and pyrolysis conditions on the thermal decomposition of wood particles and firebrands. International Journal of Heat and Mass Transfer 107, 319–328. doi:10.1016/j.ijheatmasstransfer.2016.11.051

Bai, X., Huang, Y., Ren, W., Coyne, M., Jacinthe, P.A., Tao, B., Hui, D., Yang, J., Matocha, C., 2019. Responses of soil carbon sequestration to climate-smart agriculture practices: A meta-analysis. Global Change Biology 25, 2591–2606. doi:10.1111/gcb.14658

Bakken, L.R., Bergaust, L., Liu, B., Frostegård, Å., 2012. Regulation of denitrification at the cellular level: A clue to the understanding of N2O emissions from soils. Philosophical Transactions of the Royal Society B: Biological Sciences 367, 1226–1234. doi:10.1098/rstb.2011.0321

Baral, K.R., Thomsen, A.G., Olesen, J.E., Petersen, S.O., 2014. Controls of nitrous oxide emission after simulated cattle urine deposition. Agriculture, Ecosystems and Environment 188, 103–110. doi:10.1016/j.agee.2014.02.029

Barnes, R.T., Gallagher, M.E., Masiello, C.A., Liu, Z., Dugan, B., 2014. Biochar-Induced Changes in Soil Hydraulic Conductivity and Dissolved Nutrient Fluxes Constrained by Laboratory Experiments 9. doi:10.1371/journal.pone.0108340

Basso, A.S., Miguez, F.E., Laird, D.A., Horton, R., Westgate, M., 2013. Assessing potential of biochar for increasing water-holding capacity of sandy soils. GCB Bioenergy 5, 132–143. doi:10.1111/gcbb.12026

Bateman, E.J., Baggs, E.M., 2005. Contributions of nitrification and denitrification to N2O emissions from soils at different water-filled pore space. Biology and Fertility of Soils 41, 379–388. doi:10.1007/s00374-005-0858-3

Batjes, N.H., 2014. Total carbon and nitrogen in the soils of the world. European Journal of Soil Science 65, 10–21. doi:10.1111/ejss.12114_2

Bellon-Maurel, V., McBratney, A., 2011. Near-infrared (NIR) and mid-infrared (MIR) spectroscopic techniques for assessing the amount of carbon stock in soils - Critical review and research perspectives. Soil Biology and Biochemistry 43, 1398–1410. doi:10.1016/j.soilbio.2011.02.019

Ben-Dor, E., Banin, A., 1995. Near-Infrared Analysis as a Rapid Method to Simultaneously Evaluate Several Soil Properties. Soil Science Society of America Journal 59, 364. doi:10.2136/sssaj1995.03615995005900020014x

Bird, M.I., McBeath, A. V., Ascough, P.L., Levchenko, V.A., Wurster, C.M., Munksgaard, N.C., Smernik, R.J., Williams, A., 2017. Loss and gain of carbon during char degradation. Soil Biology and Biochemistry 106, 80–89. doi:10.1016/j.soilbio.2016.12.012

Blackwell, P., Riethmuller, G., Collins, M., 2009. Biochar application to soil. Biochar for Environmental Management: Science and Technology 1, 207–226.

Blakemore, L.C., 1987. Soil Bureau Laboratory Methods. A. Methods for chemical analysis of soils. NZ Soil Bureau Scientific Report 80, 44–45.

Blanco-Canqui, H., 2017. Biochar and Soil Physical Properties. Soil Science Society of

America Journal 81, 687. doi:10.2136/sssaj2017.01.0017

Blanco-Canqui, H., Laird, D.A., Heaton, E.A., Rathke, S., Acharya, B.S., 2020. Soil carbon increased by twice the amount of biochar carbon applied after 6 years: Field evidence of negative priming. GCB Bioenergy 12, 240–251. doi:10.1111/gcbb.12665

Borchard, N., Schirrmann, M., Cayuela, M.L., Kammann, C., Wrage-Mönnig, N., Estavillo, J.M., Fuertes-Mendizábal, T., Sigua, G., Spokas, K., Ippolito, J.A., Novak, J., 2019. Biochar, soil and land-use interactions that reduce nitrate leaching and N2O emissions: A meta-analysis. Science of the Total Environment 651, 2354–2364. doi:10.1016/j.scitotenv.2018.10.060

Brewer, C.E., Chuang, V.J., Masiello, C.A., Gonnermann, H., Gao, X., Dugan, B., Driver, L.E., Panzacchi, P., Zygourakis, K., Davies, C.A., 2014. New approaches to measuring biochar density and porosity. Biomass and Bioenergy 66, 176–185. doi:10.1016/j.biombioe.2014.03.059

Brodowski, S., Amelung, W., Haumaier, L., Abetz, C., Zech, W., 2005. Morphological and chemical properties of black carbon in physical soil fractions as revealed by scanning electron microscopy and energy-dispersive X-ray spectroscopy. Geoderma 128, 116–129. doi:10.1016/j.geoderma.2004.12.019

Brodowski, S., John, B., Flessa, H., Amelung, W., 2006. Aggregate-occluded black carbon in soil. European Journal of Soil Science 57, 539–546. doi:10.1111/j.1365-2389.2006.00807.x

Brunet, D., Bernoux, M., Barthès, B.G., 2008. Comparison between predictions of C and N contents in tropical soils using a Vis–NIR spectrometer including a fibre-optic probe versus a NIR spectrometer including a sample transport module. Biosystems Engineering 100, 448–452.

Bruun, E.W., Ambus, P., Egsgaard, H., Hauggaard-Nielsen, H., 2012. Effects of slow and fast pyrolysis biochar on soil C and N turnover dynamics. Soil Biology and Biochemistry 46, 73–79. doi:10.1016/j.soilbio.2011.11.019

Bruun, E.W., Müller-Stöver, D., Ambus, P., Hauggaard-Nielsen, H., 2011. Application of biochar to soil and N2O emissions: Potential effects of blending fast-pyrolysis biochar with anaerobically digested slurry. European Journal of Soil Science 62, 581–589. doi:10.1111/j.1365-2389.2011.01377.x

Burns, D.A., Ciurczak, E.W. (Eds.), 2007. Handbook of Near-Infrared Analysis, third. ed. CRC Press.

Buss, W., Mašek, O., 2014. Mobile organic compounds in biochar – A potential source of contamination – Phytotoxic effects on cress seed (Lepidium sativum) germination. Journal of Environmental Management 137, 111–119. doi:10.1016/j.jenvman.2014.01.045

Calvelo Pereira, R., Arbestain, M.C., Sueiro, M.V., Macia-Agullo, J.A., 2015. Assessment of the surface chemistry of wood-derived biochars using wet chemistry, Fourier transform infrared spectroscopy and X-ray photoelectron spectroscopy. Soil Research 53, 753–762. doi:10.1071/SR14194

Calvelo Pereira, R., Hedley, M., Camps Arbestain, M., Wisnubroto, E., Green, S., Saggar, S., Kusumo, B.H., Mahmud, A.F., 2016. Net changes of soil C stocks in two grassland soils 26 months after simulated pasture renovation including biochar addition. GCB Bioenergy 8. doi:10.1111/gcbb.12271

Calvelo Pereira, R., Kaal, J., Camps Arbestain, M., Pardo Lorenzo, R., Aitkenhead, W., Hedley, M., Macías, F., Hindmarsh, J., Maciá-Agulló, J.A., 2011a. Contribution to characterisation of biochar to estimate the labile fraction of carbon. Organic Geochemistry 42, 1331–1342. doi:10.1016/j.orggeochem.2011.09.002

Calvelo Pereira, R., Kaal, J., Camps Arbestain, M., Pardo Lorenzo, R., Aitkenhead, W., Hedley, M., Macías, F., Hindmarsh, J., Maciá-Agulló, J.A., 2011b. Contribution to characterisation of biochar to estimate the labile fraction of carbon. Organic Geochemistry 42, 1331–1342. doi:10.1016/j.orggeochem.2011.09.002

Calvelo Pereira, R., Wisnubroto, E., Hedley, M.J., Camps Arbestain, M., Green, S., Saggar, S., n.d. Can a deep application of biochar mitigate a pulse of greenhouse gas emissions after a fertilizer application to mature pastures?

Camps-Arbestain, M., Amonette, J.E., Singh, B., Wang, T., Schmidt, H.P., 2015. A biochar classification system and associated test methods. Biochar for Environmental Management: Science, Technology and Implementation 165–193.

Cantrell, K.B., Hunt, P.G., Uchimiya, M., Novak, J.M., Ro, K.S., 2012. Impact of pyrolysis temperature and manure source on physicochemical characteristics of biochar. Bioresource Technology 107, 419–428. doi:10.1016/j.biortech.2011.11.084

Carter, M.., 2007. Contribution of nitrification and denitrification to N 2 O emissions from urine patches. Soil Biology and Biochemistry 39, 2091–2102. doi:10.1016/j.soilbio.2007.03.013

Case, S.D.C., McNamara, N.P., Reay, D.S., Whitaker, J., 2012. The effect of biochar addition on N 2O and CO 2 emissions from a sandy loam soil - The role of soil aeration. Soil Biology and Biochemistry 51, 125–134. doi:10.1016/j.soilbio.2012.03.017

Cayuela, M.L., Jeffery, S., van Zwieten, L., 2015. The molar H: Corg ratio of biochar is a key factor in mitigating N2O emissions from soil. Agriculture, Ecosystems & Environment 202, 135–138.

Cayuela, M.L., Sanchez-Monedero, M.A., Roig, A., Hanley, K., Enders, A., Lehmann, J., 2013. Biochar and denitrification in soils: when, how much and why does biochar reduce N(2)O emissions? Scientific Reports 3, 1732. doi:10.1038/srep01732

Cayuela, M.L., van Zwieten, L., Singh, B.P., Jeffery, S., Roig, A., S??nchez-Monedero, M.A., 2014. Biochar's role in mitigating soil nitrous oxide emissions: A review and meta-analysis. Agriculture, Ecosystems and Environment 191, 5–16. doi:10.1016/j.agee.2013.10.009

Chang, C.-W., Laird, D.A., 2002. Near-infrared reflectance spectroscopic analysis of soil C and N. Soil Science 167, 110–116.

Chang, C.-W., Laird, D.A., Mausbach, M.J., Hurburgh, C.R., 2001. Near-Infrared Reflectance Spectroscopy–Principal Components Regression Analyses of Soil

Properties. Soil Science Society of America Journal 65, 480–490. doi:10.2136/sssaj2001.652480x

Chapuis-lardy, L., Wrage, N., Metay, A., Chotte, J.L., Bernoux, M., 2007. Soils, a sink for N 2 O? A review. Global Change Biology 13, 1–17. doi:10.1111/j.1365-2486.2006.01280.x

Charlton, J.F.L., Stewart, a V, 1999. Pasture species and cultivars used in New Zealand – a list. Proceedings of the New Zealand Grassland Association 61, 147–166.

Chen, H., Pan, T., Chen, J., Lu, Q., 2011. Waveband selection for NIR spectroscopy analysis of soil organic matter based on SG smoothing and MWPLS methods. Chemometrics and Intelligent Laboratory Systems 107, 139–146. doi:10.1016/j.chemolab.2011.02.008

Chen, J., Kim, H., Yoo, G., 2015. Effects of biochar addition on CO2 and N2O emissions following fertilizer application to a cultivated grassland soil. PLoS ONE 10, 1–17. doi:10.1371/journal.pone.0126841

Chen, W., Meng, J., Han, X., Lan, Y., Zhang, W., 2019. Past, present, and future of biochar. Biochar 1, 75–87. doi:10.1007/s42773-019-00008-3

Chenu, C., Angers, D.A., Barré, P., Derrien, D., Arrouays, D., Balesdent, J., 2019. Increasing organic stocks in agricultural soils: Knowledge gaps and potential innovations. Soil and Tillage Research 188, 41–52. doi:10.1016/j.still.2018.04.011

Chintala, R., Mollinedo, J., Schumacher, T.E., Malo, D.D., Julson, J.L., 2014. Effect of biochar on chemical properties of acidic soil. Archives of Agronomy and Soil Science 60, 393–404. doi:10.1080/03650340.2013.789870

Clark, R.N., 1999. Spectroscopy of rocks and minerals, and principles of spectroscopy. Manual of Remote Sensing 3, 2.

Clark, R.N., King, T.V. V, Klejwa, M., Swayze, G.A., Vergo, N., 1990. High spectral resolution reflectance spectroscopy of minerals. Journal of Geophysical Research: Solid Earth 95, 12653–12680.

Clough, T.J., 2018. Personal Communication.

Clough, T.J., Bertram, J.E., Ray, J.L., Condron, L.M., O'Callaghan, M., Sherlock, R.R., Wells, N.S., 2010. Unweathered Wood Biochar Impact on Nitrous Oxide Emissions from a Bovine-Urine-Amended Pasture Soil. Soil Science Society of America Journal 74, 852–860. doi:10.2136/Sssaj2009.0185

Clough, T.J., Condron, L.M., Kammann, C., Müller, C., 2013. A Review of Biochar and Soil Nitrogen Dynamics. Agronomy 3, 275–293. doi:10.3390/agronomy3020275

Costa, A.C.P.R., Ramalho, F.M.G., Ribeiro, L.C., Trugilho, P.F., Hein, P.R.G., 2019. Classification of commercial charcoal for domestic use by near infrared spectroscopy. Biomass and Bioenergy 127, 105280. doi:10.1016/j.biombioe.2019.105280

Costa, L.R., Trugilho, P.F., Hein, P.R.G., 2018. Evaluation and classification of eucalypt charcoal quality by near infrared spectroscopy. Biomass and Bioenergy 112, 85–92. doi:10.1016/j.biombioe.2018.02.017

Criscuoli, I., Alberti, G., Baronti, S., Favilli, F., Martinez, C., Calzolari, C., Pusceddu, E., Rumpel, C., Viola, R., Miglietta, F., 2014. Carbon sequestration and fertility after centennial time scale incorporation of charcoal into soil. PLoS ONE 9, 1–11. doi:10.1371/journal.pone.0091114

Cui, J., Ge, T., Kuzyakov, Y., Nie, M., Fang, C., Tang, B., Zhou, C., 2017. Interactions between biochar and litter priming: A three-source 14C and d13C partitioning study. Soil Biology and Biochemistry 104, 49–58. doi:10.1016/j.soilbio.2016.10.014

Dalal, R.C., Henry, R.J., 1986. Simultaneous Determination of Moisture, Organic Carbon, and Total Nitrogen by Near Infrared Reflectance Spectrophotometry1. Soil Science Society of America Journal 50, 120. doi:10.2136/sssaj1986.03615995005000010023x

Dane, J.H., Hopmans, J.H., 2002. Water retention and storage. p. 671–717. JH Dane and GC Topp (ed.) Methods of soil analysis. Part 4. SSSA Book Ser. 5. SSSA, Madison, WI. Water Retention and Storage. p. 671–717. In JH Dane and GC Topp (Ed.) Methods of Soil Analysis. Part 4. SSSA Book Ser. 5. SSSA, Madison, WI.

Davis, M.R., Alves, B.J.R., Karlen, D.L., Kline, K.L., Galdos, M., Abulebdeh, D., 2018. Review of soil organic carbon measurement protocols: A US and Brazil comparison and recommendation. Sustainability (Switzerland) 10, 4–8. doi:10.3390/su10010053

Davrieux, F., Rousset, P.L.A., Pastore, T.C.M., De Macedo, L.A., Quirino, W.F., 2010. Discrimination of native wood charcoal by infrared spectroscopy. Quimica Nova 33, 1093–1097. doi:10.1590/S0100-40422010000500016

de Figueiredo, C.C., Chagas, J.K.M., da Silva, J., Paz-Ferreiro, J., 2019. Short-term effects of a sewage sludge biochar amendment on total and available heavy metal content of a tropical soil. Geoderma 344, 31–39.

de Klein, C.A.., Logtesjin, R.S.P. van, 1994. Denitrification and N20 emission from urine-affected grassland soil. Plant and Soil 163, 235–241.

de Klein, C.A.M., Ledgard, S.F., 2005. Nitrous oxide emissions from New Zealand agriculture–key sources and mitigation strategies. Nutrient Cycling in Agroecosystems 72, 77–85.

de Klein, C.A.M., Sherlock, R.R., Cameron, K.C., 2001. Nitrous oxide emissions from agricultural soils in New Zealand — A review of current knowledge and directions for future research. Journal of the Royal Society of New Zealand 31, 37–41. doi:10.1080/03014223.2001.9517667

De Muñiz, G.I.B., Carneiro, M.E., Nisgoski, S., Ramirez, M.G.L., Magalhães, W.L.E., 2013. SEM and NIR characterization of four forest species charcoal. Wood Science and Technology 47, 815–823. doi:10.1007/s00226-013-0539-6

De Vos, B., Vandecasteele, B., Deckers, J., Muys, B., 2005. Capability of loss-on-ignition as a predictor of total organic carbon in non-calcareous forest soils. Communications in Soil Science and Plant Analysis 36, 2899–2921. doi:10.1080/00103620500306080

Deiss, L., Franzluebbers, A.J., de Moraes, A., 2017. Soil texture and organic carbon fractions predicted from near-infrared spectroscopy and geostatistics. Soil Science

Society of America Journal 81, 1222–1234.

Demirbas, A., Arin, G., 2002. An Overview of Biomass Pyrolysis. Energy Sources 24, 471–482. doi:10.1080/00908310252889979

Di Blasi, C., 2008. Modeling chemical and physical processes of wood and biomass pyrolysis. Progress in Energy and Combustion Science 34, 47–90. doi:10.1016/j.pecs.2006.12.001

Di Blasi, C., Branca, C., Galgano, A., D'Agostino, P., 2015. Thermal Behavior of Beech Wood during Sulfuric Acid Catalyzed Pyrolysis. Energy and Fuels 29, 6476–6484. doi:10.1021/acs.energyfuels.5b01315

Di Blasi, C., Branca, C., Lombardi, V., Ciappa, P., Giacomo, C. Di, 2013. Effects of Particle Size and Density on the Packed-Bed Pyrolysis of Wood. Energy and Fuels 27, 6781–6791.

Di Blasi, C., Branca, C., Sarnataro, F.E., Gallo, A., 2014. Thermal Runaway in the Pyrolysis of Some Lignocellulosic Biomasses. Energy and Fuels 28, 2684–2696.

Dignac, M., Derrien, D., Barré, P., Barot, S., Cécillon, L., Chenu, C., Chevallier, T., Freschet, G.T., Garnier, P., Guenet, B., Hedde, M., Klumpp, K., Lashermes, G., Maron, P., Nunan, N., Roumet, C., Basile-doelsch, I., 2017. Increasing soil carbon storage : mechanisms , effects of agricultural practices and proxies . A review. Agronomy for Sustainable Development 37, 14. doi:10.1007/s13593-017-0421-2

Ding, F., Van Zwieten, L., Zhang, W., Weng, Z. (Han), Shi, S., Wang, J., Meng, J., 2018. A meta-analysis and critical evaluation of influencing factors on soil carbon priming following biochar amendment. Journal of Soils and Sediments 18, 1507–1517. doi:10.1007/s11368-017-1899-6

Dong, X., Singh, B.P., Li, G., Lin, Q., Zhao, X., 2018. Biochar application constrained native soil organic carbon accumulation from wheat residue inputs in a long-term wheat-maize cropping system. Agriculture, Ecosystems and Environment 252, 200–207. doi:10.1016/j.agee.2017.08.026

Dunn, B.W., Batten, G.D., Beecher, H.G., Ciavarella, S., 2002. The potential of near-infrared reflectance spectroscopy for soil analysis—a case study from the Riverine Plain of south-eastern Australia. Animal Production Science 42, 607–614.

Ellert, B.H., Bettany, J.R., 1995. Calculation of organic matter and nutrients stored in soils under contrasting management regimes. Canadian Journal of Soil Science 75, 529–538.

Ellert, B.H., Janzen, H.H., VandenBygaart, A.J., Bremer, E., 2007. Measuring Change in Soil Organic Carbon Storage, in: Soil Sampling and Methods of Analysis. pp. 25–38.

Enders, A., Hanley, K., Whitman, T., Joseph, S., Lehmann, J., 2012. Characterization of biochars to evaluate recalcitrance and agronomic performance. Bioresource Technology 114, 644–653. doi:10.1016/j.biortech.2012.03.022

Enders, A., Lehmann, J., 2012. Comparison of Wet-Digestion and Dry-Ashing Methods for Total Elemental Analysis of Biochar. Communications in Soil Science and Plant Analysis 43, 1042–1052. doi:10.1080/00103624.2012.656167

England, J.R., Rossel, R.A.V., 2018. Proximal sensing for soil carbon accounting. Soil 4, 101–122. doi:10.5194/soil-4-101-2018

Esbensen, K.H., Guyot, D., Westad, F., Houmoller, L.P., 2002. Multivariate data analysis: in practice: an introduction to multivariate data analysis and experimental design. CAMO Process AS, Oslo, Norway.

European Biochar Certificate, 2012. European Biochar Certificate- Guidelines for a Sustainable Production of Biochar. doi:10.13140/RG.2.1.4658.7043

European Biochar Certificate (EBC), 2016. European Biochar Certificate-Guidelines for a Sustainable Production of Biochar. European Biochar Foundation (EBC) 1–22. doi:10.13140/RG.2.1.4658.7043

Fang, Y., Singh, B.P., Matta, P., Cowie, A.L., Van Zwieten, L., 2017. Temperature sensitivity and priming of organic matter with different stabilities in a Vertisol with aged biochar. Soil Biology and Biochemistry 115, 346–356. doi:10.1016/j.soilbio.2017.09.004

FAO, 2019. Measuring and modelling soil carbon stocks and stock changes in livestock production systems: Guidelines for assessment (Version 1). Livestock Environmental Assessment and Performance (LEAP) Partnership. doi:Licence: CC BY-NC-SA 3.0 IGO.

FAO, 2015. Revised World Soil Charter [WWW Document]. Food and Agriculture Organization. doi:10.1016/s0378-777x(82)80097-8

Felber, R., Leifeld, J., 2013. Nitrous oxide emission reduction with greenwaste biochar : Comparison of laboratory and field experiments. doi:10.1111/ejss.12093

Franzluebbers, A.J., 1999. Potential C and N mineralization and microbial biomass from intact and increasingly disturbed soils of varying texture. Soil Biology and Biochemistry 31, 1083–1090. doi:10.1016/S0038-0717(99)00022-X

Fu, P., Hu, S., Xiang, J., Sun, L., Su, S., Wang, J., 2012. Evaluation of the porous structure development of chars from pyrolysis of rice straw: Effects of pyrolysis temperature and heating rate. Journal of Analytical and Applied Pyrolysis 98, 177–183.

Fuss, S., Lamb, W.F., Callaghan, M.W., Hilaire, J., Creutzig, F., Amann, T., Beringer, T., De Oliveira Garcia, W., Hartmann, J., Khanna, T., Luderer, G., Nemet, G.F., Rogelj, J., Smith, P., Vicente, J.V., Wilcox, J., Del Mar Zamora Dominguez, M., Minx, J.C., 2018. Negative emissions - Part 2: Costs, potentials and side effects. Environmental Research Letters 13. doi:10.1088/1748-9326/aabf9f

Gani, A., Naruse, I., 2007. Effect of cellulose and lignin content on pyrolysis and combustion characteristics for several types of biomass. Renewable Energy 32, 649–661. doi:10.1016/j.renene.2006.02.017

Gonzaga, M.I.S., Mackowiak, C., de Almeida, A.Q., de Carvalho Junior, J.I.T., Andrade, K.R., 2018. Positive and negative effects of biochar from coconut husks, orange bagasse and pine wood chips on maize (Zea mays L.) growth and nutrition. Catena 162, 414–420.

Graber, E.R., Harel, Y.M., Kolton, M., Cytryn, E., Silber, A., David, D.R., Tsechansky, L., Borenshtein, M., Elad, Y., 2010. Biochar impact on development and

productivity of pepper and tomato grown in fertigated soilless media. Plant and Soil 337, 481–496. doi:10.1007/s11104-010-0544-6

Graves, D., 2013. A comparison of methods to apply biochar into temperate soils, in: Ladygina, N., Rineau, F. (Eds.), Biochar and Soil Biota. CRC Press, pp. 202–260. doi:10.1097/01.prs.0000475744.10344.1e

Gregory, S.J., Anderson, C.W.N., Camps Arbestain, M., McManus, M.T., 2014. Response of plant and soil microbes to biochar amendment of an arsenic-contaminated soil. Agriculture, Ecosystems and Environment 191, 133–141. doi:10.1016/j.agee.2014.03.035

Guizani, C., Jeguirim, M., Valin, S., Limousy, L., Salvador, S., 2017. Biomass chars: The effects of pyrolysis conditions on their morphology, structure, chemical properties and reactivity. Energies 10. doi:10.3390/en10060796

Guo, L., Chen, Y., Shi, T., Zhao, C., Liu, Y., Wang, S., Zhang, H., 2017. Exploring the Role of the Spatial Characteristics of Visible and Near-Infrared Reflectance in Predicting Soil Organic Carbon Density. ISPRS International Journal of Geo-Information 6, 308. doi:10.3390/ijgi6100308

Guo, L., Zhang, H., Shi, T., Chen, Y., Jiang, Q., Linderman, M., 2019. Prediction of soil organic carbon stock by laboratory spectral data and airborne hyperspectral images. Geoderma 337, 32–41. doi:10.1016/j.geoderma.2018.09.003

Haider, G., Steffens, D., Müller, C., Kammann, C., 2017. Biochar may physically entrap nitrate during field aging or co-composting which become plant available under controlled conditions, in: EGU General Assembly Conference Abstracts. p. 15274.

Hale, S.E., Lehmann, J., Rutherford, D., Zimmerman, A.R., Bachmann, R.T., Shitumbanuma, V., O'Toole, A., Sundqvist, K.L., Arp, H.P.H., Cornelissen, G., 2012. Quantifying the total and bioavailable polycyclic aromatic hydrocarbons and dioxins in biochars. Environmental Science and Technology 46, 2830–2838. doi:10.1021/es203984k

Han, L., Sun, K., Yang, Y., Xia, X., Li, F., Yang, Z., Xing, B., 2020. Biochar's stability and effect on the content, composition and turnover of soil organic carbon. Geoderma 364, 114184. doi:10.1016/j.geoderma.2020.114184

Harsh, J.B., Abu-lail, N.I., Fortuna, A., 2016. Influence of feedstock source and pyrolysis temperature on biochar bulk and surface properties. Biomass and Bioenergy 84, 37–48. doi:10.1016/j.biombioe.2015.11.010

Hasan, M.D.M., Hu, X., Gunawan, R., Li, C., 2017. Pyrolysis of large mallee wood particles : Temperature gradients within a pyrolysing particle and effects of moisture content. Fuel Processing Technology 158, 163–171. doi:10.1016/j.fuproc.2016.12.018

Heincke, M., Kaupenjohann, M., 1999. Effects of soil solution on the dynamics of N2O emissions: a review. Nutrient Cycling in Agroecosystems 55, 133–157.

Herath, H.M.S.K., Camps-arbestain, M., Hedley, M., 2013. Effect of biochar on soil physical properties in two contrasting soils : An Alfisol and an Andisol. Geoderma 209–210, 188–197. doi:10.1016/j.geoderma.2013.06.016

Herath, H.M.S.K., Camps-Arbestain, M., Hedley, M., Van Hale, R., Kaal, J., 2014. Fate of biochar in chemically- and physically-defined soil organic carbon pools. Organic Geochemistry 73, 35–46. doi:10.1016/j.orggeochem.2014.05.001

Herath, H.M.S.K., Camps-Arbestain, M., Hedley, M.J., Kirschbaum, M.U.F., Wang, T., van Hale, R., 2015. Experimental evidence for sequestering C with biochar by avoidance of CO2 emissions from original feedstock and protection of native soil organic matter. GCB Bioenergy 7, 512–526. doi:10.1111/gcbb.12183

Hernandez-Soriano, M.C., Kerré, B., Goos, P., Hardy, B., Dufey, J., Smolders, E., 2016. Long-term effect of biochar on the stabilization of recent carbon: Soils with historical inputs of charcoal. GCB Bioenergy 8, 371–381. doi:10.1111/gcbb.12250

Hewitt, A., Dymond, J., 2013. Survey of New Zealand Soil Orders. Ecosystem Services in New Zealand: Conditions and Trends 121–131.

Hillel, D., 1998. 14. Entry of Water into Soil, in: Environmental Soil Physics: Fundamentals, Applications, and Environmental Considerations. Elsevier, p. 385.

Hina, K., Bishop, P., Arbestain, M.C., Calvelo-Pereira, R., MacIá-Agulló, J.A., Hindmarsh, J., Hanly, J.A., MacÍas, F., Hedley, M.J., 2010. Producing biochars with enhanced surface activity through alkaline pretreatment of feedstocks. Australian Journal of Soil Research 48, 606–617. doi:10.1071/SR10015

Hutengs, C., Seidel, M., Oertel, F., Ludwig, B., Vohland, M., 2019. In situ and laboratory soil spectroscopy with portable visible-to-near-infrared and mid-infrared instruments for the assessment of organic carbon in soils. Geoderma 355. doi:10.1016/j.geoderma.2019.113900

Igalavithana, A.D., Mandal, S., Niazi, N.K., Vithanage, M., Parikh, S.J., Mukome, F.N.D., Rizwan, M., Oleszczuk, P., Al-Wabel, M., Bolan, N., Tsang, D.C.W., Kim, K.H., Ok, Y.S., 2017. Advances and future directions of biochar characterization methods and applications. Critical Reviews in Environmental Science and Technology 47, 2275–2330. doi:10.1080/10643389.2017.1421844

International Biochar Initiative, 2015. Standardized Product Definition and Product Testing Guidelines for Biochar That Is Used in Soil. International Biochar Initiative 23. doi:http://www.biochar-international.org/characterizationstandard. 22

International Biochar Initiative, 2012. Standardized Product Definition and Product Testing Guidelines for Biochar that is Used in Soil.

IPCC, 2019. 2019 Refinement to the 2006 IPCC Guidelines for National Greenhouse Gas Inventories.

IPCC, 2006. 2006 IPCC Guidelines for National Greenhouse Gas Inventories, Prepared by the National Greenhouse Gas Inventories Programme.

Isadora, E., Pereira, P., Conz, R.F., 2019. Biochar Enhances Nitrous Oxide Reduction in Acidic but Not in Near-Neutral pH Soil. Soil Systems 3, 69.

Jahirul, M.I., Rasul, M.G., Chowdhury, A.A., Ashwath, N., 2012. Biofuels Production through Biomass Pyrolysis—A Technological Review. Energies 5, 4952–5001. doi:10.3390/en5124952

Jeffery, S., Verheijen, F.G.A., Kammann, C., Abalos, D., 2016. Biochar effects on methane emissions from soils: A meta-analysis. Soil Biology and Biochemistry 101, 251–258. doi:10.1016/j.soilbio.2016.07.021

Jensen, J., Frear, C., Ma, J., Kruger, C., Hummel, R., Yorgey, G., 2016. Digested Fiber Solids: Methods for Adding Value.

Jestel, N.L., 2010. Raman spectroscopy, in: Process Analytical Technology: Spectroscopic Tools and Implementation Strategies for the Chemical and Pharmaceutical Industries. John Wiley & Sons, Ltd, New York., pp. 195–243.

Jindo, K., Mizumoto, H., Sawada, Y., Sanchez-Monedero, M.A., Sonoki, T., 2014. Physical and chemical characterization of biochars derived from different agricultural residues. Biogeosciences 11, 6613–6621.

Jones, D.L., Rousk, J., Edwards-Jones, G., DeLuca, T.H., Murphy, D. V., 2012. Biochar-mediated changes in soil quality and plant growth in a three year field trial. Soil Biology and Biochemistry 45, 113–124. doi:10.1016/j.soilbio.2011.10.012

Jones, S.K., Famulari, D., Di Marco, C.F., Nemitz, E., Skiba, U.M., Rees, R.M., Sutton, M.A., 2011. Nitrous oxide emissions from managed grassland: A comparison of eddy covariance and static chamber measurements. Atmospheric Measurement Techniques 4, 2179–2194. doi:10.5194/amt-4-2179-2011

Joseph, S., Graber, E.R., Chia, C., Munroe, P., Donne, S., Thomas, T., Nielsen, S., Marjo, C., Rutlidge, H., Pan, G., Li, L., Taylor, P., Rawal, a, Hook, J., 2013. Shifting paradigms: development of high-efficiency biochar fertilizers based on nano-structures and soluble components. Carbon Management 4, 323–343. doi:10.4155/cmt.13.23

Joseph, S.D., Camps-Arbestain, M., Lin, Y., Munroe, P., Chia, C.H., Hook, J., Van Zwieten, L., Kimber, S., Cowie, A., Singh, B.P., Lehmann, J., Foidl, N., Smernik, R.J., Amonette, J.E., 2010. An investigation into the reactions of biochar in soil. Australian Journal of Soil Research 48, 501–515. doi:10.1071/SR10009

Kaal, J., Schneider, M.P.W., Schmidt, M.W.I., 2012. Rapid molecular screening of black carbon (biochar) thermosequences obtained from chestnut wood and rice straw: A pyrolysis-GC/MS study. Biomass and Bioenergy 45, 115–129. doi:10.1016/j.biombioe.2012.05.021

Kainiemi, V., Kirchmann, H., Kätterer, T., 2016. Structural disruption of arable soils under laboratory conditions causes minor respiration increases. Journal of Plant Nutrition and Soil Science 179, 88–93. doi:10.1002/jpln.201500139

Kammann, C., Ippolito, J., Hagemann, N., Borchard, N., Cayuela, M.L., Estavillo, J.M., Fuertes-Mendizabal, T., Jeffery, S., Kern, J., Novak, J., Rasse, D., Saarnio, S., Schmidt, H.P., Spokas, K., Wrage-Mönnig, N., 2017. Biochar as a tool to reduce the agricultural greenhouse-gas burden–knowns, unknowns and future research needs. Journal of Environmental Engineering and Landscape Management 25, 114–139. doi:10.3846/16486897.2017.1319375

Kammann, C., Ratering, S., Eckhard, C., Muller, C., 2012. Biochar and Hydrochar Effects on Greenhouse Gas (Carbon Dioxide, Nitrous Oxide, and Methane) Fluxes from

Soils. Journal of Environmental Quality 41, 1052–1066. doi:10.2134/jeq2011.0132

Kammann, C.I., Schmidt, H.P., Messerschmidt, N., Linsel, S., Steffens, D., Müller, C., Koyro, H.W., Conte, P., Stephen, J., 2015. Plant growth improvement mediated by nitrate capture in co-composted biochar. Scientific Reports 5, 1–13. doi:10.1038/srep11080

Kamruzzaman, M., Elmasry, G., Sun, D.W., Allen, P., 2011. Application of NIR hyperspectral imaging for discrimination of lamb muscles. Journal of Food Engineering 104, 332–340. doi:10.1016/j.jfoodeng.2010.12.024

Kan, T., Strezov, V., Evans, T.J., 2016a. Lignocellulosic Biomass Pyrolysis : A Review of Product Properties and Effects of Pyrolysis Parameters and effects of pyrolysis parameters. Renewable and Sustainable Energy Reviews 57, 1126–1140. doi:10.1016/j.rser.2015.12.185

Kan, T., Strezov, V., Evans, T.J., 2016b. Lignocellulosic biomass pyrolysis: A review of product properties and effects of pyrolysis parameters. Renewable and Sustainable Energy Reviews 57, 1126–1140. doi:10.1016/j.rser.2015.12.185

Kang, H., Gao, H., Yu, W., 2017. Evaluation of spectral pretreatments, spectral range, and regression methods for quantitative spectroscopic analysis of soil organic carbon composition. Spectroscopy Letters 50, 143–149.

Kanouo, B.M.D., Allaire, S.E., Munson, A.D., 2019. Quantifying the influence of eucalyptus bark and corncob biochars on the physico-chemical properties of a tropical oxisol under two soil tillage modes. International Journal of Recycling of Organic Waste in Agriculture 1–14.

Kawano, S., 2008. Application to agricultural products and foodstuffs, in: Near-Infrared Spectroscopy: Principles, Instruments, Applications. pp. 269–284.

Keiluweit, M., Nico, P.S., Johnson, M.G., Kleber, M., 2010. Dynamic molecular structure of plant biomass-derived black carbon (biochar). Environmental Science and Technology 44, 1247–1253.

Keith, A., Singh, B., Dijkstra, F.A., 2015. Biochar reduces the rhizosphere priming effect on soil organic carbon. Soil Biology and Biochemistry 88, 372–379. doi:10.1016/j.soilbio.2015.06.007

Kerré, B., Hernandez-Soriano, M.C., Smolders, E., 2016. Partitioning of carbon sources among functional pools to investigate short-term priming effects of biochar in soil: A 13C study. Science of the Total Environment 547, 30–38. doi:10.1016/j.scitotenv.2015.12.107

Khalil, M.I., Baggs, E.M., 2005. CH4 oxidation and N2O emissions at varied soil water-filled pore spaces and headspace CH4 concentrations. Soil Biology and Biochemistry 37, 1785–1794. doi:10.1016/j.soilbio.2005.02.012

Knadel, M., Gislum, R., Hermansen, C., Peng, Y., Moldrup, P., de Jonge, L.W., Greve, M.H., 2017. Comparing predictive ability of laser-induced breakdown spectroscopy to visible near-infrared spectroscopy for soil property determination. Biosystems Engineering 156, 157–172. doi:10.1016/j.biosystemseng.2017.01.007

Kuang, B., Mouazen, A.M., 2011. On-the-go soil sensing – results of field measurement

in a UK farm. Precision Agriculture 12, 585–591.

Kusumo, B., Arbestain, M., Mahmud, A., Hedley, M., Hedley, C., Pereira, R., Wang, T., Singh, B., 2014. Assessing biochar stability indices using near infrared spectroscopy. Journal of Near Infrared Spectroscopy 22, 313–328. doi:10.1255/jnirs.1125

Kusumo, B.H., Hedley, M.J., Hedley, C.B., Arnold, G.C., Tuohy, M.P., 2010. Predicting pasture root density from soil spectral reflectance: Field measurement. European Journal of Soil Science 61, 1–13. doi:10.1111/j.1365-2389.2009.01199.x

Kusumo, B.H., Hedley, M.J., Hedley, C.B., Hueni, A., Arnold, G.C., Tuohy, M.P., 2009. The use of Vis-NIR spectral reflectance for determining root density: Evaluation of ryegrass roots in a glasshouse trial. European Journal of Soil Science 60, 22–32. doi:10.1111/j.1365-2389.2008.01093.x

Kusumo, B.H., Hedley, M.J., Hedley, C.B., Tuohy, M.P., 2011. Measuring carbon dynamics in field soils using soil spectral reflectance: Prediction of maize root density, soil organic carbon and nitrogen content. Plant and Soil 338, 233–245. doi:10.1007/s11104-010-0501-4

Ladoni, M., Bahrami, H.A., Alavipanah, S.K., Norouzi, A.A., 2010. Estimating soil organic carbon from soil reflectance: A review. Precision Agriculture 11, 82–99. doi:10.1007/s11119-009-9123-3

Laird, D., Flemming, P., Wang, B., Horton, R., Karlen, D., 2010. Biochar impact on nutrient leaching from a Midwestern agricultural soil. Geoderma 158, 436–442. doi:10.1016/j.geoderma.2010.05.012

Lal, R., 2018. Digging deeper: A holistic perspective of factors affecting soil organic carbon sequestration in agroecosystems. Global Change Biology 24, 3285–3301. doi:10.1111/gcb.14054

Lal, R., 2008. Carbon sequestration in soil. CAB Reviews: Perspectives in Agriculture, Veterinary Science, Nutrition and Natural Resources 3. doi:10.1079/PAVSNNR20083030

Lehmann, J., 2007. A handful of carbon. Nature 447, 143–144.

Lehmann, J., Joseph, S. (Eds.), 2015. Biochar for Environmental Management: Science, Technology and Implementation Second Edition. Biochar for Environmental Management. doi:10.4324/9781849770552

Leng, L., Huang, H., 2018. An overview of the effect of pyrolysis process parameters on biochar stability. Bioresource Technology 270, 627–642. doi:10.1016/j.biortech.2018.09.030

Leng, L., Huang, H., Li, H., Li, J., Zhou, W., 2019. Biochar stability assessment methods: A review. Science of the Total Environment 647, 210–222. doi:10.1016/j.scitotenv.2018.07.402

Lestander, T.A., Rudolfsson, M., Pommer, L., Nordin, A., 2014. NIR provides excellent predictions of properties of biocoal from torrefaction and pyrolysis of biomass. Green Chemistry 16, 4906–4913. doi:10.1039/c3gc42479k

Li, A.M., Li, X.D., Li, S.Q., Ren, Y., Chi, Y., Yan, J.H., Cen, K.F., 1999. Pyrolysis of

solid waste in a rotary kiln: Influence of final pyrolysis temperature on the pyrolysis products. Journal of Analytical and Applied Pyrolysis 50, 149–162. doi:10.1016/S0165-2370(99)00025-X

Li, S., Chen, G., 2018. Thermogravimetric, thermochemical, and infrared spectral characterization of feedstocks and biochar derived at different pyrolysis temperatures. Waste Management 78, 198–207. doi:10.1016/j.wasman.2018.05.048

Li, S., Harris, S., Anandhi, A., Chen, G., 2019. Predicting biochar properties and functions based on feedstock and pyrolysis temperature: A review and data syntheses. Journal of Cleaner Production 215, 890–902. doi:10.1016/j.jclepro.2019.01.106

Liang, C., Gascó, G., Fu, S., Méndez, A., Paz-Ferreiro, J., 2016. Biochar from pruning residues as a soil amendment: Effects of pyrolysis temperature and particle size. Soil and Tillage Research 164, 3–10. doi:10.1016/j.still.2015.10.002

Liaw, S.B., Wu, H., 2015. Tuning Biochar Properties via Partial Gasification: Facilitating Inorganic Nutrients Recycling and Altering Organic Matter Leaching. Energy and Fuels 29, 4407–4417. doi:10.1021/acs.energyfuels.5b01020

Lim, T.J., Spokas, K.A., Feyereisen, G., Novak, J.M., 2016. Predicting the impact of biochar additions on soil hydraulic properties. Chemosphere 142, 136–144. doi:10.1016/j.chemosphere.2015.06.069

Linsler, D., Sawallisch, A., Höper, H., Schmidt, H., Vohland, M., Ludwig, B., 2017. Near-infrared spectroscopy for determination of soil organic C, microbial biomass C and C and N fractions in a heterogeneous sample of German arable surface soils. Archives of Agronomy and Soil Science 63, 1499–1509.

Liu, Q., Zhang, Y., Liu, B., Amonette, J.E., Lin, Z., Liu, G., Ambus, P., Xie, Z., 2018. How does biochar influence soil N cycle? A meta-analysis. Plant and Soil 426, 211–225. doi:10.1007/s11104-018-3619-4

Liu, S., Zhang, Y., Zong, Y., Hu, Z., Wu, S., Zhou, J., Jin, Y., Zou, J., 2016. Response of soil carbon dioxide fluxes, soil organic carbon and microbial biomass carbon to biochar amendment: A meta-analysis. GCB Bioenergy 8, 392–406. doi:10.1111/gcbb.12265

Liu, Y., Chen, Y., Wang, Y., Lu, H., He, L., Yang, S., 2018. Negative priming effect of three kinds of biochar on the mineralization of native soil organic carbon. Land Degradation and Development 29, 3985–3994. doi:10.1002/ldr.3147

Liu, Z., Dugan, B., Masiello, C.A., Barnes, R.T., Gallagher, M.E., Gonnermann, H., 2016. Impacts of Biochar Concentration and Particle Size on Hydraulic Conductivity and DOC Leaching of Biochar-Sand Mixtures. Journal of Hydrology 533, 461–472.

Ludwig, B., Khanna, P.K., Bauhus, J., Hopmans, P., 2002. Near infrared spectroscopy of forest soils to determine chemical and biological properties related to soil sustainability. Forest Ecology and Management 171, 121–132.

Luo, J., Lindsey, S.B., Ledgard, S.F., 2008. Nitrous oxide emissions from application of urea on New Zealand pasture. Biology and Fertility of Soils 44, 463–470. doi:10.1007/s00374-007-0228-4

Luo, Y., Durenkamp, M., De Nobili, M., Lin, Q., Brookes, P.C., 2011. Short term soil

priming effects and the mineralisation of biochar following its incorporation to soils of different pH. Soil Biology and Biochemistry 43, 2304–2314. doi:10.1016/j.soilbio.2011.07.020

Maestrini, B., Herrmann, A.M., Nannipieri, P., Schmidt, M.W.I., Abiven, S., 2014. Ryegrass-derived pyrogenic organic matter changes organic carbon and nitrogen mineralization in a temperate forest soil. Soil Biology and Biochemistry 69, 291–301. doi:10.1016/j.soilbio.2013.11.013

Maestrini, B., Nannipieri, P., Abiven, S., 2015. A meta-analysis on pyrogenic organic matter induced priming effect. GCB Bioenergy 7, 577–590. doi:10.1111/gcbb.12194

Mahmud, A., Camps-Arbestain, M., Hedley, M., 2018. Investigating the Influence of Biochar Particle Size and Depth of Placement on Nitrous Oxide (N2O) Emissions from Simulated Urine Patches. Agriculture 8, 175. doi:10.3390/agriculture8110175

Majumder, S., Neogi, S., Dutta, T., Powel, M.A., Banik, P., 2019. The impact of biochar on soil carbon sequestration: Meta-analytical approach to evaluating environmental and economic advantages. Journal of Environmental Management 250, 109466. doi:10.1016/j.jenvman.2019.109466

Masiello, C.A., Dugan, B., Brewer, C.E., Spokas, K.A., Novak, J.M., Liu, Z., Sorrenti, G., 2015. Biochar effects on soil hydrology, in: Biochar for Environmental Management. Routledge, pp. 543–562.

McDonald-Wharry, J., Manley-Harris, M., Pickering, K., 2013. Carbonisation of biomass-derived chars and the thermal reduction of a graphene oxide sample studied using Raman spectroscopy. Carbon 59, 383–405. doi:10.1016/j.carbon.2013.03.033

Mia, S., Dijkstra, F.A., Singh, B., 2017. Long-Term Aging of Biochar: A Molecular Understanding With Agricultural and Environmental Implications, 1st ed, Advances in Agronomy. Elsevier Inc. doi:10.1016/bs.agron.2016.10.001

Miller, J.M., Miller, J.C., 2010. Statistics and Chemometrics for Analytical Chemistry, 6th Editio. ed. Pearson Education. doi:10.1198/tech.2004.s248

Ministry for the Environment, 2019a. New Zealand's Fourth Biennial Report under the United Nations Framework Convention on Climate Change.

Ministry for the Environment, 2019b. New Zealand's Greenhouse Gas Inventory 1990-2017.

Ministry for the Environment, 2018a. New Zealand's Greenhouse Gas Inventory 1990-2016 [WWW Document]. URL https://www.mfe.govt.nz/sites/default/files/media/Climate Change/National GHG Inventory Report 1990-2016-final.pdf (accessed 9.30.18).

Ministry for the Environment, 2018b. About New Zealand's Emissions Reduction Targets [WWW Document]. URL https://www.mfe.govt.nz/climate-change/what-government-doing/emissions-reduction-targets/about-our-emissions-reduction (accessed 9.30.18).

Mitchell, E., Scheer, C., Rowlings, D., Conant, R.T., Cotrufo, M.F., Grace, P., 2018. Amount and incorporation of plant residue inputs modify residue stabilisation dynamics in soil organic matter fractions. Agriculture, Ecosystems and Environment

256, 82–91. doi:10.1016/j.agee.2017.12.006

Mørkved, P.T., Dörsch, P., Bakken, L.R., 2007. The N2O product ratio of nitrification and its dependence on long-term changes in soil pH. Soil Biology and Biochemistry 39, 2048–2057.

Moron, A., Cozzolino, D., 2004. Determination of potentially mineralizable nitrogen and nitrogen in particulate organic matter fractions in soil by visible and near-infrared reflectance spectroscopy. The Journal of Agricultural Science 142, 335–343.

Mouazen, A.M., De Baerdemaeker, J., Ramon, H., 2005a. Towards development of on-line soil moisture content sensor using a fibre-type NIR spectrophotometer. Soil and Tillage Research 80, 171–183. doi:10.1016/j.still.2004.03.022

Mouazen, A.M., Karoui, R., De Baerdemaeker, J., Ramon, H., 2005b. Classification of soil texture classes by using soil visual near infrared spectroscopy and factorial discriminant analysis techniques. Journal of near Infrared Spectroscopy 13, 231–240.

Mukherjee, A., Lal, R., 2013. Biochar Impacts on Soil Physical Properties and Greenhouse Gas Emissions. Agronomy 3, 313–339. doi:10.1016/S0268-0890(99)90085-3

Mukome, F.N.D., Six, J., Parikh, S.J., 2013. The effects of walnut shell and wood feedstock biochar amendments on greenhouse gas emissions from a fertile soil. Geoderma 200–201, 90–98. doi:10.1016/j.geoderma.2013.02.004

Nassau, K., 2001. The physics and chemistry of color: the fifteen causes of color. The Physics and Chemistry of Color: The Fifteen Causes of Color, 2nd Edition, by Kurt Nassau, Pp. 496. ISBN 0-471-39106-9. Wiley-VCH, July 2001. 496.

Nayak, A.K., Rahman, M.M., Naidu, R., Dhal, B., Swain, C.K., Nayak, A.D., Tripathi, R., Shahid, M., Islam, M.R., Pathak, H., 2019. Current and emerging methodologies for estimating carbon sequestration in agricultural soils: A review. Science of the Total Environment 665, 890–912. doi:10.1016/j.scitotenv.2019.02.125

Nelissen, V., Saha, B.K., Ruysschaert, G., Boeckx, P., 2014. Effect of different biochar and fertilizer types on N2O and NO emissions. Soil Biology and Biochemistry 70, 244–255. doi:10.1016/j.soilbio.2013.12.026

Ngo, P.T., Rumpel, C., Thu, T.D., Henry-Des-Tureaux, T., Dang, D.K., Jouquet, P., 2014. Use of organic substrates for increasing soil organic matter quality and carbon sequestration of tropical degraded soil: A 3-year mesocosms experiment. Carbon Management 5, 155–168. doi:10.1080/17583004.2014.912868

Nocita, M., Stevens, A., van Wesemael, B., Aitkenhead, M., Bachmann, M., Barthès, B., Dor, E. Ben, Brown, D.J., Clairotte, M., Csorba, A., Dardenne, P., Demattê, J.A.M., Genot, V., Guerrero, C., Knadel, M., Montanarella, L., Noon, C., Ramirez-Lopez, L., Robertson, J., Sakai, H., Soriano-Disla, J.M., Shepherd, K.D., Stenberg, B., Towett, E.K., Vargas, R., Wetterlind, J., 2015a. Soil Spectroscopy: An Alternative to Wet Chemistry for Soil Monitoring. Advances in Agronomy 132, 139–159. doi:10.1016/bs.agron.2015.02.002

Nocita, M., Stevens, A., van Wesemael, B., Brown, D.J., Shepherd, K.D., Towett, E., Vargas, R., Montanarella, L., 2015b. Soil spectroscopy: An opportunity to be seized.

Global Change Biology 21, 10–11. doi:10.1111/gcb.12632

Novak, J.M., Lima, I.M., Xing, B., Gaskin, J.W., Steiner, C., Das, K.C., Ahmedna, M., Rehrah, D., Watts, D.W., Busscher, W.J., Schomberg, H., 2009. Characterization of designer biochar produced at different temperatures and their effects on a loamy sand. Annals of Environmental Science 3, 195–206.

Obia, A., Cornelissen, G., Mulder, J., Dörsch, P., 2015. Effect of soil pH increase by biochar on NO, N 2 O and N 2 production during denitrification in acid soils. PLoS ONE 10, 1–19. doi:10.1371/journal.pone.0138781

Omondi, M.O., Xia, X., Nahayo, A., Liu, X., Korai, P.K., Pan, G., 2016. Quantification of biochar effects on soil hydrological properties using meta-analysis of literature data. Geoderma 274, 28–34.

Ouyang, L., Wang, F., Tang, J., Yu, L., Zhang, R., 2013. Effects of biochar amendment on soil aggregates and hydraulic properties. Journal of Plant Nutrition and Soil Science 13, 991–1002. doi:10.2136/sssaj2012.0180

Paetsch, L., Mueller, C.W., Kögel-Knabner, I., Von Lützow, M., Girardin, C., Rumpel, C., 2018. Effect of in-situ aged and fresh biochar on soil hydraulic conditions and microbial C use under drought conditions. Scientific Reports 8, 1–11. doi:10.1038/s41598-018-25039-x

Palansooriya, K.N., Wong, J.T.F., Hashimoto, Y., Huang, L., Rinklebe, J., Chang, S.X., Bolan, N., Wang, H., Ok, Y.S., 2019. Response of microbial communities to biochar-amended soils: a critical review. Biochar 1, 3–22. doi:10.1007/s42773-019-00009-2

Panwar, N.L., Pawar, A., Salvi, B.L., 2019. Comprehensive review on production and utilization of biochar. SN Applied Sciences 1, 1–19. doi:10.1007/s42452-019-0172-6

Pariyar, P., Kumari, K., Jain, M.K., Jadhao, P.S., 2020. Evaluation of change in biochar properties derived from different feedstock and pyrolysis temperature for environmental and agricultural application. Science of the Total Environment 713. doi:10.1016/j.scitotenv.2019.136433

Park, W.C., Atreya, A., Baum, H.R., 2010. Experimental and theoretical investigation of heat and mass transfer processes during wood pyrolysis. Combustion and Flame 157, 481–494. doi:10.1016/j.combustflame.2009.10.006

Paustian, K., Collier, S., Baldock, J., Burgess, R., Creque, J., DeLonge, M., Dungait, J., Ellert, B., Frank, S., Goddard, T., Govaerts, B., Grundy, M., Henning, M., Izaurralde, R.C., Madaras, M., McConkey, B., Porzig, E., Rice, C., Searle, R., Seavy, N., Skalsky, R., Mulhern, W., Jahn, M., 2019. Quantifying carbon for agricultural soil management: from the current status toward a global soil information system. Carbon Management 10, 567–587. doi:10.1080/17583004.2019.1633231

Peng, X., Shi, T., Song, A., Chen, Y., Gao, W., 2014. Estimating soil organic carbon using VIS/NIR spectroscopy with SVMR and SPA methods. Remote Sensing 6, 2699–2717. doi:10.3390/rs6042699

Rajkovich, S., Enders, A., Hanley, K., Hyland, C., Zimmerman, A.R., Lehmann, J., 2012. Corn growth and nitrogen nutrition after additions of biochars with varying

properties to a temperate soil. Biology and Fertility of Soils 48, 271–284. doi:10.1007/s00374-011-0624-7

Ramalho, F.M.G., Hein, P.R.G., Andrade, J.M., Napoli, A., 2017. Potential of Near-Infrared Spectroscopy for Distinguishing Charcoal Produced from Planted and Native Wood for Energy Purpose. Energy and Fuels 31, 1593–1599. doi:10.1021/acs.energyfuels.6b02446

Rayment, G.E., Higginson, F.R., 1992. Australian laboratory handbook of soil and water chemical methods. Inkata Press Pty Ltd.

Reeves, J.B., Iii, a, B, N.P.S.F., C, N.C., 2010. Spectral effects of biochar on NIR and mid-IR spectra of soil / char mixtures. 19th World Congress of Soil Science, Soil Solutions for a Changing World 8, 98–101.

Reeves, J.B., McCarty, G.W., Rutherford, D.W., Wershaw, R.L., 2008. Mid-infrared diffuse reflectance spectroscopic examination of charred pine wood, bark, cellulose, and lignin: Implications for the quantitative determination of charcoal in soils. Applied Spectroscopy 62, 182–189. doi:10.1366/000370208783575618

Reeves, J.B., McCarty, G.W., Rutherford, D.W., Wershaw, R.L., 2007. Near infrared spectroscopic examination of charred pine wood, bark, cellulose and lignin: implications for the quantitative determination of charcoal in soils. Journal of Near Infrared Spectroscopy 15, 307–315.

Ripberger, G.D., Jones, J.R., Paterson, A.H.J., Holt, R., 2015. Is it possible to produce biochar at different highest treatment temperatures in the pyrolysis range?-The exothermic nature of pyrolysis., in: Asia Pacific Confederation of Chemical Engineering Congress 2015: APCChE 2015, Incorporating CHEMECA 2015. Melbourne: Engineers Australia, 2015, pp. 1950–1957.

Robertson, G.P., Tiedje, J.M., 1984. Denitrification and Nitrous Oxide Production in Successional and Old-Growth Michigan Forests. Soil Science Society of America Journal 48, 383–389. doi:10.2136/sssaj1984.03615995004800020032x

Rodionov, A., Pätzold, S., Welp, G., Pude, R., Amelung, W., 2016. Proximal field Vis-NIR spectroscopy of soil organic carbon: A solution to clear obstacles related to vegetation and straw cover. Soil and Tillage Research 163, 89–98. doi:10.1016/j.still.2016.05.008

Rogovska, N., Laird, D., Cruse, R., Fleming, P., Parkin, T., Meek, D., 2011. Impact of biochar on manure carbon stabilization and greenhouse gas emissions. Soil Science Society of America Journal 75, 871–879. doi:10.2136/sssaj2010.0270

Ronsse, F., Dickinson, D., Prins, W., 2013. Production and characterization of slow pyrolysis biochar : Influence of feedstock type and pyrolysis conditions Production and characterization of slow pyrolysis biochar : influence of feedstock type and pyrolysis conditions. GCB Bioenergy 5, 104–115. doi:10.1111/gcbb.12018

Rose, T.J., Keen, B., Morris, S.G., Quin, P., Rust, J., Kearney, L., Kimber, S., Van Zwieten, L., 2016. Application of woody biochar and woody mulch to mitigate nitrous oxide emissions from a poultry litter-amended soil in the subtropics. Agriculture, Ecosystems and Environment 228, 1–8.

doi:10.1016/j.agee.2016.05.004

Roudier, P., Hedley, C.B., Ross, C.W., 2015. Prediction of volumetric soil organic carbon from field-moist intact soil cores. European Journal of Soil Science 1–10. doi:10.1111/ejss.12259

Saarnio, S., Heimonen, K., Kettunen, R., 2013. Biochar addition indirectly affects N2O emissions via soil moisture and plant N uptake. Soil Biology and Biochemistry 58, 99–106. doi:10.1016/j.soilbio.2012.10.035

Saggar, S., Andrew, R., Tate, K.R., Rodda, N., Hedley, C.B., Townsend, J.A., 2004. Modelling nitrous oxide emissions from New Zealand grazed pastures. Nutrient Cycling in Agroecosystems 68, 243–255.

Saleh, M.E., Mahmoud, A.H., Rashad, M., 2012. Peanut biochar as a stable adsorbent for removing NH4-N from wastewater: A preliminary study. Advances in Environmental Biology 6, 2170–2176.

Sanderman, J., Hengl, T., Fiske, G.J., 2018. Soil carbon debt of 12,000 years of human land use. Proceedings of the National Academy of Sciences 115, E1700–E1700. doi:10.1073/pnas.1800925115

Santos, L.B., Striebeck, M. V., Crespi, M.S., Ribeiro, C.A., De Julio, M., 2015. Characterization of biochar of pine pellet. Journal of Thermal Analysis and Calorimetry 122, 21–32. doi:10.1007/s10973-015-4740-8

Sarkhot, D. V., Grunwald, S., Ge, Y., Morgan, C.L.S., 2011. Comparison and detection of total and available soil carbon fractions using visible/near infrared diffuse reflectance spectroscopy. Geoderma 164, 22–32. doi:10.1016/j.geoderma.2011.05.006

Savitzky, A., Golay, M.J., 1964. Smoothing and differentiation of data by simplified least squares procedures. Analytical Chemistry 36, 1627–1639.

Schimmelpfennig, S., Müller, C., Grünhage, L., Koch, C., Kammann, C., 2014. Biochar, hydrochar and uncarbonized feedstock application to permanent grassland-Effects on greenhouse gas emissions and plant growth. Agriculture, Ecosystems and Environment 191, 39–52. doi:10.1016/j.agee.2014.03.027

Schmidt, M.W.I., Hilf, M.D., Wiesenberg, G.L.B., 2017. 15 Analysis of biochars using benzene polycarboxylic acids, in: Biochar: A Guide to Analytical Methods. CSIRO PUBLISHING, p. 162.

Schneider, M.P.W., Hilf, M., Vogt, U.F., Schmidt, M.W.I., 2010. The benzene polycarboxylic acid (BPCA) pattern of wood pyrolyzed between 200??C and 1000??C. Organic Geochemistry 41, 1082–1088. doi:10.1016/j.orggeochem.2010.07.001

Schulte, E.E., Hoskins, B., 1995. Recommended Soil Organic Matter Tests. Recommended Soil Testing Procedures for the North Eastern USA.

Schwanninger, M., Rodrigues, J.C., Fackler, K., 2011. A review of band assignments in near infrared spectra of wood and wood components. Journal of Near Infrared Spectroscopy 19, 287–308. doi:10.1255/jnirs.955

Segnini, A., Posadas, A., da Silva, W.T.L., Milori, D.M.B.P., Gavilan, C., Claessens, L., Quiroz, R., 2019. Quantifying soil carbon stocks and humification through spectroscopic methods: A scoping assessment in EMBU-Kenya. Journal of Environmental Management 234, 476–483. doi:10.1016/j.jenvman.2018.12.108

Selbie, D.R., Buckthought, L.E., Shepherd, M.A., 2015. The Challenge of the Urine Patch for Managing Nitrogen in Grazed Pasture Systems, Advances in Agronomy. Elsevier Ltd. doi:10.1016/bs.agron.2014.09.004

Shen, Q., Hedley, M., Arbestain, M.C., Kirschbaum, M.U.F., 2016. Can biochar increase the bioavailability of phosphorus ? 16, 268–286. doi:dx.doi.org/10.4067/S0718-95162016005000022

Shi, R.Y., Hong, Z.N., Li, J.Y., Jiang, J., Baquy, M.A. Al, Xu, R.K., Qian, W., 2017. Mechanisms for Increasing the pH Buffering Capacity of an Acidic Ultisol by Crop Residue-Derived Biochars. Journal of Agricultural and Food Chemistry 65, 8111–8119. doi:10.1021/acs.jafc.7b02266

Si, B., Dyck, M., Parkin, G., 2011. Flow and Transport in Layered Soils. Canadian Journal of Soil Science 91, 127–132. doi:10.4141/cjss11501

Sigua, G.C., Novak, J.M., Cantrell, K.B., Shumaker, P.D., Johnson, M.G., Watts, D.W., Szögi, A.A., 2014. Carbon mineralization in two ultisols amended with different sources and particle sizes of pyrolyzed biochar. Chemosphere 103, 313–321. doi:10.1016/j.chemosphere.2013.12.024

Singh, B., Dolk, M.M., Shen, Q., Camps-Arbestain, M., 2017. Biochar pH, electrical conductivity and liming potential, in: Biochar: A Guide to Analytical Methods. Csiro Publishing, Clayton, Australia., pp. 23–38. doi:10.13040/IJPSR.0975-8232.5(2).607-1

Singh, B.P., Cowie, A.L., 2014. Long-term influence of biochar on native organic carbon mineralisation in a low-carbon clayey soil. Scientific Reports 4. doi:10.1038/srep03687

Singh, B.P., Cowie, A.L., Smernik, R.J., 2012. Biochar carbon stability in a clayey soil as a function of feedstock and pyrolysis temperature. Environmental Science and Technology 46, 11770–11778. doi:10.1021/es302545b

Singh, B.P., Hatton, B.J., Singh, B., Cowie, A.L., Kathuria, A., 2010. Influence of Biochars on Nitrous Oxide Emission and Nitrogen Leaching from Two Contrasting Soils. Journal of Environmental Quality 39, 1224–1235. doi:10.2134/Jeq2009.0138

Six, J., Conant, R.T., Paul, E. a, Paustian, K., 2002. Stabilization mechanisms of soil organic matter: Implications for C-saturatin of soils. Plant and Soil 241, 155–176. doi:10.1023/A:1016125726789

Smith, E., Dent, G., 2019. Modern Raman Spectroscopy: A Practical Approach. Wiley. doi:10.1002/9781119440598

Smith, P., 2008. Land use change and soil organic carbon dynamics. Nutrient Cycling in Agroecosystems 81, 169–178.

Smith, P., Soussana, J.F., Angers, D., Schipper, L., Chenu, C., Rasse, D.P., Batjes, N.H., van Egmond, F., McNeill, S., Kuhnert, M., Arias-Navarro, C., Olesen, J.E., Chirinda,

N., Fornara, D., Wollenberg, E., Álvaro-Fuentes, J., Sanz-Cobena, A., Klumpp, K., 2020. How to measure, report and verify soil carbon change to realize the potential of soil carbon sequestration for atmospheric greenhouse gas removal. Global Change Biology 26, 219–241. doi:10.1111/gcb.14815

Soil Survey Staff, 2014. Keys to Soil Taxonomy. Usda 12, 410. doi:10.1063/1.1698257

Soriano-Disla, J.M., Janik, L.J., Viscarra Rossel, R. a, Macdonald, L.M., McLaughlin, M.J., 2014. The Performance of Visible, Near-, and Mid-Infrared Reflectance Spectroscopy for Prediction of Soil Physical, Chemical, and Biological Properties. Applied Spectroscopy Reviews 49, 139–186. doi:10.1080/05704928.2013.811081

Spelter, H., Winandy, J., Zauche, T., 2008. Anaerobically digested bovine biofiber as a source of fiber for particleboard manufacturing: an economic analysis. BioResources 3, 1256–1266.

Spokas, K.A., Reicosky, D.C., 2009. Impacts of sixteen different biochars on soil greenhouse gas production. Ann. Environ. Sci. 3, 179–193.

Stenseng, M., Jensen, A., Dam-johansen, K., 2001. Investigation of biomass pyrolysis by thermogravimetric analysis and differential scanning calorimetry. Journal of Analytical and Applied Pyrolysis 59, 765–780.

Sudduth, K.A., Hummel, J.W., 1993. Soil organic matter, CEC, and moisture sensing with a portable NIR spectrophotometer. Transactions of the ASAE 36, 1571–1582.

Sun, D.-W., Rinnan, Å., Nørgaard, L., Berg, F. van den, Thygesen, J., Bro, R., Engelsen, S.B., 2009. Infrared Spectroscopy for Food Quality Analysis and Control. Infrared Spectroscopy for Food Quality Analysis and Control 3, 29–50. doi:10.1016/B978-0-12-374136-3.00002-X

Taghizadeh-Toosi, A., Clough, T.J., Condron, L.M., Sherlock, R.R., Anderson, C.R., Craigie, R. a., 2011. Biochar incorporation into pasture soil suppresses in situ nitrous oxide emissions from ruminant urine patches. Journal of Environmental Quality 40, 468. doi:10.2134/jeq2010.0419

Terhoeven-Urselmans, T., Michel, K., Helfrich, M., Flessa, H., Ludwig, B., 2006. Near-infrared spectroscopy can predict the composition of organic matter in soil and litter. Journal of Plant Nutrition and Soil Science 169, 168–174. doi:10.1002/jpln.200521712

Thomazini, A., Spokas, K., Hall, K., Ippolito, J., Lentz, R., Novak, J., 2015. GHG impacts of biochar: Predictability for the same biochar. Agriculture, Ecosystems and Environment 207, 183–191. doi:10.1016/j.agee.2015.04.012

Tiedje, J.M., 1988. Ecology of denitrification and dissimilatory nitrate reduction to ammonium. Environmental Microbiology of Anaerobes 179–244.

Tripathi, M., Sahu, J.N., Ganesan, P., 2016. Effect of process parameters on production of biochar from biomass waste through pyrolysis : A review. Renewable and Sustainable Energy Reviews 55, 467–481. doi:10.1016/j.rser.2015.10.122

Troy, Shane M., Lawlor, P.G., O' Flynn, C.J., Healy, M.G., 2013. Impact of biochar addition to soil on greenhouse gas emissions following pig manure application. Soil Biology and Biochemistry 60, 173–181. doi:10.1016/j.soilbio.2013.01.019

Troy, Shane M, Nolan, T., Leahy, J.J., Peadar, G., Healy, M.G., Kwapinski, W., 2013. Effect of sawdust addition and composting of feedstock on renewable energy and biochar production from pyrolysis of anaerobically digested pig manure. Biomass and Bioenergy 49, 1–9.

Uchimiya, M., Franzluebbers, A.J., Liu, Z., Lamb, M.C., Sorensen, R.B., 2019. Detection of Biochar Carbon by Fluorescence and Near-Infrared-Based Chemometrics. Aquatic Geochemistry 24, 345–361. doi:10.1007/s10498-018-9347-9

Ulusoy, Y., Tekin, Y., Tümsavaş, Z., Mouazen, A.M., 2016. Prediction of soil cation exchange capacity using visible and near infrared spectroscopy. Biosystems Engineering 152, 79–93.

Van de Velden, M., Baeyens, J., Brems, A., Janssens, B., Dewil, R., 2010. Fundamentals, kinetics and endothermicity of the biomass pyrolysis reaction. Renewable Energy 35, 232–242. doi:10.1016/j.renene.2009.04.019

Van der Weerden, T.J., Cox, N., Luo, J., Di, H.J., Podolyan, A., Phillips, R.L., Saggar, S., de Klein, C.A.M., Ettema, P., Rys, G., 2016. Refining the New Zealand nitrous oxide emission factor for urea fertiliser and farm dairy effluent. Agriculture, Ecosystems and Environment 222, 133–137. doi:10.1016/j.agee.2016.02.007

Van Zwieten, L., Kammen, C., Cayuela, M.L., Singh, B.P., Joseph, S., Kimber, S., Donne, S., Clough, T.J., Spokas, K. a., 2015. Biochar effects on nitrous oxide and methane emissions from soil. Biochar for Environmental Management: Science, Technology and Implementation 489–520.

Van Zwieten, L, Kimber, S., Morris, S., Chan, K.., Downie, A., Rust, J., Cowie, A., Joseph, S., 2010. Effects of biochar from slow pyrolysis of papermill waste on agronomic performance and soil fertility. Plant and Soil 327, 235–246.

Van Zwieten, L., Kimber, S., Morris, S., Downie, A., Berger, E., Rust, J., Scheer, C., 2010. Influence of biochars on flux of N2O and CO2 from Ferrosol. Australian Journal of Soil Research 48, 555–568. doi:10.1071/SR10004

van Zwieten, L., Kimber, S., Morris, S., Macdonald, L.M., Rust, J., Petty, S., Joseph, S., Rose, T., 2019. Biochar improves dairy pasture yields by alleviating P and K constraints with no influence on soil respiration or N2O emissions. Biochar 1, 115–126. doi:10.1007/s42773-019-00005-6

Van Zwieten, L., Singh, B.P., Kimber, S.W.L., Murphy, D. V, Macdonald, L.M., Rust, J., Morris, S., 2014. An incubation study investigating the mechanisms that impact N2O flux from soil following biochar application. Agriculture, Ecosystems & Environment 191, 53–62.

Varmuza, K., Filzmoser, P., 2009. Introduction to Multivariate Statistical Analysis in Chemometrics. CRC Press, Boca Raton.

Verheijen, F., Jeffery, S., Bastos, A.C., van der Velde, M., Diafas, I., 2010. Biochar application to soils. A critical scientific review of effects on soil properties, processes, and functions, EUR 24099. doi:10.2788/472

Verhoeven, E., Pereira, E., Decock, C., Suddick, E., Angst, T., Six, J., 2017. Toward a better assessment of biochar-nitrous oxide mitigation potential at the field scale.

Journal of Environmental Quality 46, 237–246. doi:10.2134/jeq2016.10.0396

Verhoeven, E., Six, J., 2014. Biochar does not mitigate field-scale N2O emissions in a Northern California vineyard: An assessment across two years. Agriculture, Ecosystems and Environment 191, 27–38. doi:10.1016/j.agee.2014.03.008

Viscarra Rossel, R.A., 2008. ParLeS: Software for chemometric analysis of spectroscopic data. Chemometrics and Intelligent Laboratory Systems 90, 72–83. doi:10.1016/j.chemolab.2007.06.006

Viscarra Rossel, R.A., Behrens, T., Ben-Dor, E., Brown, D.J., Demattê, J.A.M., Shepherd, K.D., Shi, Z., Stenberg, B., Stevens, A., Adamchuk, V., Aïchi, H., Barthès, B.G., Bartholomeus, H.M., Bayer, A.D., Bernoux, M., Böttcher, K., Brodský, L., Du, C.W., Chappell, A., Fouad, Y., Genot, V., Gomez, C., Grunwald, S., Gubler, A., Guerrero, C., Hedley, C.B., Knadel, M., Morrás, H.J.M., Nocita, M., Ramirez-Lopez, L., Roudier, P., Campos, E.M.R., Sanborn, P., Sellitto, V.M., Sudduth, K.A., Rawlins, B.G., Walter, C., Winowiecki, L.A., Hong, S.Y., Ji, W., 2016. A global spectral library to characterize the world's soil. Earth-Science Reviews 155, 198–230. doi:10.1016/j.earscirev.2016.01.012

Viscarra Rossel, R.A., McGlynn, R.N., McBratney, A.B., 2006. Determining the composition of mineral-organic mixes using UV-vis-NIR diffuse reflectance spectroscopy. Geoderma 137, 70–82. doi:10.1016/j.geoderma.2006.07.004

Viscarra Rossel, R.A., Webster, R., 2011. Discrimination of Australian soil horizons and classes from their visible-near infrared spectra. European Journal of Soil Science 62, 637–647. doi:10.1111/j.1365-2389.2011.01356.x

Walkley, A., Black, I.A., 1934. An examination of the Degtjareff method for determining soil organic matter, and a proposed modification of the chromic acid titration method. Soil Science 37, 29–38.

Wang, J., Xiong, Z., Kuzyakov, Y., 2016. Biochar stability in soil: Meta-analysis of decomposition and priming effects. GCB Bioenergy 8, 512–523. doi:10.1111/gcbb.12266

Wang, T., Camps-Arbestain, M., Hedley, M., 2013. Predicting C aromaticity of biochars based on their elemental composition. Organic Geochemistry 62, 1–6. doi:10.1016/j.orggeochem.2013.06.012

Wang, T., Camps-Arbestain, M., Hedley, M., Bishop, P., 2012a. Predicting phosphorus bioavailability from high-ash biochars. Plant and Soil 357, 173–187. doi:10.1007/s11104-012-1131-9

Wang, T., Camps Arbestain, M., Hedley, M., Bishop, P., 2012b. Chemical and bioassay characterisation of nitrogen availability in biochar produced from dairy manure and biosolids. Organic Geochemistry 51, 45–54. doi:10.1016/j.orggeochem.2012.07.009

Weber, K., Quicker, P., 2018. Properties of biochar. Fuel 217, 240–261. doi:10.1016/j.fuel.2017.12.054

Wei, S., Zhu, M., Fan, X., Song, J., Peng, P., Li, K., Jia, W., Song, H., 2019. Influence of pyrolysis temperature and feedstock on carbon fractions of biochar produced from pyrolysis of rice straw, pine wood, pig manure and sewage sludge. Chemosphere

218, 624–631.

Wendt, J.W., Hauser, S., 2013. An equivalent soil mass procedure for monitoring soil organic carbon in multiple soil layers. European Journal of Soil Science 64, 58–65. doi:10.1111/ejss.12002

Weng, Z., Van Zwieten, L., Singh, B.P., Kimber, S., Morris, S., Cowie, A., Macdonald, L.M., 2015. Plant-biochar interactions drive the negative priming of soil organic carbon in an annual ryegrass field system. Soil Biology and Biochemistry 90, 111–121. doi:10.1016/j.soilbio.2015.08.005

Weng, Z.H., Van Zwieten, L., Singh, B.P., Tavakkoli, E., Joseph, S., Macdonald, L.M., Rose, T.J., Rose, M.T., Kimber, S.W.L., Morris, S., Cozzolino, D., Araujo, J.R., Archanjo, B.S., Cowie, A., 2017. Biochar built soil carbon over a decade by stabilizing rhizodeposits. Nature Climate Change 7, 371–376. doi:10.1038/nclimate3276

White, J.E., Catallo, W.J., Legendre, B.L., 2011. Biomass pyrolysis kinetics : A comparative critical review with relevant agricultural residue case studies. Journal of Analytical and Applied Pyrolysis 91, 1–33. doi:10.1016/j.jaap.2011.01.004

Whitehead, D., Schipper, L.A., Pronger, J., Moinet, G.Y.K., Mudge, P.L., Calvelo Pereira, R., Kirschbaum, M.U.F., McNally, S.R., Beare, M.H., Camps-Arbestain, M., 2018. Management practices to reduce losses or increase soil carbon stocks in temperate grazed grasslands: New Zealand as a case study. Agriculture, Ecosystems and Environment 265, 432–443. doi:10.1016/j.agee.2018.06.022

Whitman, T., Hanley, K., Enders, A., Lehmann, J., 2013. Predicting pyrogenic organic matter mineralization from its initial properties and implications for carbon management. Organic Geochemistry 64, 76–83. doi:10.1016/j.orggeochem.2013.09.006

Whitman, T., Singh, B.P., Zimmerman, A.R., Lehmann, J., Joseph, S., 2015. Priming effects in biochar-amended soils: implications of biochar-soil organic matter interactions for carbon storage. Biochar for Environmental Management: Science, Technology and Implementation 2, 455–488.

Whitman, T., Zhu, Z., Lehmann, J., 2014. Carbon mineralizability determines interactive effects on mineralization of pyrogenic organic matter and soil organic carbon. Environmental Science and Technology 48, 13727–13734. doi:10.1021/es503331y

Wiesmeier, M., Urbanski, L., Hobley, E., Lang, B., von Lützow, M., Marin-Spiotta, E., van Wesemael, B., Rabot, E., Ließ, M., Garcia-Franco, N., Wollschläger, U., Vogel, H.J., Kögel-Knabner, I., 2019. Soil organic carbon storage as a key function of soils - A review of drivers and indicators at various scales. Geoderma 333, 149–162. doi:10.1016/j.geoderma.2018.07.026

Williams, P., Norris, K.H., 2001. Near-Infrared Technology in the Agricultural and Food Industries. American Association of Cereal Chemists, Inc.

Wold, S.S.M., Eriksson, L., 2001. PLS-Regression: A Basic Tool of Chemometrics 109–130.

Woolf, D., Lehmann, J., Cowie, A., Cayuela, M.L., Whitman, T., Sohi, S., 2018a. Biochar

for Climate Change Mitigation: Navigating from Science to Evidence-Based Policy, in: Soil and Climate. CRC Press, pp. 219–248.

Woolf, D., Lehmann, J., Cowie, A., Cayuela, M.L., Whitman, T., Sohi, S., 2018b. Biochar for Climate Change Mitigation: Navigating from Science to Evidence-Based Policy. Soil and Climate 219–248.

Workman Jr, J., Weyer, L., 2012. Practical guide and spectral atlas for interpretive near-infrared spectroscopy. CRC Press.

Workman Jr, J.J.J., 2016. Concise Handbook Of Analytical Spectroscopy, The: Theory, Applications, And Reference Materials (In 5 Volumes). World Scientific.

Wrage, N., Velthof, G.L., Van Beusichem, M.L., Oenema, O., 2001. Role of nitrifier denitrification in the production of nitrous oxide. Soil Biology and Biochemistry 33, 1723–1732. doi:10.1016/S0038-0717(01)00096-7

Xu, F., Yu, J., Tesso, T., Dowell, F., Wang, D., 2013. Qualitative and quantitative analysis of lignocellulosic biomass using infrared techniques: A mini-review. Applied Energy 104, 801–809. doi:10.1016/j.apenergy.2012.12.019

Xu, S., Shi, X., Wang, M., Zhao, Y., 2016. Determination of rice root density at the field level using visible and near-infrared reflectance spectroscopy. Geoderma 267, 174–184.

Yamauchi, S., Kurimoto, Y., 2003. Raman spectroscopic study on pyrolyzed wood and bark of Japanese cedar: Temperature dependence of Raman parameters. Journal of Wood Science 49, 235–240. doi:10.1007/s10086-002-0462-1

Yan, Z., Wang, T., Wang, L., Yang, X., Smith, P., Hilpert, M., Li, S., Shang, J., Bailey, V., Liu, C., 2018. Microscale water distribution and its effects on organic carbon decomposition in unsaturated soils. Science of the Total Environment 644, 1036–1043. doi:10.1016/j.scitotenv.2018.06.365

Yanai, Y., Toyota, K., Okazaki, M., 2007. Effects of charcoal addition on N2O emissions from soil resulting from rewetting air-dried soil in short-term laboratory experiments: Original article. Soil Science and Plant Nutrition 53, 181–188. doi:10.1111/j.1747-0765.2007.00123.x

Yang, H., Kuang, B., Mouazen, A.M., 2012. Quantitative analysis of soil nitrogen and carbon at a farm scale using visible and near infrared spectroscopy coupled with wavelength reduction. European Journal of Soil Science 63, 410–420. doi:10.1111/j.1365-2389.2012.01443.x

Yang, H., Sheng, K., 2012. Characterization of Biochar Properties Affected by Different Pyrolysis Temperatures Using Visible-Near-Infrared Spectroscopy. ISRN Spectroscopy 2012, 1–7. doi:10.5402/2012/712837

Yang, H., Yan, R., Chen, H., Zheng, C., Lee, D.H., Liang, D.T., 2006. In-depth investigation of biomass pyrolysis based on three major components: Hemicellulose, cellulose and lignin. Energy and Fuels 20, 388–393. doi:10.1021/ef0580117

Yao, Y., Gao, B., Zhang, M., Inyang, M., Zimmerman, A.R., 2012. Effect of biochar amendment on sorption and leaching of nitrate, ammonium, and phosphate in a sandy soil. Chemosphere 89, 1467–1471. doi:10.1016/j.chemosphere.2012.06.002

Ye, L., Camps-Arbestain, M., Shen, Q., Lehmann, J., Singh, B., Sabir, M., 2019. Biochar effects on crop yields with and without fertilizer: a meta-analysis of field studies using separate controls. Soil Use and Management 00, 1–17. doi:https://doi.org/10.1111/sum.12546

Yoo, G., Kang, H., 2012. Effects of biochar addition on greenhouse gas emissions and microbial responses in a short-term laboratory experiment. Journal of Environmental Quality 41, 1193–1202. doi:10.2134/jeq2011.0157

Yu, Z., Chen, L., Pan, S., Li, Y., Kuzyakov, Y., Xu, J., Brookes, P.C., Luo, Y., 2018. Feedstock determines biochar-induced soil priming effects by stimulating the activity of specific microorganisms. European Journal of Soil Science 69, 521–534. doi:10.1111/ejss.12542

Zar, J.H., 2010. Biostatistical Analysis, 5th ed, Pearson Prentice Hall. Pearson Prentice Hall, Upper Saddle River, New Jersey.

Zhang, A., Bian, R., Pan, G., Cui, L., Hussain, Q., Li, L., Zheng, Jinwei, Zheng, Jufeng, Zhang, X., Han, X., Yu, X., 2012. Effects of biochar amendment on soil quality, crop yield and greenhouse gas emission in a Chinese rice paddy: A field study of 2 consecutive rice growing cycles. Field Crops Research 127, 153–160. doi:10.1016/j.fcr.2011.11.020

Zhang, L., Xu, C. (Charles), Champagne, P., 2010. Overview of recent advances in thermo-chemical conversion of biomass. Energy Conversion and Management 51, 969–982. doi:10.1016/j.enconman.2009.11.038

Zheng, J., Stewart, C.E., Cotrufo, M.F., 2012. Biochar and nitrogen fertilizer alters soil nitrogen dynamics and greenhouse gas fluxes from two temperate soils. J Environ Qual 41, 1361–1370. doi:10.2134/jeq2012.0019\r10.2134/jeq2012.0019.

Zimmerman, A.R., Gao, B., Ahn, M.Y., 2011. Positive and negative carbon mineralization priming effects among a variety of biochar-amended soils. Soil Biology and Biochemistry 43, 1169–1179. doi:10.1016/j.soilbio.2011.02.005

Zimmerman, A.R., Ouyang, L., 2018. Priming of pyrogenic C (biochar) mineralization by dissolved organic matter and vice versa. Soil Biology and Biochemistry 130, 105–112. doi:10.1016/J.SOILBIO.2018.12.011

Zimmermann, M., Bird, M.I., Wurster, C., Saiz, G., Goodrick, I., Barta, J., Capek, P., Santruckova, H., Smernik, R., 2012. Rapid degradation of pyrogenic carbon. Global Change Biology 18, 3306–3316. doi:10.1111/j.1365-2486.2012.02796.x

Zornoza, R., Guerrero, C., Mataix-Solera, J., Scow, K.M., Arcenegui, V., Mataix-Beneyto, J., 2008. Near infrared spectroscopy for determination of various physical, chemical and biochemical properties in Mediterranean soils. Soil Biology and Biochemistry 40, 1923–1930.

APPENDIX

Appendix I. Supporting information for Chapter 3 (S3)

Table S3-1. Samples in calibration set (n=82)

Biochar	Maximum Pyrolysis Temperature (°C)	H/C_{org} ratio	Production condition	Source/Reference
Brush-yard waste	500	0.45	Slow pyrolysis	Enders et al. (2012)
Bull Manure	300	1.03	Slow pyrolysis	
Bull Manure	350	0.72	Slow pyrolysis	
Bull Manure	400	0.61	Slow pyrolysis	
Bull Manure	450	0.55	Slow pyrolysis	
Bull Manure	500	0.42	Slow pyrolysis	
Bull Manure	550	0.37	Slow pyrolysis	
Bull Manure	600	0.28	Slow pyrolysis	
Carbonized pine	750	0.17	Updraft pyrolysis	
Composted Dairy Manure	500	0.45*	Slow pyrolysis	
Composted Dairy Manure + Wood	500	0.24*	Slow pyrolysis	
Corn	300	0.90	Slow pyrolysis	
Corn	350	0.70	Slow pyrolysis	
Corn	400	0.72	Slow pyrolysis	
Corn	450	0.47	Slow pyrolysis	
Corn	500	0.32	Slow pyrolysis	
Corn	550	0.38	Slow pyrolysis	
Corn	600	0.39	Slow pyrolysis	
Corn 3	500	0.58	Ablative-updraft pyrolysis	
Dairy Manure	300	0.88	Slow pyrolysis	
Dairy Manure	350	0.77	Slow pyrolysis	
Dairy Manure	400	0.59	Slow pyrolysis	
Dairy Manure	450	0.60	Slow pyrolysis	
Dairy Manure	500	0.43	Slow pyrolysis	
Dairy Manure	550	0.38	Slow pyrolysis	
Dairy Manure	600	0.32	Slow pyrolysis	
Digested Dairy Manure	350	0.97*	Slow pyrolysis	
Digested Dairy Manure	400	0.70*	Slow pyrolysis	
Digested Dairy Manure	450	0.63*	Slow pyrolysis	
Digested Dairy Manure	550	0.61*	Slow pyrolysis	
Digested Dairy Manure	600	0.47*	Slow pyrolysis	
Food	300	1.02	Slow pyrolysis	
Food	400	0.95	Slow pyrolysis	

Food	500	0.88	Slow pyrolysis	
Food	600	0.50	Slow pyrolysis	
Grass Clippings-yard waste	500	0.78*	Slow pyrolysis	
Hazelnut	300	0.67	Slow pyrolysis	
Hazelnut	350	0.61	Slow pyrolysis	
Hazelnut	400	0.51	Slow pyrolysis	
Hazelnut	450	0.44	Slow pyrolysis	
Hazelnut	500	0.50	Slow pyrolysis	
Hazelnut	550	0.38	Slow pyrolysis	
Hazelnut	600	0.31	Slow pyrolysis	
Leaves-yard waste	500	0.51	Slow pyrolysis	
Mixed Hardwood	500	0.60	Fast pyrolysis	
Mixed Softwood	500	0.54	Fast pyrolysis	
Mixed Vegetation	500	0.49*	Fast pyrolysis	
Mixed Woodchips	500	0.40	Slow pyrolysis	
Mixture	220	1.43*	Torrefaction	
Mixture	240	1.03*	Torrefaction	
Oak	300	0.90	Slow pyrolysis	
Oak	350	0.54	Slow pyrolysis	
Oak	450	0.42	Slow pyrolysis	
Oak	500	0.37	Slow pyrolysis	
Oak	550	0.33	Slow pyrolysis	
Oak	600	0.42	Slow pyrolysis	
Paper	300	0.57	Slow pyrolysis	
Paper	400	0.54	Slow pyrolysis	
Paper	500	0.32	Slow pyrolysis	
Paper	600	0.25	Slow pyrolysis	
Peanut	480	0.62	Ablative-updraft pyrolysis	
Pine	300	0.88	Slow pyrolysis	
Pine	350	0.74	Slow pyrolysis	
Pine	400	0.58	Slow pyrolysis	
Pine	450	0.46	Slow pyrolysis	
Pine	500	0.42	Slow pyrolysis	
Pine	550	0.43	Slow pyrolysis	
Pine	600	0.30	Slow pyrolysis	
Pine 2	500	0.83*	Fast/intermediate pyrolysis	
Poultry Manure	300	0.83	Slow pyrolysis	
Poultry Manure	350	0.55	Slow pyrolysis	
Poultry Manure	400	0.26	Slow pyrolysis	
Poultry Manure	450	0.17	Slow pyrolysis	
Poultry Manure	500	0.22	Slow pyrolysis	
Poultry Manure	550	0.13	Slow pyrolysis	
Poultry Manure	600	0.17	Slow pyrolysis	
Poultry 2	600	1.53*	Fixed-bed gasification	
Raw Dairy Manure	500	0.43*	Slow pyrolysis	

Rice husk	800	0.47*	Gasification	
Soybean	500	0.71*	Fast pyrolysis	
Switchgrass 2	500	0.41	Fast/intermediate pyrolysis	
Switchgrass	500	0.60*	Fast pyrolysis	

-Samples which only H/C ratios were available are denoted by symbol (*).

Table S3-2. Samples used as prediction set (n=20)

Biochar	Maximum Pyrolysis Temperature (°C)	Feedstock size	H/C_{org} ratio	Production condition	Source/Reference
Pine	325	Medium	0.59	Slow pyrolysis	Ripberger et al., (2015)
	350	Large	0.58		
	356	Small	0.78		
	383	Medium	0.52		
	402	Large	0.64		
	411	Large	0.59		
	414	Large	0.62		
	416	Medium	0.56		
	523	Medium	0.48		
	541	Large	0.36		
	552	Small	0.43		
	554	Medium	0.54		
	556	Large	0.37		
	579	Large	0.33		
	606	Large	0.31		
	709	Medium	0.27		
	710	Large	0.26		
	713	Medium	0.30		
	714	Large	0.31		
	723	Large	0.26		

*Small (15 mm x 15 mm x 17.5 mm; n=2); medium (32 mm x 32 mm x 17.5 mm; n=7) and large (67 mm x 67 mm x 17.5 mm; n=11).

Appendix II. Supporting information for Chapter 4 (S4)

Table S4-1. Samples used as prediction set (n=18)

Biochar	Maximum Pyrolysis Temperature (°C)	H/C_{org} ratio	Production condition	Source/Reference
Pine	400	0.72	Slow pyrolysis	Calvelo Pereira et al. (2011)
Poplar	400	0.67	Slow pyrolysis	
Willow	400	0.63	Slow pyrolysis	
Poplar	550	0.57	Slow pyrolysis	
Willow	550	0.53	Slow pyrolysis	
Biosolid	250	1.27	Slow pyrolysis	Wang et al. (2012)
Biosolid	350	0.91	Slow pyrolysis	
Biosolid	450	0.68	Slow pyrolysis	
Biosolid	550	0.55	Slow pyrolysis	
Manure	250	1.30	Slow pyrolysis	
Manure	350	0.82	Slow pyrolysis	
Manure	450	0.60	Slow pyrolysis	
Corn stover	350	0.64	Slow pyrolysis	Herath et al. (2013)
Corn stover	550	0.45	Slow pyrolysis	
Willow	550	0.44	Slow pyrolysis	Gregory et al. (2014)
Pine	290	1.03	Slow pyrolysis	Shen et al. (2016)
Pine	550	0.37	Slow pyrolysis	
Willow	550	0.38	Slow pyrolysis	

Appendix III. Supporting information for Chapter 5 (S5)

Figure S5-1. <2 mm pine biochar (left) and >4 mm pine biochar (right)

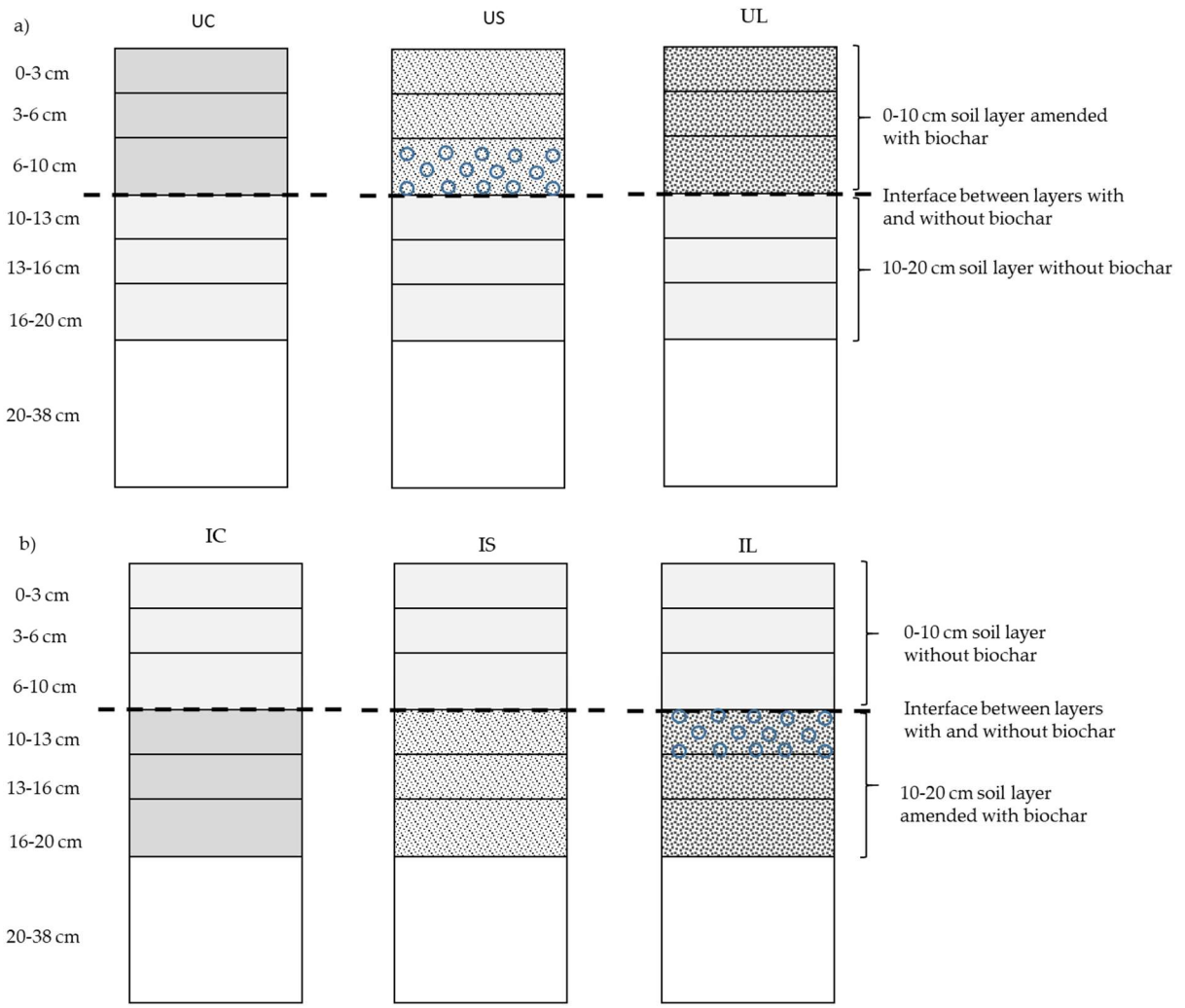

Figure S5-2. The soil in cores was packed as follows: a) Un-inverted soil; UC-control un-inverted; US – Un-inverted 0-10 cm with <2 mm biochar; UL – Un-inverted 0-10 cm with >4 mm biochar; b) Inverted soil; IC- Control inverted; IS- Inverted 0-10 cm with <2 mm biochar; IL - Inverted 0-10 cm with >4 mm biochar.

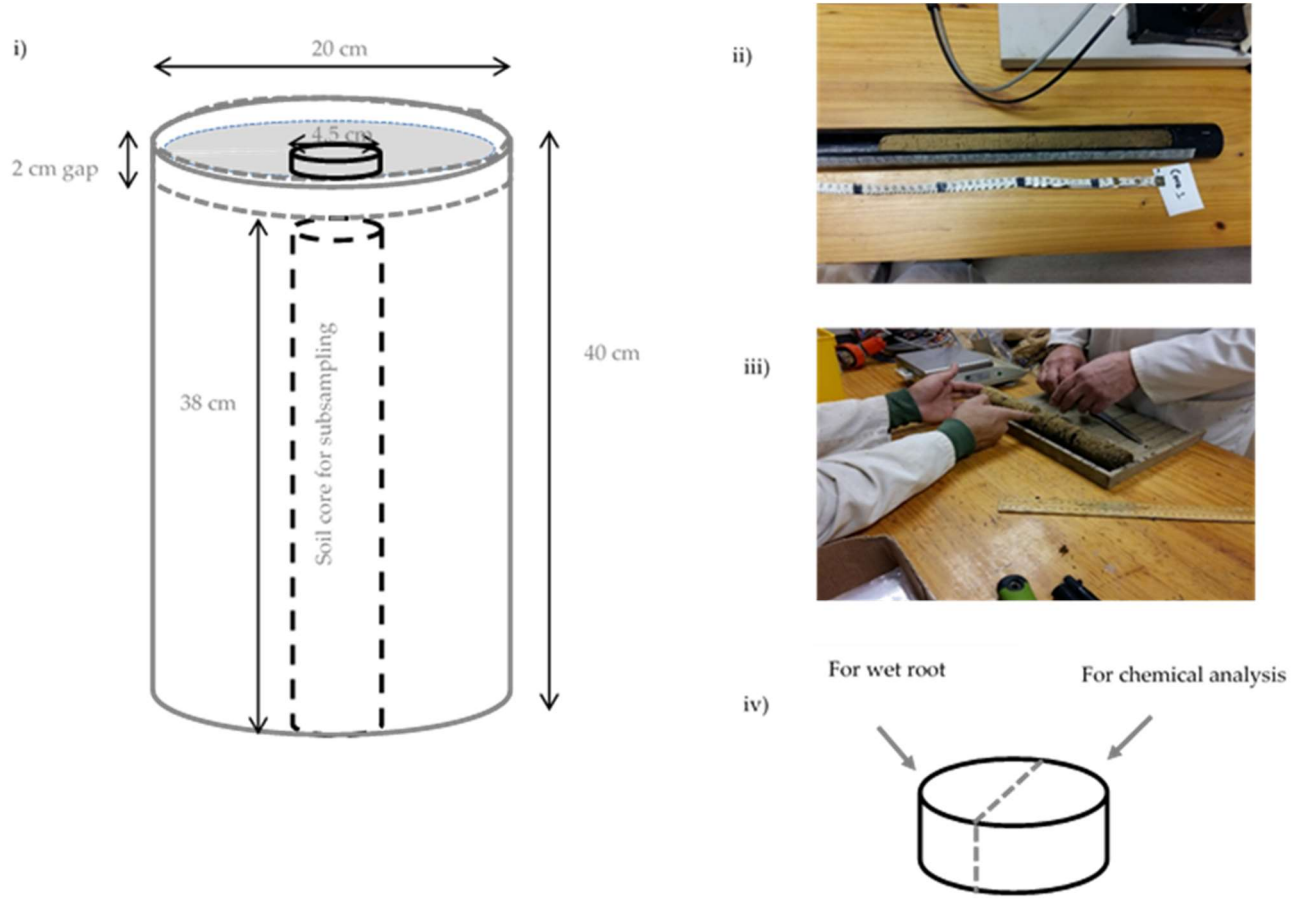

Figure S5-3. End-of-trial sampling; i) A soil core (subsample) was taken out from each core using a corer (diameter of 45 mm) from 0-38 cm depth; ii) Each core was scanned with NIRS; iii) soil was sliced according to designated depth; iv) each sliced soil was cut into half and separated for analysis.

Table S5-1. Time scale of the experiment.

Date	Week	Event
26/9/2014	1	Finish setting up all cores and first irrigation to reach 50% WFPS- topsoil (0-10 cm) has been mixed with basic fertilizer to stimulate seedlings (NPK; 60 kg N ha^{-1} ; 50 kg K ha^{-1} and 60 kg P ha^{-1}) N from urea, K from KCl and P from SSP.
10/10/2014	3	Sowing ryegrass seeds
4/11/2014	7	Thinning to 20 seedlings
13/11/2014	8	First harvest, cut to 5 cm length
24/11/2014	Week 10 & onward	Subsequent harvests
15/12/2014	13	Gas measurement to measure N_2O emission prior to urine application: sampling (day 0)-summer trial
16/12/2014	13	First application of cow urine equal to 354 kg N ha^{-1}, 3.5 mm of urine applied using syringe onto 1/3 of total area of soil core.
17/12/2014 until 3/2/2015	Weeks 13-20	Gas measurement day 1 to day 49
	Weeks 21-28	Gap
9 and 10/4/2015	29	Leaching before 2nd cow urine application
27/4/2015	32	Gas measurement to measure N_2O emission prior to urine application: sampling (day 0)-autumn trial
28/4/2015	32	Second application of cow urine equal to 563 kg N ha^{-1}
29-4-2015 until 16-6-2015	Weeks 32-39	Gas measurement day 1 to day 49

16-9-2015	52	Experiment setup dismantled. Soil cores were kept in the chiller room for further analysis.

Table S5-2. Soil pH of each layer measured at the end of the experiment.

Soil depth (cm)	Treatments							
	Un-inverted soil				Inverted soil			
	UC	US	UL	*p*-value	IC	IS	IL	*p*-value
Layer A (0-3 cm)	5.74a	5.72a	5.68a	0.906	5.68a	5.67a	5.62a	0.411
Layer B (3-6 cm)	5.65a	5.34a	5.43a	0.068	5.43a	5.39a	5.38a	0.875
Layer C (6-10 cm)	5.52a	5.43a	5.34a	0.481	5.29a	5.38a	5.37a	0.728
Layer D (10-13 cm)	5.59a	5.30a	5.34a	0.105	5.30a	5.42a	5.38a	0.745
Layer E (13-16 cm)	5.54a	5.25b	5.34b	0.034	5.29a	5.42a	5.37a	0.387
Layer F (16-20 cm)	5.53a	5.25a	5.38a	0.203	5.40a	5.43a	5.36a	0.647

UC-control un-inverted; US – Un-inverted 0-10 cm with <2 mm biochar; UL – Un-inverted 0-10 cm with >4 mm biochar; IC- Control inverted; IS- Inverted 0-10 cm with <2 mm biochar; IL - Inverted 0-10 cm with >4 mm biochar. Different letters denote significant differences at $p < 0.10$ between treatments ($n = 4$) for each layer. In the un-inverted soil biochar was at 0-10 cm depth; in the inverted soil biochar was at 10-20 cm depth.

Table S5-3. N_2O emission fluxes measured during summer and autumn trial (data showed for selected days only).

Summer Trial				
		Treatments		
Day	**Soil Inversion**	**Control**	**Small-particle size biochar**	**Large-particle size biochar**
Day prior to urine application	Un-inverted	0.12bB	1.51aA	0.50bA
	Inverted	**2.08**aA	1.63aA	0.19aA
Day after urine application with maximum N_2O peak	Un-inverted	30.5aA	60.7aA	54.2aA
	Inverted	13.9aA	25.4aA	29.1aA
Day 10 after urine application	Un-inverted	3.11aA	3.18aA	4.41aA
	Inverted	2.70aA	15.9aA	7.90aA
Autumn Trial				
		Treatments		
Day	**Soil Inversion**	**Control**	**Small-particle size biochar**	**Large-particle size biochar**
Day prior to urine application	Un-inverted	0.76bB	4.61aA	3.24aB
	Inverted	**21.8**aA	4.36bA	**24.8**aA
Day after urine application with maximum N_2O peak	Un-inverted	40.9aA	85.7aA	69.7aA
	Inverted	66.9aA	59.7aA	93.8aA
Day 10 after urine application	Un-inverted	14.6aA	28.6aA	14.1aA
	Inverted	9.43aA	23.4aA	22.7aA

Within a specific season, (i) different small letters within a row indicate differences between biochar treatments ($n = 4$) and $p < 0.10$), and (ii) different uppercase letters within a column indicate differences between un-inverted and inverted treatments ($n = 4$ and $p < 0.10$).

Table S5-4. Treatment effects on the amount of NO_3-N measured for every leaching event.

Leaching event	NO_3-N leachate (NO_3^-N g m^{-2} / % of added N leached as NO_3^-N)							
	UC	**US**	**UL**	***p*-value**	**IC**	**IS**	**IL**	***p*-value**
1st	0.073/0.21a	0.036/0.10a	0.066/0.19a	0.680	0.030/0.08a	0.035/0.10a	0.036/0.10a	0.933
2nd	0.015/0.04a	0.026/0.07a	0.018/0.05a	0.683	0.013/0.04a	0.060/0.17a	0.021/0.06a	0.132
3rd	0.015/0.03a	0.022/0.04a	0.015/0.03a	0.634	0.020/0.03a	0.025/0.04a	0.036/0.06a	0.426

UC - control un-inverted; US – Un-inverted 0-10 cm with <2 mm biochar; UL – un-inverted 0-10 cm with >4 mm biochar; IC - control inverted; IS - inverted 0-10 cm with <2 mm biochar; IL - inverted 0-10 cm with >4 mm biochar. Different letters denote significant differences at $p < 0.10$ between treatments at each leaching event ($n = 4$).

Table S5-5. Soil bulk density (g/cm^{-3}) at each depth measured at the end of the experiment.

Soil depth (cm)	Treatments							
	Un-inverted soil				Inverted soil			
	UC	US	UL	*p*-value	IC	IS	IL	*p*-value
Layer A (0-3 cm)	0.92a	0.93a	0.84a	0.115	1.16a	1.06a	1.12a	0.271
Layer B (3-6 cm)	1.04a	0.99a	0.94a	0.106	1.14a	1.19a	1.18a	0.792
Layer C (6-10 cm)	0.97a	1.06a	0.99a	0.101	1.05a	1.17a	1.08a	0.186
Layer D (10-13 cm)	1.18a	1.18a	1.12a	0.741	0.92a	0.95a	1.00a	0.327
Layer E (13-16 cm)	1.17a	1.10a	1.11a	0.599	1.00a	0.94a	0.92a	0.417
Layer F (16-20 cm)	1.18a	1.10a	1.08a	0.183	1.00a	0.91a	0.93a	0.267

UC - control un-inverted; US – Un-inverted 0-10 cm with <2 mm biochar; UL – un-inverted 0-10 cm with >4 mm biochar; IC - control inverted; IS - inverted 0-10 cm with <2 mm biochar; IL - inverted 0-10 cm with >4 mm biochar. Different letters denote significant differences at $p < 0.10$ between treatments ($n = 4$) for each layer. In the un-inverted soil biochar was at 0-10 cm depth; in the inverted soil biochar was at 10-20 cm depth.

Table S5-6. Volumetric soil moisture contents (%) at different matric potentials including the available water content (AWC) measured after the end of the experiment.

Matric potential	Soil depth (cm)	Treatments							
		Un-inverted soil				Inverted soil			
		UC	US	UL	*p*-value	IC	IS	IL	*p*-value
-15bar	0-3	14.79±0.60	14.35±0.94	14.12±0.91	ns	14.79±0.85	14.02±0.12	14.61±0.86	ns
	3-6	19.78±0.67	19.36±0.78	18.58±0.77	ns	17.25±0.15	20.34±2.16	19.27±2.61	ns
	6-10	17.45b±0.01	19.37a±0.62	19.11a±0.03	**0.058**	18.51±6.70	18.25±0.60	17.25±2.09	ns
	10-13	18.85±1.06	19.98±0.10	16.46±1.91	ns	14.73b±0.90	16.22b±0.50	19.68a±0.35	**0.024**
	13-16	20.45±0.45	21.38±0.15	19.32±3.11	ns	20.28±0.21	16.21±0.82	18.52±1.08	ns
	16-20	20.79±0.62	20.81±0.12	19.49±1.75	ns	20.73±0.75	17.32±0.91	18.64±1.94	ns
-1bar	0-3	21.62±0.85	21.40±1.82	19.82±1.28	ns	19.98±1.34	19.22±0.17	19.96±0.98	ns
	3-6	26.17±0.27	24.89±2.21	23.45±1.02	ns	22.72±2.07	24.67±2.50	23.15±2.81	ns
	6-10	22.81b±0.14	27.81a±0.88	24.01b±0.37	**0.016**	15.43±1.02	22.15±1.01	20.74±2.52	ns
	10-13	26.16±1.93	26.96±0.88	22.37±2.60	ns	20.43b±0.95	21.66b±0.81	24.77a±0.28	**0.053**
	13-16	24.20±0.22	25.72±0.12	22.79±3.63	ns	24.00±1.04	20.99±1.53	22.86±1.18	ns
	16-20	24.05±1.46	21.13±2.53	21.92±2.31	ns	24.71±0.61	20.76±0.92	23.13±1.70	ns
-0.3 bar	0-3	27.31±1.08	26.99±2.18	24.58±1.67	ns	26.36±1.99	24.92±0.01	26.15±1.01	ns
	3-6	34.22±0.49	32.06±1.72	30.68±0.01	ns	27.66±0.25	32.72±2.87	30.71±3.15	ns
	6-10	28.76b±0.41	34.04a±1.24	30.06b±0.02	**0.032**	19.57±1.43	28.07±1.01	26.49±3.00	ns
	10-13	32.16±5.09	29.68±1.03	25.44±3.24	ns	23.52b±1.25	25.24b±0.72	28.99a±1.13	**0.074**
	13-16	29.07±0.27	29.23±0.08	26.85±4.42	ns	29.45±0.40	25.15±1.99	26.74±1.42	ns
	16-20	30.51±0.98	28.32±0.51	27.51±2.83	ns	28.89±0.50	26.61±1.01	27.57±2.37	ns
AWC	0-3	12.52±0.48	12.64±1.24	10.46±0.76	ns	11.58±1.14	10.90±0.12	11.55±0.16	ns
	3-6	14.45±0.19	12.69±0.94	12.10±0.76	ns	10.42±0.10	12.39±0.72	11.44±0.54	ns
	6-10	11.31±0.40	14.68±1.86	10.94±0.05	ns	4.38±1.94	9.82±0.41	9.24±0.91	ns
	10-13	13.31±4.04	9.70±0.93	8.98±1.32	ns	8.79±0.35	9.02±0.22	9.31±0.78	ns
	13-16	8.63±0.19	7.85±0.23	7.53±1.32	ns	9.17±0.20	8.94±1.17	8.21±0.35	ns
	16-20	9.73±0.36	7.51±0.39	8.02±1.08	ns	8.17±0.25	9.30±0.10	8.93±0.44	ns

UC-control un-inverted; US – Un-inverted 0-10 cm with <2 mm biochar; UL – Un-inverted 0-10 cm with >4 mm biochar; IC- Control inverted; IS- Inverted 0-10 cm with <2mm biochar; IL - Inverted 0-10 cm with >4 mm biochar. SEM (n = 4) and significant differences were detected at $p < 0.10$. Different letters denote significant differences between treatments for each layer. In the un-inverted soil biochar was at 0-10 cm depth; in the inverted soil biochar was at 10-20 cm depth.

Table S5-7. Soil total C (%) of each layer measured at the end of the experiment.

Soil depth (cm)	Treatments							
	Un-inverted soil				Inverted soil			
	UC	US	UL	*p*-value	IC	IS	IL	*p*-value
Layer A (0-3 cm)	3.85 b	5.64 a	5.23 a	**0.000**	2.49a	2.47a	2.33a	0.187
Layer B (3-6 cm)	3.76 b	5.18 a	4.91 a	**0.000**	2.27a	2.34a	2.35a	0.176
Layer C (6-10 cm)	3.23 b	4.93 a	4.77 a	**0.001**	2.32a	2.30a	2.32a	0.900
Layer D (10-13 cm)	2.30a	2.30a	2.31a	0.971	3.42 b	5.04 a	4.79 a	**0.003**
Layer E (13-16 cm)	2.24a	2.29a	2.29a	0.299	3.61 c	5.20 a	4.58 b	**0.000**
Layer F (16-20 cm)	1.96a	2.17a	2.30a	0.100	3.24 c	5.22 a	4.09 b	**0.000**

UC - control un-inverted; US – Un-inverted 0-10 cm with <2 mm biochar; UL – un-inverted 0-10 cm with >4 mm biochar; IC - control inverted; IS - inverted 0-10 cm with <2 mm biochar; IL - inverted 0-10 cm with >4 mm biochar. Different letters denote significant differences at $p < 0.10$ between treatments ($n = 4$) for each layer. In the un-inverted soil, biochar was at 0-10 cm depth; in the inverted soil biochar was at 10-20 cm depth.

Table S5-8. Dry root (mg cm^{-3}) in each soil layer measured at the end of the experiment.

Soil depth (cm)	Treatments							
	Un-inverted soil				Inverted soil			
	UC	US	UL	*p*-value	IC	IS	IL	*p*-value
Layer A (0-3 cm)	5.61a	10.99a	5.61a	0.522	5.83a	9.87a	7.63a	0.415
Layer B (3-6 cm)	4.04a	1.35a	3.59a	0.318	1.57a	0.90a	1.79a	0.539
Layer C (6-10 cm)	0.68a	0.85a	0.85a	0.908	0.34 a	1.88 b	1.54 b	**0.078**
Layer D (10-13 cm)	0.45a	0.67a	0.90a	0.192	2.69 a	1.12 b	0.67 b	**0.009**
Layer E (13-16 cm)	0.45a	0.43a	0.44a	1.000	0.67a	0.90a	0.89a	0.898
Layer F (16-20 cm)	0.34a	0.33a	0.51a	0.829	0.34a	0.51a	0.85a	0.563

UC - control un-inverted; US – Un-inverted 0-10 cm with <2 mm biochar; UL – un-inverted 0-10 cm with >4 mm biochar; IC - control inverted; IS - inverted 0-10 cm with <2 mm biochar; IL - inverted 0-10 cm with >4 mm biochar. Different letters denote significant differences at $p < 0.10$ between treatments ($n = 4$) for each layer. In the un-inverted soil, biochar was at 0-10 cm depth; in the inverted soil biochar was at 10-20 cm depth

Appendix IV. Supporting information on Chapter 6 (S6)

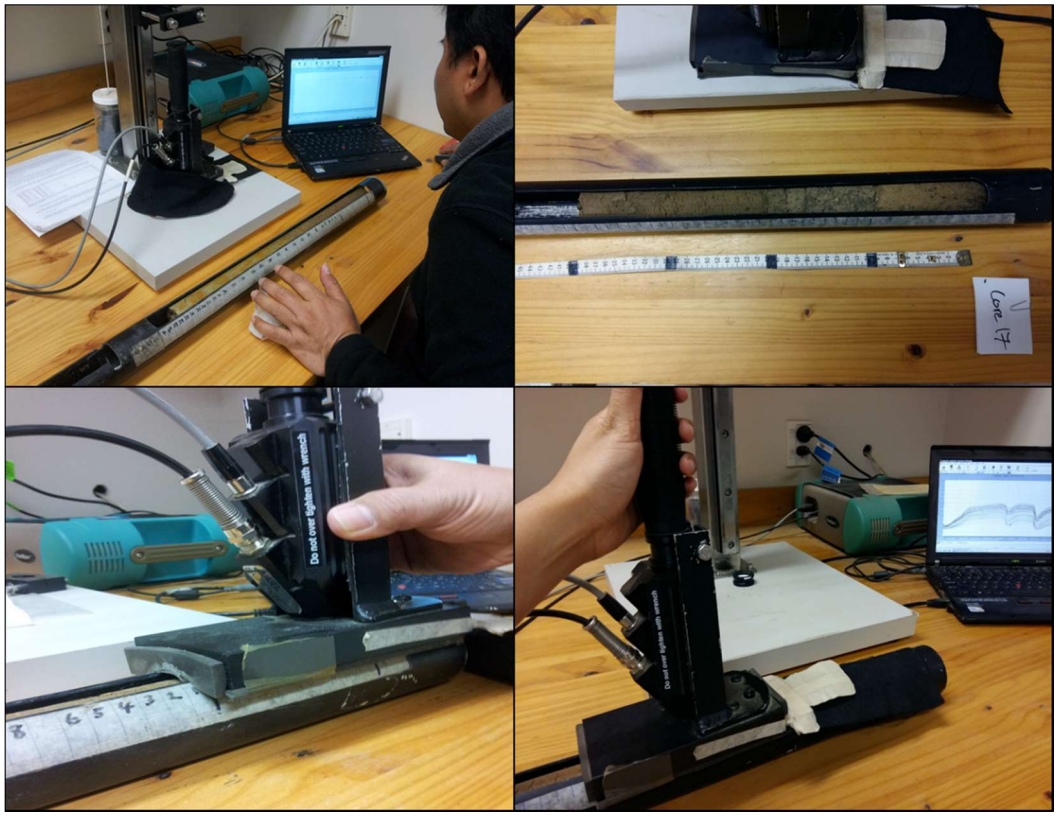

Figure S6-1. Each soil core was then scanned using a modified contact probe of ASD FieldSpec 3 Vis-NIR Spectrometer (Kusumo et al., 2009) to collect the UV-Visible NIR spectral reflectance at 1-cm intervals between 0 and 20 cm

Table S6-1. Total dry root (mg cm^{-3}) content in each treatment measured at overall 0-20 cm depth by the end of the experiment, with treatment or soil inversion as the factor

	Treatments		
Soil Inversion	**Control**	**Small-particle size biochar**	**Large-particle size biochar**
Un-inverted	11.6aA	14.7aA	11.9aA
Inverted	11.4aA	15.2aA	13.4aA

Different small letters within a row indicate differences between biochar treatments ($n = 4$) and $p < 0.10$), and (ii) different uppercase letters within a column indicate differences between un-inverted and inverted treatments ($n = 4$ and $p < 0.10$).

Table S6-2. Average C concentration (g kg^{-1}) at 0-10 and 10-20 cm depth measured at the end of the experiment, with treatment or soil inversion as the factor.

	Treatments		
Soil Inversion (depth in the soil column)	**Control**	**Small-particle size biochar**	**Large-particle size biochar**
Un-inverted topsoil (at 0-10 cm depth)	36.1bA	52.5aA	49.7aA
Inverted topsoil (at 10-20 cm depth)	34.2cA	51.8aA	44.8bB
Un-inverted subsoil (at 10-20 cm depth)	21.7aB	22.6aB	23.0aA
Inverted subsoil (at 0-10 cm depth)	23.6aA	23.7aA	23.3aA

Different small letters within a row indicate differences between biochar treatments ($n = 4$) and $p < 0.10$), and (ii) different uppercase letters within a column indicate differences between un-inverted and inverted treatments ($n = 4$ and $p < 0.10$). In the un-inverted soil, biochar was at 0-10 cm depth while in the inverted soil biochar was at 10-20 cm depth.

Table S6-3. *Soil total C (g kg^{-1}) of each layer measured at the end of the experiment.*

Soil depth (cm)	Treatments							
	Un-inverted soil				Inverted soil			
	UC	US	UL	*p*-value	IC	IS	IL	*p*-value
Layer A (0-3 cm)	38.5b	56.4a	52.3a	**0.000**	24.9a	24.7a	23.3a	0.187
Layer B (3-6 cm)	37.6b	51.8a	49.1a	**0.000**	22.7a	23.4a	23.5a	0.176
Layer C (6-10 cm)	32.3b	49.3a	47.7a	**0.001**	23.2a	23.0a	23.2a	0.900
Layer D (10-13 cm)	23.0a	23.0a	23.1a	0.971	34.2b	50.4a	47.9a	**0.003**
Layer E (13-16 cm)	22.4a	22.9a	22.9a	0.299	36.1c	52.0a	45.8b	**0.000**
Layer F (16-20 cm)	19.6a	21.7a	23.0a	0.100	32.4c	52.2a	40.9b	**0.000**

UC - control un-inverted; US – Un-inverted 0-10 cm with <2 mm biochar; UL – un-inverted 0-10 cm with >4 mm biochar; IC - control inverted; IS - inverted 0-10 cm with <2 mm biochar; IL - inverted 0-10 cm with >4 mm biochar. Different letters denote significant differences at $p < 0.10$ between treatments ($n = 4$) for each layer. In the un-inverted soil, biochar was at 0-10 cm depth; in the inverted soil biochar was at 10-20 cm depth.

Table S6-4. Non-oxidisable C (g kg^{-1}) at each depth measured at the end of the experiment.

Soil depth (cm)	Treatments							
	Un-inverted soil				Inverted soil			
	UC	US	UL	*p*-value	IC	IS	IL	*p*-value
Layer A (0-3 cm)	3.73b	18.18a	17.81a	**0.017**	0.92a	1.33a	2.74a	0.569
Layer B (3-6 cm)	5.06c	17.69a	11.68b	**0.000**	3.47a	2.48a	0.99a	0.170
Layer C (6-10 cm)	5.22b	17.63a	15.57a	**0.004**	3.21a	2.35a	1.45a	0.588
Layer D (10-13 cm)	3.64a	3.24a	2.44a	0.461	3.87b	18.16a	16.98a	**0.009**
Layer E (13-16 cm)	3.44a	2.78a	1.87a	0.493	4.58c	19.79a	12.95b	**0.000**
Layer F (16-20 cm)	2.70a	2.58a	3.45a	0.760	2.03c	20.07a	9.08b	**0.001**

UC - control un-inverted; US – Un-inverted 0-10 cm with <2 mm biochar; UL – un-inverted 0-10 cm with >4 mm biochar; IC - control inverted; IS - inverted 0-10 cm with <2 mm biochar; IL - inverted 0-10 cm with >4 mm biochar. Different letters denote significant differences at $p < 0.10$ between treatments ($n = 4$) for each layer. In the un-inverted soil, biochar was at 0-10 cm depth; in the inverted soil biochar was at 10-20 cm depth.

Table S6-5. Soil bulk density (g/cm^{-3}) at each depth measured at the end of the experiment.

Soil depth (cm)	Treatments							
	Un-inverted soil				Inverted soil			
	UC	US	UL	*p*-value	IC	IS	IL	*p*-value
Layer A (0-3 cm)	0.92a	0.93a	0.84a	0.115	1.16a	1.06a	1.12a	0.271
Layer B (3-6 cm)	1.04a	0.99a	0.94a	0.106	1.14a	1.19a	1.18a	0.792
Layer C (6-10 cm)	0.97a	1.06a	0.99a	0.101	1.05a	1.17a	1.08a	0.186
Layer D (10-13 cm)	1.18a	1.18a	1.12a	0.741	0.92a	0.95a	1.00a	0.327
Layer E (13-16 cm)	1.17a	1.10a	1.11a	0.599	1.00a	0.94a	0.92a	0.417
Layer F (16-20 cm)	1.18a	1.10a	1.08a	0.183	1.00a	0.91a	0.93a	0.267

UC - control un-inverted; US – Un-inverted 0-10 cm with <2 mm biochar; UL – un-inverted 0-10 cm with >4 mm biochar; IC - control inverted; IS - inverted 0-10 cm with <2 mm biochar; IL - inverted 0-10 cm with >4 mm biochar. Different letters denote significant differences at $p < 0.10$ between treatments ($n = 4$) for each layer. In the un-inverted soil biochar was at 0-10 cm depth; in the inverted soil biochar was at 10-20 cm depth.

Table S6-6. Soil C stock (Mg ha^{-1}) calculated at equivalent soil mass measured at overall 0-20 cm depth by the end of the experiment, with treatment or soil inversion as the factor.

Soil Inversion	Treatments		
	Control	Small-particle size biochar	Large-particle size biochar
Un-inverted	57.9bA	74.4aA	72.2aA
Inverted	58.3cA	75.4aA	68.1bB

Different small letters within a row indicate differences between biochar treatments ($n = 4$) and $p < 0.10$), and (ii) different uppercase letters within a column indicate differences between un-inverted and inverted treatments ($n = 4$ and $p < 0.10$). In the un-inverted soil, biochar was at 0-10 cm depth while in the inverted soil biochar was at 10-20 cm depth.

Table S6-7. Comparison between measured and NIR/PLSR predicted mean Soil C stock (Mg ha^{-1}) calculated at equivalent soil mass measured at overall 0-20 cm depth

Soil depth (cm)	Un-inverted soil			Inverted soil		
	UC	**US**	**UL**	**IC**	**IS**	**IL**
Measured	57.9a	74.4a	72.2a	58.3a	75.4a	68.0a
Predicted	58.0a	76.6a	66.2b	58.7a	79.5a	67.8a
***p*-value**	0.913	0.640	0.008	0.902	0.071	0.903

UC - control un-inverted; US – Un-inverted 0-10 cm with <2 mm biochar; UL – un-inverted 0-10 cm with >4 mm biochar; IC - control inverted; IS - inverted 0-10 cm with <2 mm biochar; IL - inverted 0-10 cm with >4 mm biochar. Different letters denote significant differences at $p < 0.05$, analysed using paired t-test (α=0.05; n = 4).

Table S6-8. Predicted soil C stock (Mg ha^{-1}) calculated at equivalent soil mass measured at overall 0-20 cm depth by the end of the experiment, with treatment or soil inversion as the factor.

	Treatments		
Soil Inversion	**Control**	**Small-particle size biochar**	**Large-particle size biochar**
Un-inverted	58.0cA	76.6aA	66.2bA
Inverted	58.7cA	79.5aA	67.8bA

Different small letters within a row indicate differences between biochar treatments (n = 4) and $p < 0.05$), and (ii) different uppercase letters within a column indicate differences between un-inverted and inverted treatments (n = 4 and $p < 0.05$). In the un-inverted soil, biochar was at 0-10 cm depth while in the inverted soil biochar was at 10-20 cm depth.

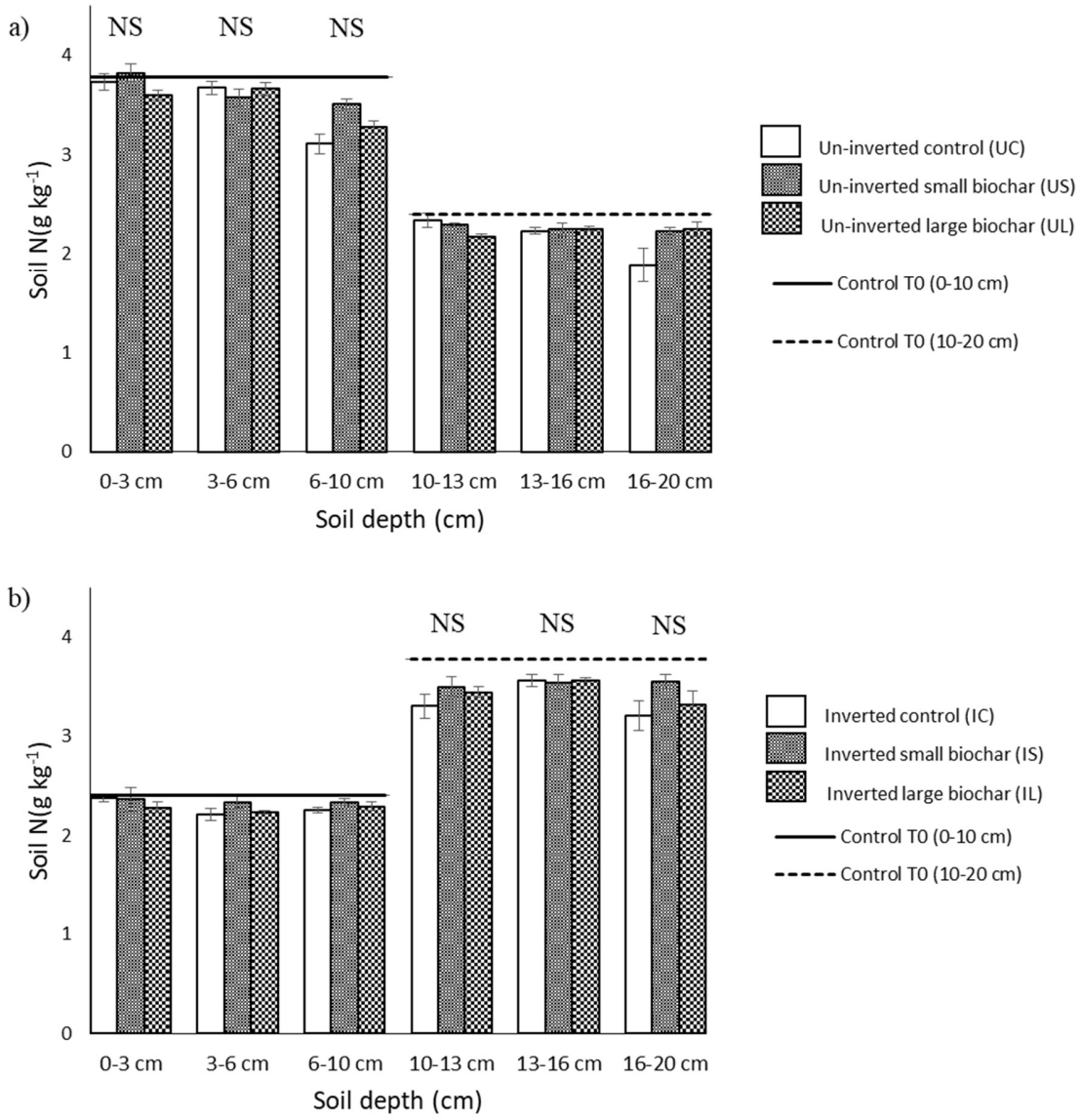

Figure S6-2. Soil N concentration distribution with depth at the end of the trial. Error bars indicate the standard error of the mean (SEM). Within a specific soil inversion; (a) un-inverted soil and (b) inverted soil, different small letters would indicate differences in soil N between treatments for each soil depth ($n = 4$ and $p < 0.10$), however, no significant difference was detected.

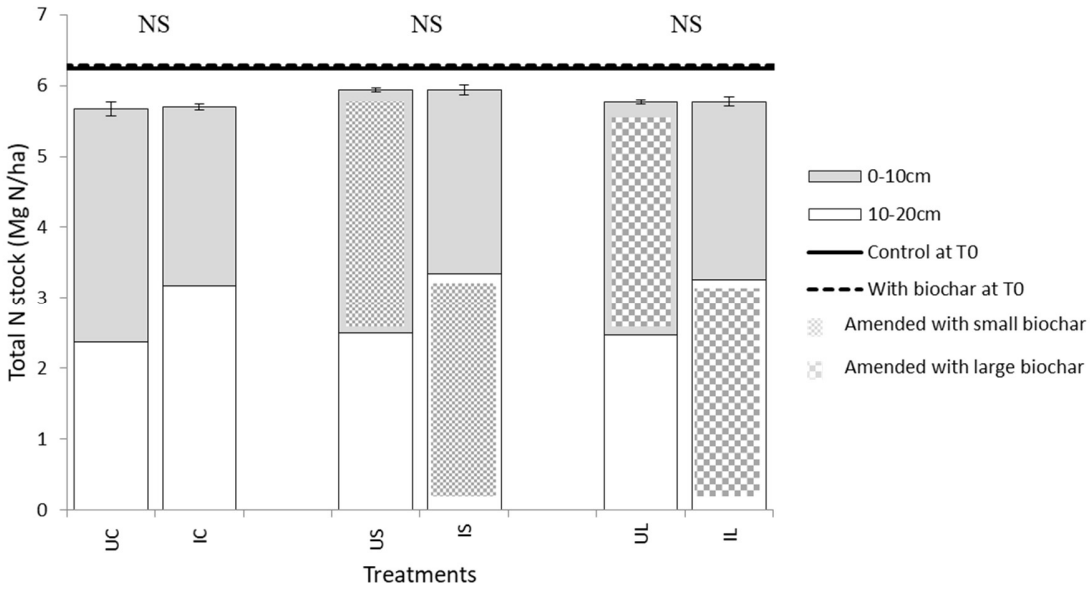

Figure S6-3. Soil N stocks calculated at an equivalent soil mass for overall depth of 0 to 20 cm. Error bars indicate the standard error of the mean (SEM). Within a specific soil inversion, different small letters would indicate differences in soil N stock between treatments ($n = 4$ and $p < 0.10$) while, within specific biochar treatment, different uppercase letters indicate differences between un-inverted and inverted treatments ($n = 4$ and $p < 0.10$), however, no significant difference was detected.

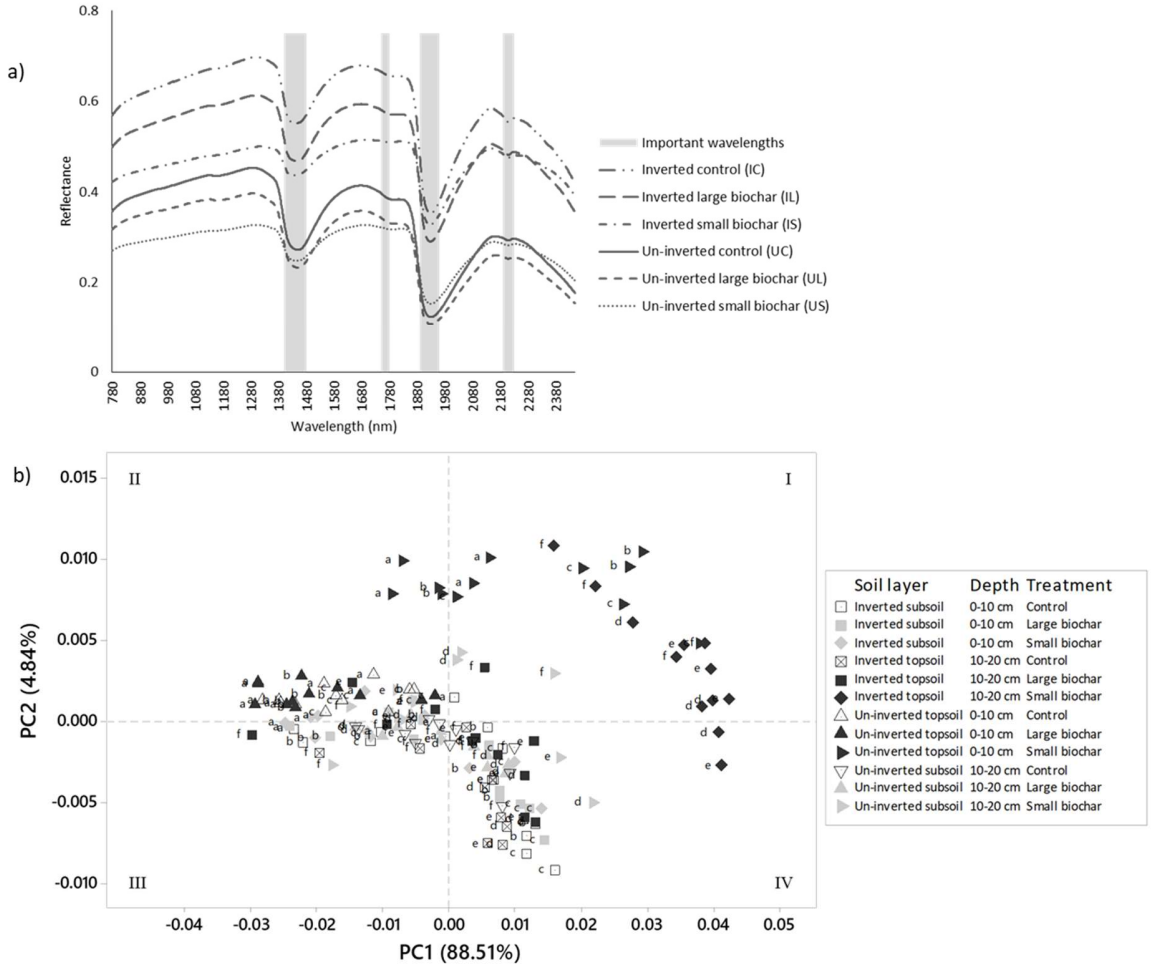

Figure S6-4. a) The average NIR reflectance spectra of the soils layers intended for biochar application (0-10 cm of un-inverted soil or 10-20 cm of inverted soil) according to each treatment; b) Score plots for the first two principal components in a principal component analysis (PCA) of the pre-processed NIR spectra from 144 soil samples.

MASSEY UNIVERSITY
TE KUNENGA KI PŪREHUROA
UNIVERSITY OF NEW ZEALAND

GRADUATE RESEARCH SCHOOL

STATEMENT OF CONTRIBUTION
DOCTORATE WITH PUBLICATIONS/MANUSCRIPTS

We, the candidate and the candidate's Primary Supervisor, certify that all co-authors have consented to their work being included in the thesis and they have accepted the candidate's contribution as indicated below in the *Statement of Originality*.

Name of candidate:	Ainul Faizah Mahmud
Name/title of Primary Supervisor:	Professor Marta Camps Arbestain
In which chapter is the manuscript /published work:	Chapter Three

Please select one of the following three options:

○ The manuscript/published work is published or in press

- Please provide the full reference of the Research Output:

○ The manuscript is currently under review for publication – please indicate:

- The name of the journal:

- The percentage of the manuscript/published work that was contributed by the candidate:

- Describe the contribution that the candidate has made to the manuscript/published work:

◉ It is intended that the manuscript will be published, but it has not yet been submitted to a journal

Candidate's Signature:	AINUL FAIZAH MAHMUD Digitally signed by AINUL FAIZAH MAHMUD Date: 2020.06.16 01:26:35 +08'00'
Date:	16-Jun-2020
Primary Supervisor's Signature:	Marta Camps-Arbestain Digitally signed by Marta Camps-Arbestain Date: 2020.06.16 19:06:18 +12'00'
Date:	

This form should appear at the end of each thesis chapter/section/appendix submitted as a manuscript/ publication or collected as an appendix at the end of the thesis.

MASSEY UNIVERSITY
TE KUNENGA KI PŪREHUROA
UNIVERSITY OF NEW ZEALAND

GRADUATE RESEARCH SCHOOL

STATEMENT OF CONTRIBUTION
DOCTORATE WITH PUBLICATIONS/MANUSCRIPTS

We, the candidate and the candidate's Primary Supervisor, certify that all co-authors have consented to their work being included in the thesis and they have accepted the candidate's contribution as indicated below in the *Statement of Originality*.

Name of candidate:	Ainul Faizah Mahmud
Name/title of Primary Supervisor:	Professor Marta Camps Arbestain
In which chapter is the manuscript /published work:	Chapter Four

Please select one of the following three options:

○ The manuscript/published work is published or in press

- Please provide the full reference of the Research Output:

○ The manuscript is currently under review for publication – please indicate:

- The name of the journal:

- The percentage of the manuscript/published work that was contributed by the candidate:

- Describe the contribution that the candidate has made to the manuscript/published work:

◉ It is intended that the manuscript will be published, but it has not yet been submitted to a journal

Candidate's Signature:	AINUL FAIZAH MAHMUD Digitally signed by AINUL FAIZAH MAHMUD Date: 2020.06.16 01:26:35 +08'00'
Date:	16-Jun-2020
Primary Supervisor's Signature:	Marta Camps-Arbestain Digitally signed by Marta Camps-Arbestain Date: 2020.06.16 19:07:06 +12'00'
Date:	

This form should appear at the end of each thesis chapter/section/appendix submitted as a manuscript/ publication or collected as an appendix at the end of the thesis.

MASSEY UNIVERSITY
TE KUNENGA KI PŪREHUROA
UNIVERSITY OF NEW ZEALAND

GRADUATE RESEARCH SCHOOL

STATEMENT OF CONTRIBUTION
DOCTORATE WITH PUBLICATIONS/MANUSCRIPTS

We, the candidate and the candidate's Primary Supervisor, certify that all co-authors have consented to their work being included in the thesis and they have accepted the candidate's contribution as indicated below in the *Statement of Originality*.

Name of candidate:	Ainul Faizah Mahmud
Name/title of Primary Supervisor:	Professor Marta Camps Arbestain
In which chapter is the manuscript /published work:	Chapter Five

Please select one of the following three options:

(●) The manuscript/published work is published or in press

- Please provide the full reference of the Research Output:

Mahmud, A. F., Camps-Arbestain, M., & Hedley, M. (2018). Investigating the Influence of Biochar Particle Size and Depth of Placement on Nitrous Oxide (N2O) Emissions from Simulated Urine Patches. Agriculture, 8(11), 175.

( ) The manuscript is currently under review for publication – please indicate:

- The name of the journal:

- The percentage of the manuscript/published work that was contributed by the candidate:

- Describe the contribution that the candidate has made to the manuscript/published work:

( ) It is intended that the manuscript will be published, but it has not yet been submitted to a journal

Candidate's Signature:	AINUL FAIZAH MAHMUD Digitally signed by AINUL FAIZAH MAHMUD Date: 2020.06.16 01:26:35 +08'00'
Date:	16-Jun-2020
Primary Supervisor's Signature:	Marta Camps-Arbestain Digitally signed by Marta Camps-Arbestain Date: 2020.06.16 19:07:48 +12'00'
Date:	

This form should appear at the end of each thesis chapter/section/appendix submitted as a manuscript/ publication or collected as an appendix at the end of the thesis.

MASSEY UNIVERSITY
TE KUNENGA KI PŪREHUROA
UNIVERSITY OF NEW ZEALAND

GRADUATE RESEARCH SCHOOL

STATEMENT OF CONTRIBUTION
DOCTORATE WITH PUBLICATIONS/MANUSCRIPTS

We, the candidate and the candidate's Primary Supervisor, certify that all co-authors have consented to their work being included in the thesis and they have accepted the candidate's contribution as indicated below in the *Statement of Originality*.

Name of candidate:	Ainul Faizah Mahmud
Name/title of Primary Supervisor:	Professor Marta Camps Arbestain
In which chapter is the manuscript /published work:	Chapter Six

Please select one of the following three options:

○ The manuscript/published work is published or in press

- Please provide the full reference of the Research Output:

○ The manuscript is currently under review for publication – please indicate:

- The name of the journal:

- The percentage of the manuscript/published work that was contributed by the candidate:

- Describe the contribution that the candidate has made to the manuscript/published work:

◉ It is intended that the manuscript will be published, but it has not yet been submitted to a journal

Candidate's Signature:	AINUL FAIZAH MAHMUD Digitally signed by AINUL FAIZAH MAHMUD Date: 2020.06.16 01:26:35 +08'00'
Date:	16-Jun-2020
Primary Supervisor's Signature:	Marta Camps-Arbestain Digitally signed by Marta Camps-Arbestain Date: 2020.06.16 19:08:53 +12'00'
Date:	

This form should appear at the end of each thesis chapter/section/appendix submitted as a manuscript/ publication or collected as an appendix at the end of the thesis.